PL-TR-96-2207

# DISCRIMINATION OF SEISMIC SOURCES USING ISRAEL SEISMIC NETWORK

Yefim Gitterman
Vladimir Pinsky
Avi Shapira

Institute for Petroleum Research and Geophysics
P.O. Box 2286
Holon 58122, ISRAEL

July 1996

**19961104 109**

Scientific Report No. 1

**PHILLIPS LABORATORY**
**Directorate of Geophysics**
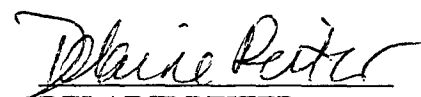**AIR FORCE MATERIEL COMMAND**
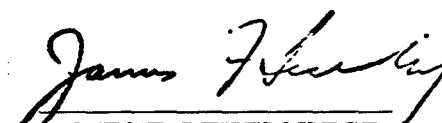**HANSCOM AFB, MA 01731-3010**

DTIC QUALITY INSPECTED 1

SPONSORED BY
Department of Energy
Office of Non-Proliferation and National Security

MONITORED BY
Phillips Laboratory
CONTRACT No. F19628-95-K-0006

DELAINE REITER
Contract Manager
Earth Sciences Division

JAMES F. LEWKOWICZ
Director
Earth Sciences Division

| REPORT DOCUMENTATION PAGE | Form Approved OMB No. 0704-0188 |
|---|---|

| 1. AGENCY USE ONLY (Leave blank) | 2. REPORT DATE<br>July 1996 | 3. REPORT TYPE AND DATES COVERED<br>Scientific Report No. 1 |
|---|---|---|

| 4. TITLE AND SUBTITLE<br><br>Discrimination of seismic sources<br>using Israel Seismic Network | 5. FUNDING NUMBERS<br>PE 69120H<br>PR DENN TA GM WU AL<br>Contract F19628-95-K-0006 |
|---|---|

**6. AUTHOR(S)**

Yefim Gitterman, Vladimir Pinsky, Avi Shapira

| 7. PERFORMING ORGANIZATION NAME(S) AND ADDRESS(ES)<br><br>The Institute for Petroleum Research and Geophysics<br>P.O.B. 2286, Holon 58122<br>ISRAEL | 8. PERFORMING ORGANIZATION REPORT NUMBER<br><br>555/53/96(4) |
|---|---|

| 9. SPONSORING / MONITORING AGENCY NAME(S) AND ADDRESS(ES)<br>Phillips Laboratory<br>29 Randolph Road<br>Hanscom AFB, MA 01731-3010<br><br>Contract Manager: Delaine Reiter/GPE | 10. SPONSORING / MONITORING AGENCY REPORT NUMBER<br><br>PL-TR-96-2207 |
|---|---|

**11. SUPPLEMENTARY NOTES**

| 12a. DISTRIBUTION / AVAILABILITY STATEMENT<br><br>Approved for Public Release; Distribution Unlimited | 12b. DISTRIBUTION CODE |
|---|---|

**13. ABSTRACT** (Maximum 200 words)

Regional Densed Seismic Networks (RDSN) have additional as yet uninvestigated potential for discriminating weak local earthquakes and quarry blasts. Even conventional single station discriminants, such as P/S and spectral ratios are significantly improved, after averaging across the Israel Seismic Network, which consists of 36 short period stations. This report documents a study aimed at the development of new techniques specially designed for RDSN oriented discrimination: (1) subnet average of the seismic energy ratio between the low (1-6 Hz) and high (6-11 Hz) frequency ranges; (2) spectral semblance, measuring subnet spectral shapes coherency; (3) velogram analysis evaluating the different kinematic features of seismic waves for shallow and deep events.

The algorithms were tested on 212 events: earthquakes, quarry ripple-fired and single blasts, and underwater explosions from some areas of the Middle East region with a 97-100% success rate. The study of this physically approved algorithms was complimented by testing of the multivariate procedures based on formal Integrative Approach: King's clustering procedure, Linear Discrimination Function and Artificial Neural Networks. When applied to a vector of spectral parameters derived from the Galilee data base, they provided 99-100% of true classification in a cross-validation test. All the procedures are applicable to routine processing of seismograms, thus significantly improving discrimination performance.

| 14. SUBJECT TERMS<br>Regional discrimination, seismic network, velogram analysis, spectra modulation and coherency, spectral ratios, multivariate discrimination procedures | 15. NUMBER OF PAGES<br>98 |
|---|---|
| | 16. PRICE CODE |

| 17. SECURITY CLASSIFICATION OF REPORT<br>Unclassified | 18. SECURITY CLASSIFICATION OF THIS PAGE<br>Unclassified | 19. SECURITY CLASSIFICATION OF ABSTRACT<br>Unclassified | 20. LIMITATION OF ABSTRACT<br>SAR |
|---|---|---|---|

# TABLE OF CONTENTS

# ILLUSTRATIONS

# TABLES

## ACKNOWLEDGMENTS

## PUBLICATIONS RESULTING FROM SPONSORSHIP OF THE CONTRACT:

Shapira, A., Gitterman, Y., Pinsky, V. and Malitzky, A., 1995. Detection, location and discrimination of seismic events by the Seismic Network of Israel, Proceedins, 17th Seismic Research Symposium on Monitoring a CTBT, September 1995, AZ, 911-919. PL-TR-95-2108, ADA 310037

Gitterman, Y., Pinsky, V. and Shapira, A., 1996. Semblance and energy spectral statistics for discrimination of seismic events, Annual Meeting of Isr. Geol. Survey, March, 1996.

Pinsky, V., Shapira, A. and Gitterman, Y., 1996. Multi-channel velogram analysis for discriminating between earthquakes and quarry blasts, 27th Nordic Seminar on Detection Seismology, XXV ESC General Assembly, September 1996, Reykjavik, Iceland (submitted).

Gitterman, Y., Shapira, A. and Pinsky, V., 1996. Spectral semblance statistics as effective regional discriminants of seismic events in Israel, 27th Nordic Seminar on Detection Seismology, XXV ESC General Assembly, September 1996, Reykjavik, Iceland (submitted).

Shapira, A., Gitterman, Y., and Pinsky, V., 1996. Discrimination of seismic sources using the Israel Seismic Network, Proceedings of 18th Seismic Research Symposium on Monitoring a CTBT, September 1996, Annapolis. PL-TR-96-2153

# SUMMARY

The primary objective of this research is to utilize the advantages of the Regional Dense Seismic Network (RDSN) efficiently as a multichannel, spatially distributed system for discrimination of low magnitude events ($m_b < 2.5$). In this study the Israel Seismic Network (ISN) is used to discriminate between earthquakes and explosions in the Middle East region. This issue is most important for CTBT monitoring, especially with regard to small nuclear tests which may be conducted under evasive conditions.

We began with the application of conventional single station/array methods, such as P/Lg and spectral short period ratios, to the ISN. This led to the development of new RDSN oriented algorithms based on different spectral and space-time characteristics of seismic radiation from explosions and earthquakes, i.e., spectral semblance statistics and multi-channel velogram analysis. These developments were followed by the integration of different approaches into a multidimensional procedure for the achievement of high automatic performance in routine operation of the RDSN.

Two hundred and twelve quarry blasts, underwater explosions and earthquakes within the magnitude range $M_L = 1.0-2.8$ and distances of 10-320km recorded by the ISN were selected for the discrimination study. Discriminants based on spectral features of seismograms appeared to be the most efficient. The analysis is based on smoothed (0.5 Hz window) FFT spectra of the whole signal, without picking out separate wave phases. The seismic energy ratio between the low frequency (1-6 Hz) and the high frequency (6-11 Hz) bands showed an overlap between quarry blasts and earthquakes. When averaging the ratios over a RDSN subnetwork, the resolving power is enhanced and the two classes of seismic events are separated.

We also computed rms spectral amplitudes in five sequential, equal frequency windows within the 1-11 Hz band and applied multiparametric classification procedures (i.e. Linear Fisher Discriminator, Artificial Neural Network and King's cluster algorithm) to the subnetwork averages of these data. The results of a leave-one-out test showed a low rate of classification mistakes for all the methods.

We developed and tested a new multi-station discriminant based on the Low Frequency Spectral Modulation (LFSM) method. The LFSM is associated with ripple-firing in quarry blasts and with the bubbling effect in underwater explosions. The method demonstrates a distinct azimuth-invariant coherency of spectral shapes in the low-frequency range (1-12 Hz) for a

broad range of distances (up to 320km) and for arbitrary delay times. The coherency of modulated spectra for different RDSN stations was measured by semblance statistics commonly used in seismic prospecting for phase correlation in the time domain. After modification, the statistics provided a complete separation of earthquakes and explosions.

Another new RDSN discriminant is based on velograms (signal envelopes versus group velocity). We measured velocities $V_{ms}$ and $V_{mp}$ at which the velogram reaches its local maximum $S_{max}$, $P_{max}$ within the range 1-4 km/sec and 4-8 km/s, respectively. It was observed that the empirical relationship between $V_{ms}$ and distance R (in the range 10-150 km), is different for blasts and earthquakes. This effect can be attributed to the different excitation of surface waves from these two types of seismic events and/or different S-wave group velocities for shallow and deep sources. A simple statistic, derived from the $V_{ms}(R)$ parametric approximation, provides true identification of the events.

As a part of the investigation we tested the $P_{max}/S_{max}$ ratio, which worked well only for a small number of relatively strong events ($m_b > 2$) and coda discriminants, which failed completely, showing severe dependency on the SNR ratio.

Discrimination results for weak and remote events can be improved by application of the array technique, providing efficient enhancement of the signal-to-noise ratio. We began by analyzing the limited amount of data obtained from the micro-array deployed in the Negev desert, Israel, in June 1995. The initial results of experiments with beamforming and the implementation of a new phase correlation algorithm for detection and event characterization are optimistic.

# 1. INTRODUCTION

The monitoring of a Comprehensive Test Ban Treaty (CTBT) requires the enhanced ability to discriminate between small earthquakes and man-made activities, e.g. mining, quarry blasts and explosions of different types. For example, a kiloton clandestine nuclear explosion carried out in a large cavity may lead to a seismic decoupling factor of 50 (Jarpe et al., 1996), with a magnitude $m_b$ of 2.1, comparable with that of quarry blasts. Regional Dense Seismic Networks (RDSN) have an additional potential for detecting and identifying small seismic events; therefore a study devoted to RDSN-based discrimination between quarry blasts and earthquakes is of great importance.

Different amplitude ratios are used as regional discriminants. The most frequently used is the family of Pn/Sn, Pn/Lg ratios which, according to reports by Pomeroy et al. (1982), Taylor et al. (1989), Baumgardt and Young (1990), Dysart and Pully (1990), Hedlin et al. (1990) and others, are successful. A number of regional discriminants are based on spectral differences of earthquakes and explosions and various types of spectral ratios are used: ratios of separate wave phases, e.g. P to S, in selected narrow bands (see e.g. Baumgardt, 1993), or slopes of these spectral ratios in the entire recorded frequency range (Goldstein, 1995); ratios of peak, rms or average amplitude (or power) in different frequency bands for the same phase, mainly Lg (Pulli, 1986; Taylor et al., 1988; Bennett and Murphy, 1986; Baumgardt and Zigler, 1988; Suteau-Henson and Bache, 1988; Walter et al., 1995). The spectral ratio, $R_E$, of seismic energy in low-frequency and high-frequency ranges (Gitterman and Shapira, 1993) provided complete separation of earthquakes and underwater explosions off the Levant coast.

These short-period discriminants are heavily dependent upon the structure and constitution of the uppermost crust. Their performance varies from region to region and should be tested on a reliable database with ground-truth information in every case study. Most of the investigations mentioned were conducted for a single station or beamed array data. As shown by Kim et al. (1994), the discrimination effect of the single-station discriminant (P/S spectral ratio) is significantly enhanced when averaged over the New York State seismic network. We obtained similar results in this study by averaging amplitude P/S and energy spectral ratios over the ISN.

A fundamental coda wave characteristic is that its decay depends on the average properties of the region surrounding the source and station and is independent of any particular wave path. However, as shown by Su et al.

(1991) for the South-Central Mojave Desert and Eastern Transverse Ranges, coda decay rate $Q^{-1}$ for quarry blasts was significantly higher than for earthquakes at low frequencies (1.5 and 3 Hz) for lapse time to about 30 sec. This result was explained by the predominant contribution of surface waves from quarry blasts. In this study we tried to test the applicability of the coda parameter to discrimination in the Middle East region.

One of the main spectral features used in the identification of industrial explosions is spectral modulation (SM) caused by ripple firing. Most of the studies are based on time-independent patterns for a single station or array, presented in spectrograms or sonograms of the whole seismogram (e.g. Hedlin et al., 1989, 1995; Kim et al., 1994), or in spectra of different regional phases (e.g. Baumgardt and Zigler, 1988; Der and Baumgardt, 1995). These discriminants are concerned mainly with spectral maxima at high frequencies (more than 10 Hz) reciprocal to a delay time. It has been argued that SM is not observable in the United States, because delay times were too short to be observed within the limited recording bandwidth (Bennett et al., 1989) and that the bandwidth should be extended to 80 Hz to resolve delays shorter then 25 msec (Baumgardt and Zigler, 1988).

A different multi-station approach based on the azimuth-invariant SM caused by ripple firing, considered jointly for RDSN stations, is discussed by Gitterman and van Eck (1993). A similar approach was also implemented for the identification of underwater explosions in the Mediterranean using an SM caused by the bubbling phenomenon (Gitterman and Shapira, 1993, 1994). The method utilizes low frequency (1-12 Hz) minima and demonstrates the distinct coherency of spectral shapes for broad ranges of azimuths and distances (10-320km), in the whole range of delay times (20-100 msec). In this study the advantages provided by RDSN are utilized in the newly developed discriminant based on coherency of spectral shapes for quarry blasts at different azimuthally distributed stations which is not presented in earthquake patterns. The coherency is measured by "semblance" and "cross-correlation" statistics used in seismic prospecting practice in the time domain and modified for spectral application.

Besides the above mentioned dynamic discriminants, it is possible to utilize kinematic features of seismograms. Earthquake foci are usually deeper than explosions with different physical properties of the media and surface and, therefore, their respective wave fields possess different kinematic characteristics. The experimental fact emphasized in many studies

(Kafka, 1990; Walter et al., 1996) is that explosions in the vicinity of the source generate very slow (1.5-2 km/s) fundamental surface Rayleigh waves, Rg, with low frequencies and high amplitudes as compared to earthquakes. Alexander et al. (1995), using data from quarry blasts, showed that Rg scattering into body phases shifts the total dispersion of the wavetrain towards lower group velocities. In spite of the above analysis, no direct study using group velocity measurements for discrimination has previously been performed.

In our investigation a new kinematic "velogram" discriminant based on the empirical relationship between the group velocity of S waves and distance, is developed, providing effective separation between local earthquakes and explosions recorded by the ISN.

An additional effect can be achieved by the Integrative Approach using a number of different physical signal features. Even a simple majority voting of several different physical discriminants (Wuster, 1993) provides an improvement in classification results. Simultaneous application of efficient multi-dimensional discrimination procedures, such as cluster analysis (King, 1967), linear or quadratic Fisher discriminators (e.g. Tsvang et al., 1993), artificial neural network (e.g. Dowla, 1995; Pully, 1995), to a group of statistics presented in the vector form, essentially enhances the resolving power as compared to an individual discriminator or majority voting. During the period covered by this report we began application of the Integrative Approach, including the above mentioned multi-dimensional discrimination procedures, to events from northern Israel with promising preliminary results. The performance of these algorithms was tested by the leave-one-out procedure.

Further enhancement of discrimination results for week seismic events can be achieved by the implementation of the array technique due to effective noise suppression (Tsvang et al., 1993). We began realization of this study using data from a 13 station micro-array deployed in the Negev desert, Israel, in June 1995. The initial results with beamforming and testing of a new phase correlation algorithm (Gelchinsky et al., 1985) for detection and location are promising.

## 2. DATA COLLECTION

In this project 212 regional seismic events recorded by the Israel Seismic Network (ISN) were used to test different analytical discrimination procedures, both commonly used and newly-developed. The ISN is operated by the Seismology Division of the Institute for Petroleum Research and Geophysics (IPRG) (currently changing its name to the Geophysical Institute of Israel). The selected database covers a broad range of types of seismic events: ripple-firing quarry blasts, single quarry blasts, underwater explosions (UWE) and local earthquakes occurring in the region, as well as a variety of geographical-geological areas in Israel and surrounding regions: the Galilee and Tyre off-coast Mediterranean, northern Israel; the Dead Sea basin and Negev desert in the south; the Gilad region in Jordan and the Jordan-Saudi Arabia border (see map, Fig. 1). The seismic events are within the magnitude range $M_L$=1.0-2.8 and distance range 10-320km.

The local magnitude is determined from S-coda duration measurements (Shapira, 1988). It should be noted that magnitude estimates for open-pit quarry blasts and underwater explosions are rather rough and might be overestimated due to strong surface waves. A description of the network, arrival times, local magnitude determination and the original hypocenter locations used in this study may be found in "Earthquakes in and around Israel", Seismological Bulletins Nos. 6-10, 1988-1991, IPRG Seismology Division, Holon.

### 2.1 INSTRUMENTATION

The distribution of ISN stations is shown in Fig. 1. The network consists of short period (1 Hz) seismometers (either Teledyne-Geotech S-13 or Mark Products L4C). Signals are bandpass filtered (0.2 to 12.5 Hz), amplified and digitally recorded by the ISDA system (Shapira and Avirav, 1990) with a sampling rate of 50 samples per second. All seismograms used in the study are from vertical seismometers.

During the observational period the data were transmitted via FM telemetry to the National Seismology Center at IPRG. At present the Seismology Division is engaged in updating the Israel seismic network, implementing digital satellite telemetry with a resolution of 20 bit/word and a 50 Hz sampling rate.
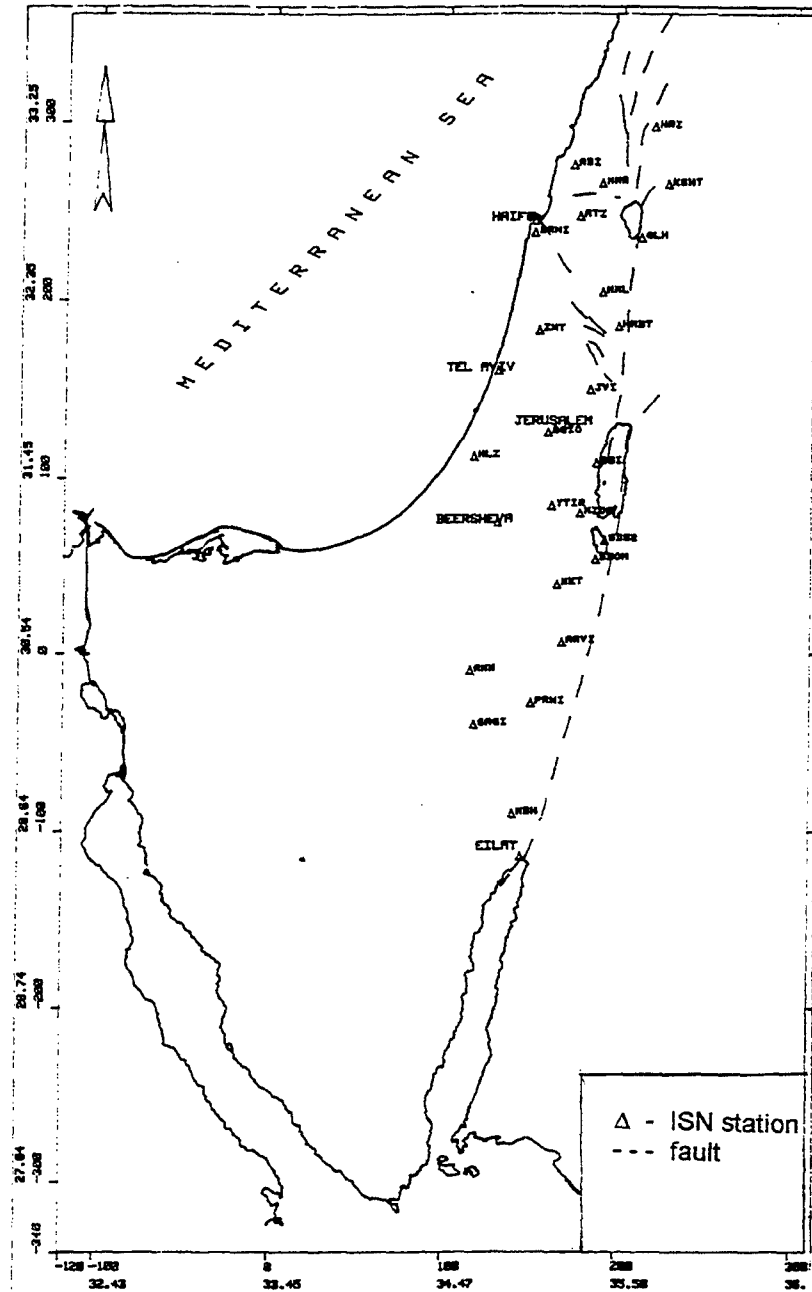
Figure 1. General view of the investigated region.

## 2.2 GALILEE GROUND-TRUTH DATASET OF EARTHQUAKES AND QUARRY BLASTS

The dataset includes 39 regionally recorded quarry blasts with ground-truth information and 30 earthquakes ($M_L$=1.0-2.6). All these events occurred in the Galilee region of Israel, relatively close to each other (a large part of this dataset was used by Gitterman and van Eck in their 1993 report). The event epicenters and quarry locations are shown in Fig. 2; earthquake and blast parameters are summarized in Table 1. Information presented in the open-pit quarries study is included in Table 2. The quarries in the Galilee mainly produce materials for construction of buildings and roads. We obtained information about the total amount of explosives used for all blasts and, in some cases, there are delay time values (usually 20-40 msec). This ground-truth information is routinely collected, based on telephone and fax communication with the quarries.

Over the years of ISN operation, quarry blasts were considered to be noise and, as such, no significant attempts were made either to locate them accurately or even determine their magnitude. Since this study requires true ground information, it was necessary to re-locate the events, match the computed locations with reports from the quarries and re-evaluate their magnitudes. For four small blasts ($M_L$<1.0) we could not estimate magnitude (close to 1) accurately owing to limitations of the magnitude formulae. Owing to the relatively high density of stations in the Galilee, we consider the earthquake hypocenters to be accurately located. Nevertheless, we checked several earthquakes with zero depth and found better solutions for deeper (3-6km) sources.

At the request of Phillips Labs., waveforms of 50 events (30 blasts and 20 earthquakes) from the selected dataset, adjusted and supplied with necessary additional information, were sent via electronic mail for further study. The events will be used as part of the Ground-Truth Database (GTDB), compiled by L. Grant (Multimax) (personal communication). This regional dataset ("The Galilee Dataset") will be available through the World Wide Web, as a contribution of IPRG. The information includes CSS3.0 arrival tables (with some modifications and additions by F. Ryall), references for the network, event coordinates, ground-truth information, characterization of quarries, etc.
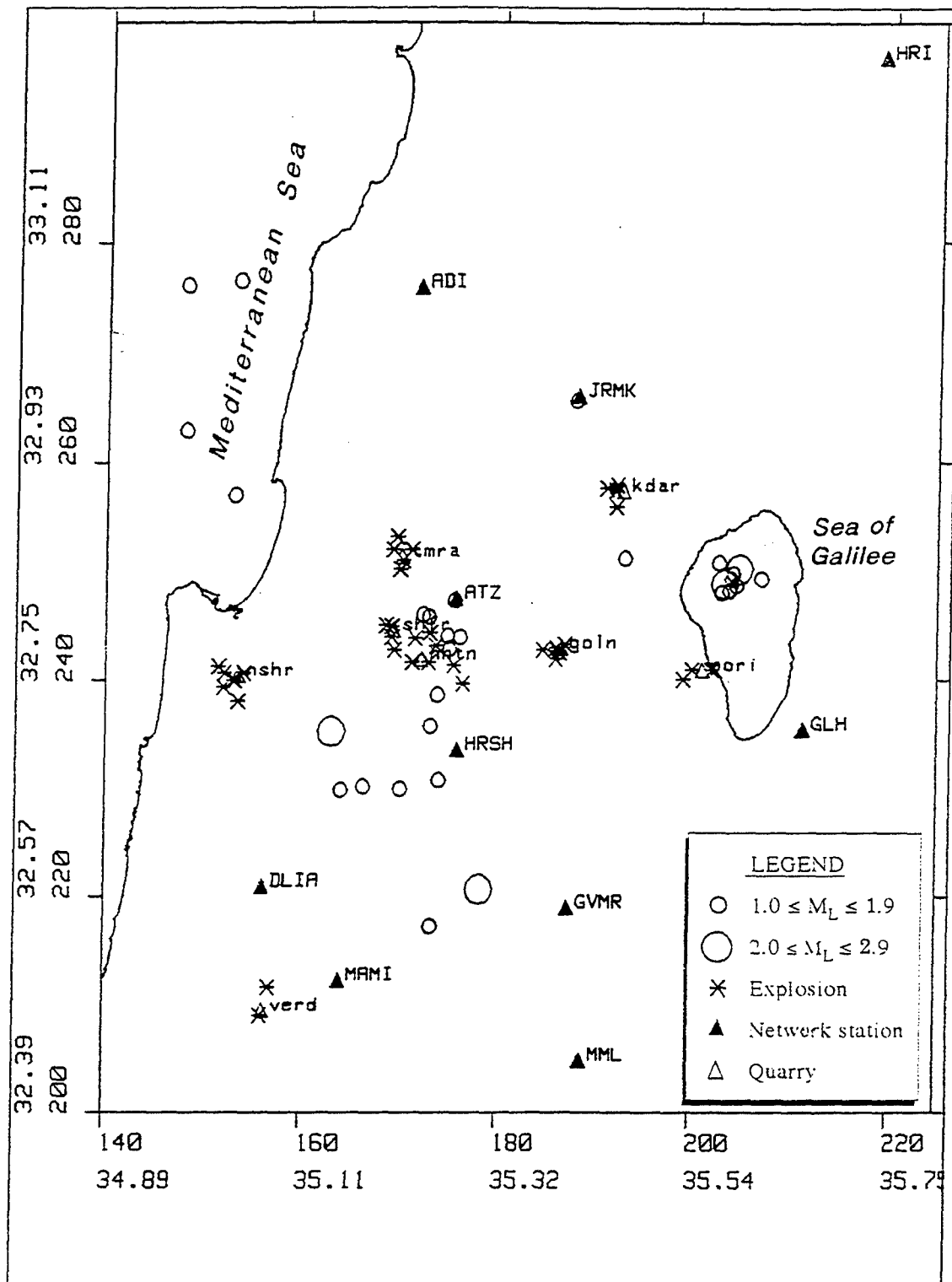
**Figure 2.** Epicenters of earthquakes, quarry blasts, quarries and ISN stations in the Galilee region.

9

Table 1. Seismic events in the Galilee region.

| Event | Origin time (yr/mo/dy/hr/mn) | ML | X (km) | Y (km) | Depth (km) | Lat. (N) | Lon. (E) | Quarry/ Local area | Size (kg) | Delay (msec) |
|---|---|---|---|---|---|---|---|---|---|---|
| | | | | | Quarry blasts | | | | | |
| EG1 | 8906201018 | 2.6 | 152.9 | 240.0 | 0 | 32.75 | 35.03 | Carmel | 12000 | 20 |
| EG2 | 8911081109 | 1.9 | 171.1 | 241.7 | 0 | 32.77 | 35.23 | Shefar | 2500 | 40 |
| EG3 | 9003271037 | 1.3 | 184.6 | 242.8 | 0 | 32.78 | 35.38 | Golani | 2800 | |
| EG4 | 9004041301 | 2.4 | 151.4 | 241.3 | 0 | 32.77 | 35.02 | Carmel | 15000 | 20 |
| EG5 | 9006121302 | 2.1 | 154.0 | 240.7 | 0 | 32.76 | 35.05 | Carmel | 13000 | 20 |
| EG6 | 9006130743 | 1.7 | 170.1 | 251.1 | 0 | 32.86 | 35.22 | Tamra | 6700 | 25 |
| EG7 | 9007231222 | 1.4 | 169.0 | 245.0 | 0 | 32.80 | 35.21 | Shefar | 1900 | 40 |
| EG8 | 9007260957 | 1.5 | 168.4 | 245.1 | 0 | 32.80 | 35.20 | Shefar | 4200 | 40 |
| EG9 | 9008120753 | 1.9 | 169.1 | 252.1 | 0 | 32.86 | 35.21 | Tamra | 6100 | 17&25 |
| EG10 | 9008281424 | 1.7 | 176.3 | 239.7 | 0 | 32.75 | 35.29 | Shefar | 2100 | 40 |
| EG11 | 9009111347 | 2.0 | 172.8 | 241.7 | 0 | 32.77 | 35.25 | Hanaton | 2500 | |
| EG12 | 9010161405 | 2.2 | 152.0 | 240.7 | 0 | 32.76 | 35.03 | Carmel | 12000 | 20 |
| EG13 | 9011061244 | 2.1 | 175.4 | 241.4 | 0 | 32.77 | 35.28 | Hanaton | 2500 | |
| EG14 | 9012181224 | 2.2 | 202.0 | 241.0 | 0 | 32.76 | 35.56 | Poria | 3700 | |
| EG15 | 9101091411 | 2.2 | 153.0 | 240.0 | 0 | 32.75 | 35.04 | Carmel | 12000 | 20 |
| EG16 | 9102040852 | 1.8 | 171.0 | 252.1 | 0 | 32.86 | 35.23 | Tamra | 4200 | |
| EG17 | 9102111255 | 2.0 | 200.0 | 241.0 | 0 | 32.76 | 35.54 | Poria | 2200 | |
| EG18 | 9102121206 | 1.4 | 186.0 | 243.0 | 0 | 32.78 | 35.39 | Golani | 3200 | |
| EG19 | 9103041333 | <1.0 | 156.0 | 209.0 | 0 | 32.47 | 35.07 | Vered | 2640 | |
| EG20 | 9103101242 | 1.4 | 186.9 | 243.3 | 0 | 32.79 | 35.40 | Golani | 5760 | |
| EG21 | 9103121107 | 2.0 | 191.9 | 257.5 | 0 | 32.91 | 35.46 | Kadarim | 2750 | |
| EG22 | 9103170920 | 1.3 | 169.8 | 250.3 | 0 | 32.85 | 35.22 | Tamra | 5000 | 17&25 |
| EG23 | 9103211208 | 1.9 | 186.2 | 242.7 | 0 | 32.78 | 35.39 | Golani | 1800 | |
| EG24 | 9103191014 | <1.0 | 192.0 | 256.0 | 0 | 32.90 | 35.46 | Kadarim | 2584 | |
| EG25 | 9103191402 | 2.3 | 151.9 | 239.4 | 0 | 32.75 | 35.02 | Carmel | 14000 | |
| EG26 | 9104140831 | 1.5 | 169.5 | 253.3 | 0 | 32.88 | 35.21 | Tamra | 5520 | |
| EG27 | 9104221043 | 1.7 | 191.0 | 257.7 | 0 | 32.92 | 35.45 | Kadarim | 4086 | |
| EG28 | 9104221231 | 1.8 | 199.1 | 240.1 | 0 | 32.76 | 35.53 | Poria | 3900 | |
| EG29 | 9104241621 | 1.3 | 173.5 | 243.2 | 0 | 32.78 | 35.26 | Hanaton | 3320 | |
| EG30 | 9104301404 | <1.0 | 169.0 | 244.0 | 0 | 32.79 | 35.21 | Shefaram | 5130 | |
| EG31 | 9105061241 | 1.6 | 192.1 | 258.0 | 0 | 32.92 | 35.46 | Kadarim | 3500 | |
| EG32 | 9105081305 | 2.6 | 153.4 | 238.1 | 0 | 32.74 | 35.04 | Carmel | 12000 | |
| EG33 | 9105090846 | 1.7 | 169.3 | 242.8 | 0 | 32.78 | 35.21 | Shefaram | 4880 | |
| EG34 | 9105121154 | 2.1 | 186.0 | 242.0 | 0 | 32.77 | 35.39 | Golani | 3300 | |
| EG35 | 9105231341 | 1.8 | 186.0 | 243.0 | 0 | 32.78 | 35.39 | Golani | 3838 | |
| EG36 | 9106171437 | <1.0 | 171.4 | 243.9 | 0 | 32.79 | 35.23 | Hanaton | 3900 | |
| EG37 | 9107281244 | 1.6 | 186.3 | 242.6 | 0 | 32.78 | 35.39 | Golani | 3000 | |
| EG38 | 9107291325 | 1.7 | 156.8 | 211.6 | 0 | 32.50 | 35.08 | Vered | 3600 | |
| EG39 | 9107291409 | 1.6 | 172.9 | 244.4 | 0 | 32.79 | 35.25 | Hanaton | 3280 | |
| | | | | | Earthquakes | | | | | |
| QG1 | 8710071515 | 1.9 | 173.9 | 230.8 | 12 | 32.67 | 35.26 | Galilee | | |
| QG2 | 8802241537 | 1.5 | 173.0 | 235.8 | 10 | 32.72 | 35.25 | Galilee | | |
| QG3 | 8803031315 | 1.1 | 173.7 | 238.7 | 12 | 32.74 | 35.26 | Galilee | | |
| QG4 | 8807292333 | 1.4 | 170.0 | 230.0 | 10 | 32.66 | 35.22 | Galilee | | |
| QG5 | 8808061449 | 2.1 | 162.9 | 235.3 | 12 | 32.71 | 35.14 | Galilee | | |
| QG6 | 8904140553 | 1.3 | 166.2 | 230.2 | 17 | 32.67 | 35.18 | Galilee | | |
| QG7 | 8908190917 | 1.7 | 176.0 | 244.0 | 21 | 32.79 | 35.28 | Galilee | | |
| QG8 | 9008112214 | 1.8 | 187.8 | 265.7 | 11 | 32.99 | 35.41 | Galilee | | |

10

| QG9 | 9008210622 | 1.8 | 163.9 | 229.9 | 16 | 32.66 | 35.15 | Galilee |
|-----|------------|-----|-------|-------|----|-------|-------|---------|
| QG10 | 9009041644 | 1.5 | 152.9 | 257.1 | 12 | 32.91 | 35.04 | Galilee |
| QG11 | 9009160941 | 1.6 | 147.9 | 263.0 | 12 | 32.96 | 34.98 | O.C. Haifa |
| QG12 | 9011170730 | 1.2 | 174.7 | 244.1 | 17 | 32.79 | 35.27 | Galilee |
| QG13 | 9012200002 | 1.5 | 173.2 | 217.3 | 3 | 32.55 | 35.25 | Galilee |
| QG14 | 9012211524 | 1.5 | 202.6 | 250.9 | 23 | 32.85 | 35.57 | Kineret |
| QG15 | 9101090230 | 1.1 | 174.9 | 242.9 | 20 | 32.78 | 35.27 | Galilee |
| QG16 | 9101261746 | 1.2 | 172.8 | 245.9 | 6 | 32.81 | 35.25 | Galilee |
| QG17 | 9101261903 | 1.2 | 172.2 | 246.1 | 7 | 32.81 | 35.24 | Galilee |
| QG18 | 9101270305 | 1.6 | 175.4 | 247.4 | 8 | 32.82 | 35.28 | Galilee |
| QG19 | 9102120832 | 1.4 | 193.0 | 251.3 | 8 | 32.86 | 35.47 | Galilee |
| QG20 | 9102250633 | 2.0 | 178.2 | 220.7 | 21 | 32.58 | 35.31 | Galilee |
| QG21 | 9104051808 | 1.4 | 153.2 | 276.6 | 17 | 33.08 | 35.04 | Tyre |
| QG22 | 9104071718 | 1.3 | 204.4 | 248.8 | 12 | 32.84 | 35.59 | Kineret |
| QG23 | 9104150121 | 2.4 | 204.7 | 250.3 | 14 | 32.85 | 35.59 | Kineret |
| QG24 | 9104150503 | 1.5 | 202.9 | 248.1 | 4 | 32.83 | 35.57 | Kineret |
| QG25 | 9104160638 | 1.9 | 204.1 | 249.9 | 6 | 32.84 | 35.59 | Kineret |
| QG26 | 9104270713 | 1.2 | 207.0 | 249.4 | 14 | 32.84 | 35.62 | Kineret |
| QG27 | 9105011436 | 1.2 | 203.9 | 249.4 | 0 | 32.84 | 35.59 | Kineret |
| QG28 | 9105012047 | 2.2 | 203.2 | 248.9 | 6 | 32.84 | 35.58 | Kineret |
| QG29 | 9105032207 | 1.0 | 203.7 | 248.3 | 6 | 32.83 | 35.58 | Kineret |
| QG30 | 9105160250 | 1.7 | 147.8 | 276.2 | 10 | 33.08 | 34.98 | O.C. Tyre |

Table 2. Information about open-pit quarries presented in the study.

| Name | short | x(km) | y(km) | Lat. | Long. | Product |
|------|-------|-------|-------|------|-------|---------|
| Golani | goln | 186.5 | 243.0 | 32.782 | 35.397 | aggregate, blocks, beton |
| Poria | pori | 201.0 | 241.0 | 32.764 | 35.553 | basalt, aggregate, beton |
| Revaya | rvya | 194.5 | 205.0 | 32.439 | 35.480 | |
| Shefaram | shfr | 169.2 | 244.7 | 32.797 | 35.211 | aggregate, asphalt, beton |
| Carmel | nshr | 153.4 | 240.5 | 32.758 | 35.040 | dolomites (constr., roads) |
| Tamra | tmra | 170.0 | 251.5 | 32.858 | 35.220 | carbonate, chalk, cement |
| Vered | verd | 156.2 | 209.5 | 32.479 | 35.069 | dolomites |
| Hanaton | hntn | 172.0 | 242.0 | 32.773 | 35.241 | dolomites (constr., roads) |
| PhosphArad | arad | 170.0 | 60.0 | 31.131 | 35.210 | phosphates |
| PhosphZin | pzin | 158.0 | 29.0 | 30.851 | 35.082 | phosphates |
| Dragot | drgt | 157.5 | 79.8 | 31.309 | 35.078 | phosphates |
| Aroar | aror | 150.5 | 59.5 | 31.125 | 35.003 | phosphates |
| Oceana | ocea | 186.5 | 68.5 | 31.208 | 35.385 | salt aggregates |
| Kadarim | kdar | 192.7 | 257.5 | 32.913 | 35.465 | |
| Gilad | | 230.0 | 207.0 | 32.457 | 35.862 | |
| Jordan | | 205.0 | 103.0 | 31.519 | 35.584 | |
| Mt.Nitzim | ntzm | 155.0 | 66.0 | 31.184 | 35.051 | calcium carbonates |

## 2.3 SOUTHERN GROUND-TRUTH DATASET OF EARTHQUAKES AND QUARRY BLASTS

The dataset includes 26 quarry blasts with ground-truth information and 16 earthquakes ($M_L$=1.5-2.8), occurring in the southern Dead Sea basin and Negev desert (see map in Fig. 3). The source parameters are presented in Table 3. The quarries in this region produce phosphates and various chemicals from Dead Sea deposits (see Table 2). Blasting of salt monoliths on the bottom (Oceana) requires only a few dozen kilograms of explosive, however, due to effective coupling of seismic energy in heavy salt water, these explosions radiate strong signals. For most of the blasts we obtained information from the quarries regarding the total amount of explosives. For the two events on the Jordanian side of the Dead Sea, we observed clear sonic waves striking the seismometers (see example in Fig. 4) from the seismograms. The locations of some of the blasts were corrected and magnitudes were determined.

## 2.4 TYRE DATASET OF UNDERWATER EXPLOSIONS AND OFF-COAST EARTHQUAKES IN THE MEDITERRANEAN

The dataset includes 16 UWE and 8 earthquakes ($M_L$=1.0-2.5), occurring off-coast Mediterranean in the Tyre region (see map in Fig. 5 and source parameters in Table 4). Unfortunately, since most of the man-made events are unauthorized fishing explosions and the reminder are naval activities, we were unable to obtain any additional information. The UWE usually occur in the morning hours, sometimes at intervals of several minutes (e.g. events EU5, EU6, EU7 in Table 4). Most of these events were used by Gitterman and Shapira (1994). The sea depth in the area of selected epicenters varies from 50 to 300m (Almagor and Hall, 1984). Charge weights for UWE possibly do not exceed a few dozen kilograms of explosives.

## 2.5 DEAD SEA GROUND-TRUTH DATASET OF EXPERIMENTAL UNDERWATER SINGLE EXPLOSIONS

A series of 78 single-shot underwater explosions was detonated in 1993 in the Dead Sea by the Tel-Aviv and Hamburg (Germany) Universities for seismic profiling in order to study the detailed structure of the crust in the Dead Sea transform fault zone. Seventy five of these UWE were recorded by the ISN. We selected 28 explosions of different sizes distributed uniformly on a line along the Dead Sea, as shown on Fig.3, for the analysis. Ground-truth information, including accurate coordinates, charge weight,
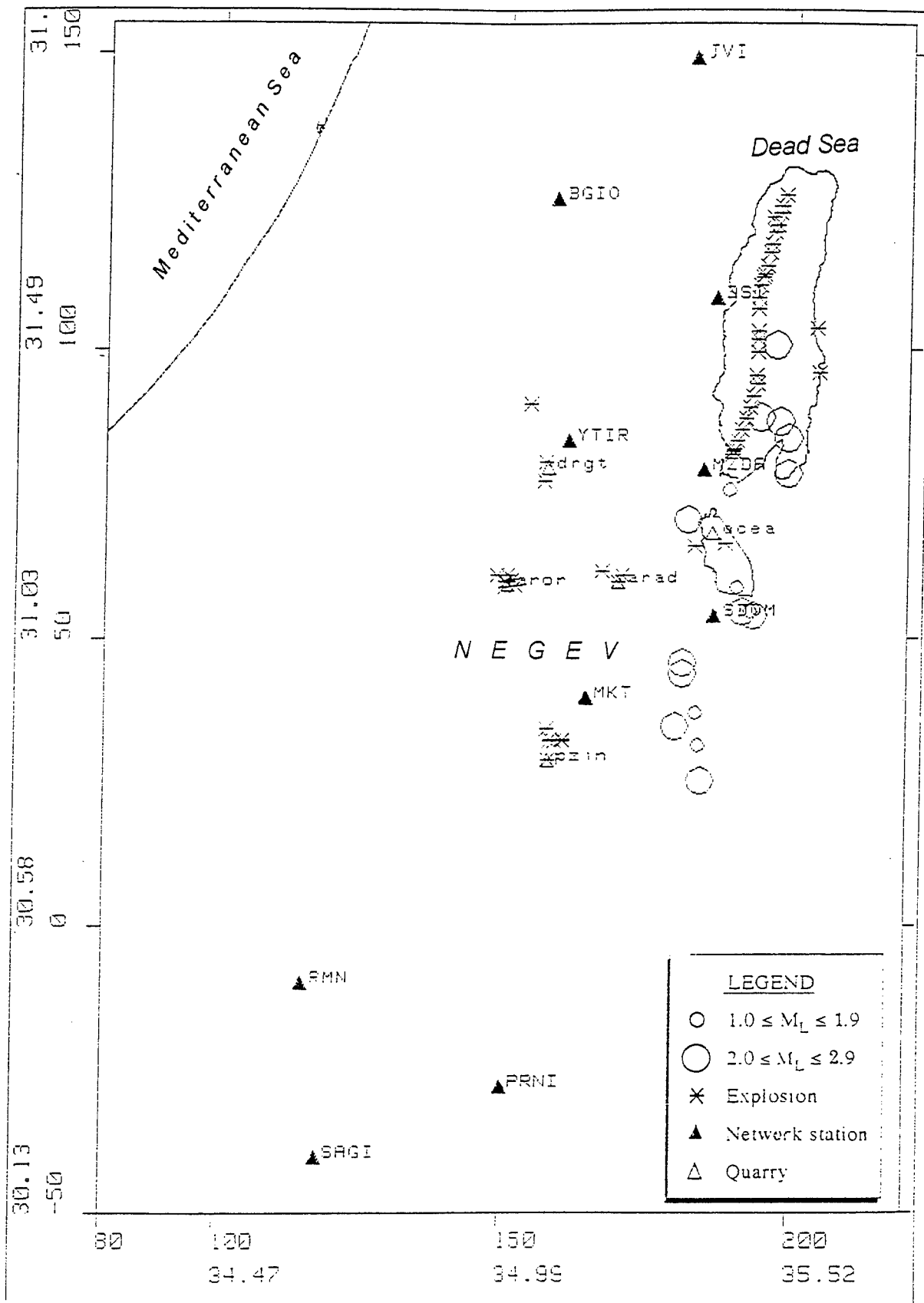
**Figure 3.** Epicenters of earthquakes, underwater explosions, quarry blasts, quarries and ISN stations in the Dead Sea and Negev region. Experimental single UWE for seismic profiling form a line along the Dead Sea.

Table 3. Seismic events in the Southern Dead Sea and Negev region.

| Event | Origin time (yr/mo/dy/hr/mn) | ML | X (km) | Y (km) | Depth (km) | Lat. (N) | Lon. (E) | Quarry/ Local area | Size (tons) |
|-------|------------------------------|-----|--------|--------|------------|----------|----------|-------------------|-------------|
| | | | | | | | | | |

Quarry blasts (including UWE), road construction

| Event | Origin time | ML | X (km) | Y (km) | Depth (km) | Lat. (N) | Lon. (E) | Quarry/ Local area | Size (tons) |
|-------|-------------|-----|--------|--------|------------|----------|----------|-------------------|-------------|
| ES1 | 8909240543 | 2.2 | 203.6 | 103.5 | 0 | 31.52 | 35.57 | Jordan | |
| ES2 | 9003261352 | 2.0 | 204.0 | 96.0 | 0 | 31.46 | 35.57 | Jordan | |
| ES3 | 9101011206 | 2.0 | 150.5 | 61.0 | 0 | 31.14 | 35.00 | Aroar | 10.5 |
| ES4 | 9101020937 | 2.2 | 170.0 | 60.0 | 0 | 31.13 | 35.21 | Arad | |
| ES5 | 9102061248 | 2.1 | 150.2 | 60.0 | 0 | 31.13 | 35.00 | Aroar | 7.4 |
| ES6 | 9102140941 | 2.1 | 170.0 | 60.0 | 0 | 31.13 | 35.21 | Arad | 10.3 |
| ES7 | 9103111012 | 2.3 | 158.6 | 32.5 | 0 | 30.88 | 35.09 | Zin | 7.8 |
| ES8 | 9103121005 | 2.2 | 158.2 | 32.3 | 0 | 30.88 | 35.08 | Zin | 8.0 |
| ES9 | 9103121231 | 2.2 | 151.6 | 60.3 | 0 | 31.13 | 35.02 | Aroar | |
| ES10 | 9103160815 | 1.9 | 158.0 | 29.0 | 0 | 30.85 | 35.08 | Zin | 2.1 |
| ES11 | 9104030830 | 2.0 | 159.2 | 32.3 | 0 | 30.88 | 35.09 | Zin | 8.8 |
| ES12 | 9104141148 | 2.2 | 152.0 | 59.3 | 0 | 31.12 | 35.02 | Aroar | 9.1 |
| ES13 | 9104160935 | 2.2 | 160.6 | 32.3 | 0 | 30.88 | 35.11 | Zin | 6.96 |
| ES14 | 9104250809 | 2.3 | 160.6 | 32.5 | 0 | 30.88 | 35.11 | Zin | 1.7 |
| ES15 | 9104301239 | 2.1 | 154.2 | 90.6 | 0 | 31.41 | 35.04 | Dragot | 3.15 |
| ES16 | 9105201219 | 1.9 | 188.5 | 66.8 | 0 | 31.19 | 35.41 | Okeana | |
| ES17 | 9105300817 | 1.7 | 160.7 | 32.5 | 0 | 30.88 | 35.11 | Zin | 8.44 |
| ES18 | 9106040929 | 1.9 | 167.2 | 61.7 | 0 | 31.15 | 35.18 | Arad | 9.12 |
| ES19 | 9106161256 | 2.1 | 150.0 | 60.0 | 0 | 31.13 | 35.00 | Aroar | 9.9 |
| ES20 | 9106240847 | 2.5 | 157.9 | 34.5 | 0 | 30.90 | 35.08 | Zin | 3.6 |
| ES21 | 9106251257 | 1.9 | 157.2 | 80.7 | 0 | 31.32 | 35.07 | Dragot | 3.6 |
| ES22 | 9106270719 | 2.2 | 170.8 | 61.2 | 0 | 31.14 | 35.22 | Arad | 3.6 |
| ES23 | 9107170827 | 1.5 | 183.4 | 66.2 | 0 | 31.19 | 35.35 | Okeana | |
| ES24 | 9109 51413 | 1.9 | 156.8 | 77.6 | 0 | 31.29 | 35.07 | Dragot | |
| ES25 | 9109201053 | 1.9 | 148.7 | 61.0 | 0 | 31.14 | 34.98 | Aroar | 10.44 |
| ES26 | 9110071257 | 1.9 | 150.0 | 59.0 | 0 | 31.12 | 35.00 | Aroar | 10.5 |

Earthquakes

| Event | Origin time | ML | X (km) | Y (km) | Depth (km) | Lat. (N) | Lon. (E) | Quarry/ Local area | Size (tons) |
|-------|-------------|-----|--------|--------|------------|----------|----------|-------------------|-------------|
| QS1 | 8901120345 | 2.2 | 194.3 | 88.5 | 18 | 31.39 | 35.47 | Dead Sea | |
| QS2 | 8901120752 | 2.4 | 197.7 | 87.8 | 18 | 31.38 | 35.51 | Dead Sea | |
| QS3 | 8908110029 | 2.4 | 182.2 | 71.0 | 18 | 31.23 | 35.34 | Dead Sea | |
| QS4 | 9001130116 | 2.0 | 181.5 | 44.0 | 17 | 30.99 | 35.33 | Arava | |
| QS5 | 9001141228 | 2.7 | 180.4 | 34.9 | 18 | 30.90 | 35.32 | Arava | |
| QS6 | 9011161920 | 2.8 | 199.1 | 84.9 | 18 | 31.36 | 35.52 | Dead Sea | |
| QS7 | 9102230059 | 1.9 | 183.8 | 37.2 | 24 | 30.93 | 35.35 | Arava | |
| QS8 | 9106031202 | 1.6 | 189.1 | 76.2 | 21 | 31.28 | 35.41 | Dead Sea | |
| QS9 | 9106232222 | 2.6 | 199.1 | 79.0 | 0 | 31.30 | 35.52 | Dead Sea | |
| QS10 | 9109040811 | 2.1 | 181.4 | 45.9 | 2 | 31.00 | 35.33 | Arava | |
| QS11 | 9109272224 | 2.6 | 191.5 | 54.7 | 11 | 31.08 | 35.44 | Dead Sea | |
| QS12 | 9109301155 | 2.1 | 193.4 | 54.1 | 10 | 31.08 | 35.46 | Dead Sea | |
| QS13 | 9110030128 | 1.5 | 184.3 | 31.5 | 17 | 30.87 | 35.36 | Arava | |
| QS14 | 9110050744 | 1.9 | 190.5 | 58.9 | 18 | 31.12 | 35.43 | Dead Sea | |
| QS15 | 9111170201 | 2.6 | 184.8 | 25.5 | 21 | 30.82 | 35.36 | Arava | |
| QS16 | 9112240106 | 1.6 | 192.9 | 54.7 | 10 | 31.08 | 35.45 | Dead Sea | |

r = 34 km

r = 29 km

r = 17 km    sonic wave
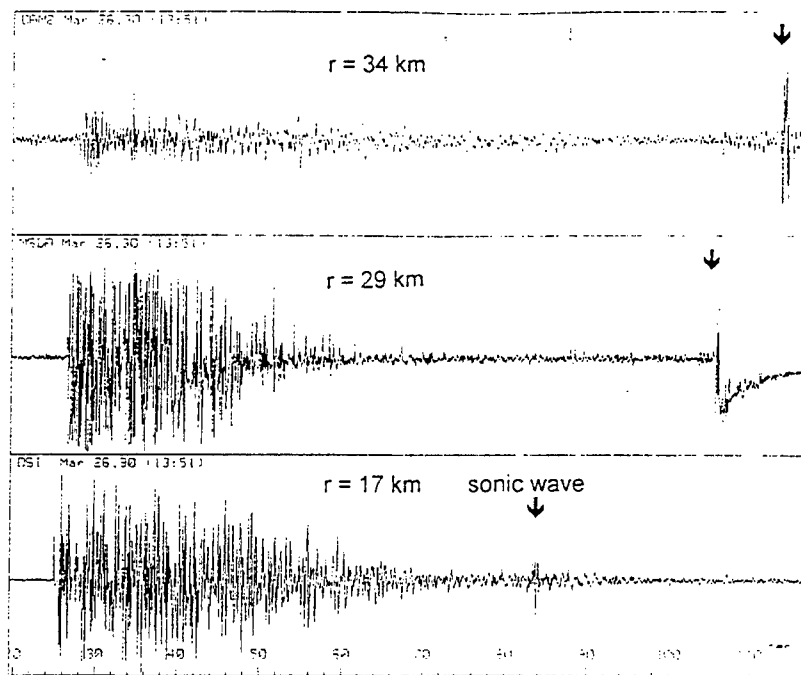
**Figure** 4. Seismogram of the event ES1 on the Jordanian side of the Dead Sea. Clear sonic waves are observed at closest stations.
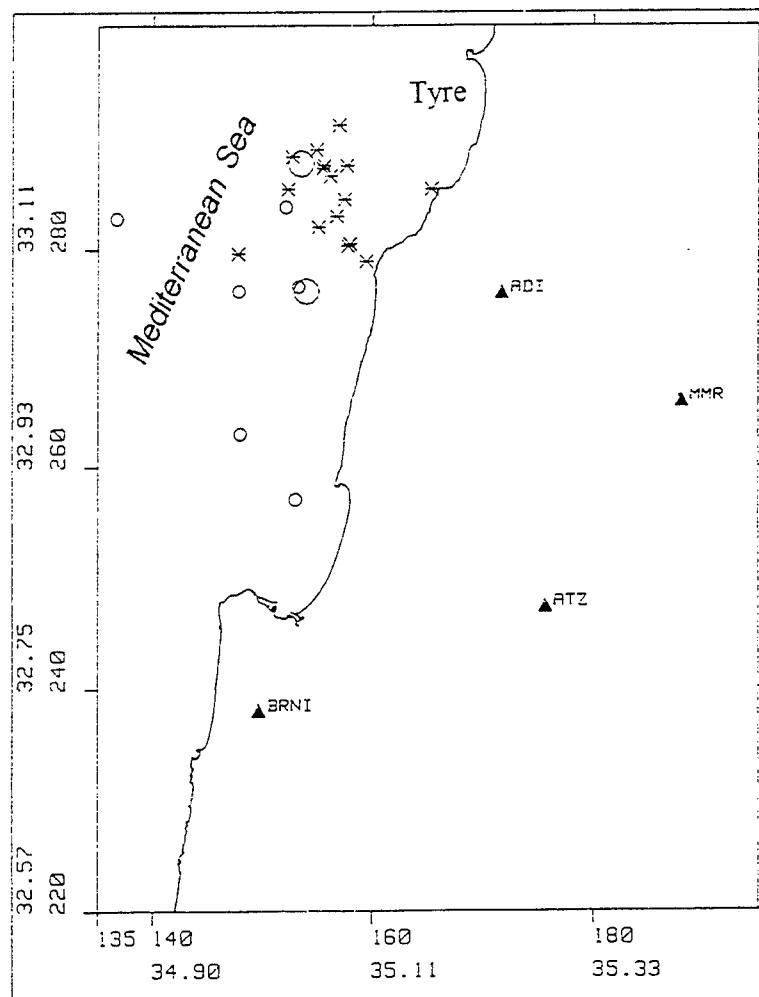


**Figure** 5. Epicenters of earthquakes and underwater explosions in the Tyre region of Mediterranean.

Table 4. Off-coast Mediterranean seismic events in the Tyre region.

| Event | Origin time (yr/mo/dy/hr/mn) | ML | X (km) | Y (km) | Depth (km) | Lat. (N) | Lon. (E) | Local area |
|---|---|---|---|---|---|---|---|---|
| | | | | | | | | |

Underwater explosions

| Event | Origin time (yr/mo/dy/hr/mn) | ML | X (km) | Y (km) | Depth (km) | Lat. (N) | Lon. (E) | Local area |
|---|---|---|---|---|---|---|---|---|
| EU1 | 9008250629 | 1.5 | 157.7 | 280.3 | 0 | 33.12 | 35.09 | Tyre |
| EU2 | 9012010713 | 1.8 | 156.9 | 291.1 | 0 | 33.22 | 35.08 | Tyre |
| EU3 | 9102101102 | 1.7 | 154.8 | 288.9 | 0 | 33.20 | 35.06 | Tyre |
| EU4 | 9102110659 | 1.5 | 155.5 | 287.5 | 0 | 33.18 | 35.06 | Tyre |
| EU5 | 9103190611 | 1.9 | 157.6 | 287.5 | 0 | 33.18 | 35.09 | Tyre |
| EU6 | 9103190629 | 1.8 | 152.2 | 285.4 | 0 | 33.16 | 35.03 | Tyre |
| EU7 | 9103190650 | 1.8 | 156.7 | 283.0 | 0 | 33.14 | 35.08 | Tyre |
| EU8 | 9104140657 | 1.7 | 157.4 | 284.5 | 0 | 33.16 | 35.09 | Tyre |
| EU9 | 9104180628 | 1.8 | 159.4 | 278.9 | 0 | 33.10 | 35.11 | Tyre |
| EU10 | 9105300524 | 1.5 | 156.1 | 286.6 | 0 | 33.18 | 35.07 | Tyre |
| EU11 | 9106090612 | 1.6 | 147.7 | 279.6 | 0 | 33.11 | 34.98 | O.C. Tyre |
| EU12 | 9107110632 | 1.7 | 152.6 | 288.3 | 0 | 33.19 | 35.03 | Tyre |
| EU13 | 9107110653 | 1.6 | 165.4 | 285.4 | 0 | 33.16 | 35.17 | Tyre |
| EU14 | 9109070546 | 1.6 | 157.9 | 280.5 | 0 | 33.12 | 35.09 | Tyre |
| EU15 | 9109070637 | 1.5 | 155.4 | 287.3 | 0 | 33.18 | 35.06 | Tyre |
| EU16 | 9109070723 | 1.5 | 155.0 | 282.0 | 0 | 33.13 | 35.06 | Tyre |

Earthquakes

| Event | Origin time (yr/mo/dy/hr/mn) | ML | X (km) | Y (km) | Depth (km) | Lat. (N) | Lon. (E) | Local area |
|---|---|---|---|---|---|---|---|---|
| QU1 | 8802231810 | 2.0 | 153.4 | 287.7 | 6 | 33.18 | 35.04 | Tyre |
| QU2 | 8907072033 | 1.0 | 152.0 | 283.8 | 12 | 33.15 | 35.03 | Tyre |
| QU3 | 9003131521 | 2.5 | 153.9 | 276.2 | 12 | 33.08 | 35.05 | Tyre |
| QU4* | 9009041644 | 1.5 | 152.9 | 257.1 | 12 | 32.91 | 35.04 | Galilee |
| QU5* | 9009160941 | 1.6 | 147.9 | 263.0 | 12 | 32.96 | 34.98 | O.C. Haifa |
| QU6* | 9104051808 | 1.4 | 153.2 | 276.6 | 17 | 33.08 | 35.04 | Tyre |
| QU7 | 9104241857 | 1.8 | 136.7 | 282.8 | 10 | 33.14 | 34.86 | O.C. Tyre |
| QU8* | 9105160250 | 1.7 | 147.8 | 276.2 | 10 | 33.08 | 34.98 | O.C. Tyre |

* - an event is included also in the Galilee dataset.

underwater shot depth and local time of explosions, was kindly provided by Prof. A. Ginzburg (Tel-Aviv University) and is presented in Table 5.

Local magnitudes were evaluated for a few explosions of different sizes only and rather overestimated values were obtained, especially for the largest shot (W = 304kg), owing to long wavetrains of reverberations in the water layer.

## 2.6 JORDANIAN GROUND-TRUTH DATASET OF QUARRY BLASTS

The ISN regularly records many quarry blasts and road construction explosions from neighboring countries. Our Jordanian colleagues at the Jordan Seismological Observatory (Natural Resources Authority) provided ground-truth information about quarry blasts conducted in southern Jordan near the border with Saudi Arabia. The information includes the date and time of blasts, accurate locations, type and amount of explosive (see Table A1 in Appendix A). We selected five blasts which occurred in 1995 and which are clearly identified in the ISN bulletin. For some other earlier events, owing to non-accurate blasting time data, we came across the problem of reliable identification: two events at intervals of a few minutes and in very close proximity were recorded for almost each date. Parameters of the selected blasts (with locations, determined by ISN) are presented in Table 6 and the epicenters are shown in Fig. 6.

## 2.7 SINGLE QUARRY BLASTS GROUND-TRUTH DATASET

Commercial blasts without delays (i.e. non-ripple fired) differ in their temporal and spectral features from conventional ripple-fired blasts. There are only very few quarries in Israel using such blasting techniques a few times a year. They are usually of low yield and not all of them are recorded by the ISN. After a long search we selected 10 events from two quarries located in different areas (see map in Fig. 6 and Table 6). It should be noted that these are not concentrated explosions, but rather a group of shot holes, distributed in space along a horizontal bench and fired almost simultaneously.

Table 5. Underwater explosions for seismic profiling in the Dead Sea
(shots 70 m under the sea level).

| Event | Origin time (yr/mo/dy/hr/mn) | ML | X (km) | Y (km) | Lat. (N) | Lon. (E) | Size (kg) |
|-------|------------------------------|------|--------|--------|----------|----------|-----------|
| EX1   | 9301280827                   | 3.1  | 189.7  | 82.7   | 31.33    | 35.42    | 304       |
| EX2   | 9301281043                   | .0   | 189.6  | 82.3   | 31.33    | 35.42    | 24        |
| EX3   | 9301281103                   | .0   | 189.7  | 82.8   | 31.34    | 35.42    | 24        |
| EX4   | 9301281203                   | .0   | 189.9  | 83.2   | 31.34    | 35.42    | 24        |
| EX5   | 9301281237                   | .0   | 190.4  | 84.6   | 31.35    | 35.43    | 24        |
| EX6   | 9301281354                   | 2.0  | 191.1  | 86.4   | 31.37    | 35.44    | 24        |
| EX7   | 9301281446                   | .0   | 191.7  | 88.3   | 31.39    | 35.44    | 24        |
| EX8   | 9301281541                   | .0   | 192.5  | 90.2   | 31.40    | 35.45    | 24        |
| EX9   | 9301281638                   | .0   | 193.0  | 92.1   | 31.42    | 35.46    | 24        |
| EX10  | 9301290456                   | .0   | 198.0  | 126.3  | 31.73    | 35.51    | 24        |
| EX11  | 9301290636                   | .0   | 197.4  | 124.3  | 31.71    | 35.50    | 24        |
| EX12  | 9301291006                   | 2.5  | 195.9  | 122.6  | 31.69    | 35.49    | 192       |
| EX13  | 9301291155                   | .0   | 197.1  | 123.3  | 31.70    | 35.50    | 24        |
| EX14  | 9301310829                   | .0   | 193.6  | 94.1   | 31.44    | 35.46    | 24        |
| EX15  | 9301310916                   | .0   | 193.5  | 95.6   | 31.45    | 35.46    | 24        |
| EX16  | 9301311138                   | .0   | 193.6  | 99.6   | 31.49    | 35.46    | 24        |
| EX17  | 9301311242                   | .0   | 193.6  | 101.6  | 31.50    | 35.46    | 24        |
| EX18  | 9301311321                   | .0   | 193.6  | 103.1  | 31.52    | 35.46    | 24        |
| EX19  | 9301311449                   | .0   | 193.6  | 106.8  | 31.55    | 35.46    | 24        |
| EX20  | 9301311528                   | .0   | 193.6  | 108.7  | 31.57    | 35.46    | 24        |
| EX21  | 9301311621                   | .0   | 193.9  | 110.7  | 31.59    | 35.47    | 16        |
| EX22  | 9301311729                   | .0   | 194.4  | 112.2  | 31.60    | 35.47    | 16        |
| EX23  | 9301311741                   | .0   | 194.5  | 112.7  | 31.62    | 35.47    | 16        |
| EX24  | 9301311921                   | .0   | 195.0  | 114.1  | 31.62    | 35.48    | 24        |
| EX25  | 9301312030                   | .0   | 195.5  | 116.3  | 31.64    | 35.48    | 24        |
| EX26  | 9301312118                   | .0   | 195.7  | 117.8  | 31.65    | 35.49    | 24        |
| EX27  | 9301312246                   | .0   | 196.6  | 121.0  | 31.68    | 35.49    | 24        |
| EX28  | 9301312301                   | .0   | 196.3  | 120.0  | 31.67    | 35.49    | 16        |

Figure 7. Seismic events in the Gilad region (Jordan).
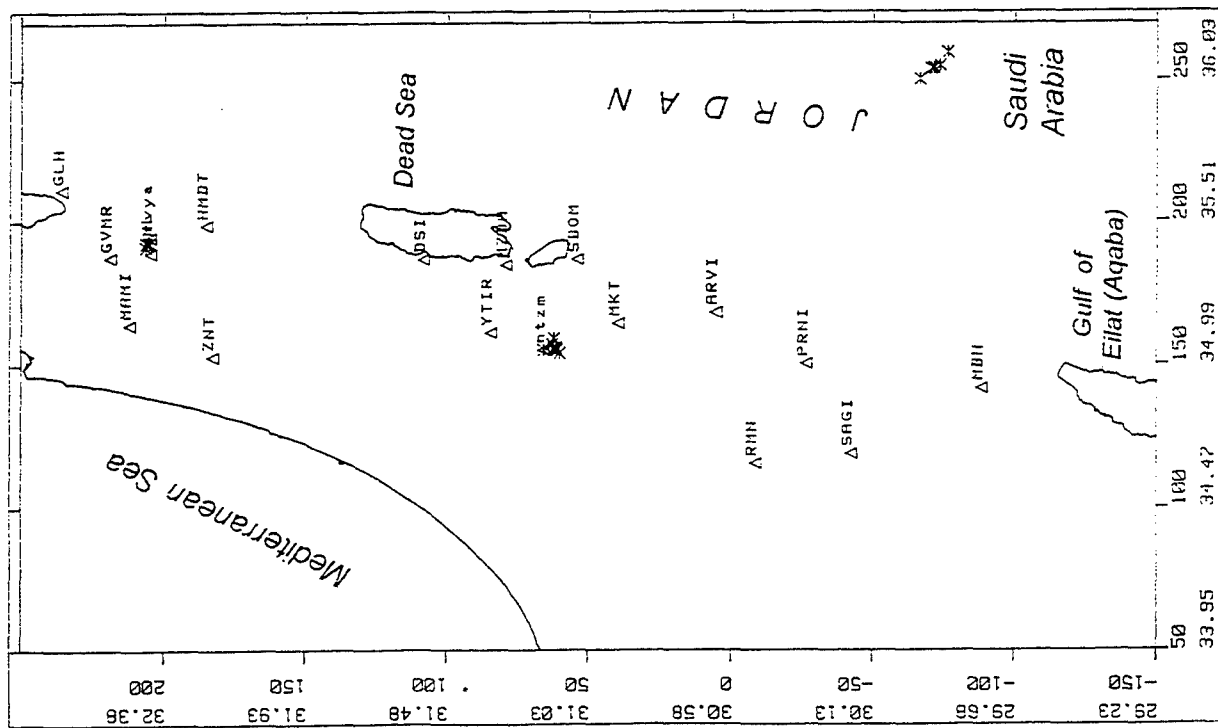
Figure 6. Epicentres of Jordanian quarry blasts and single quarry blasts
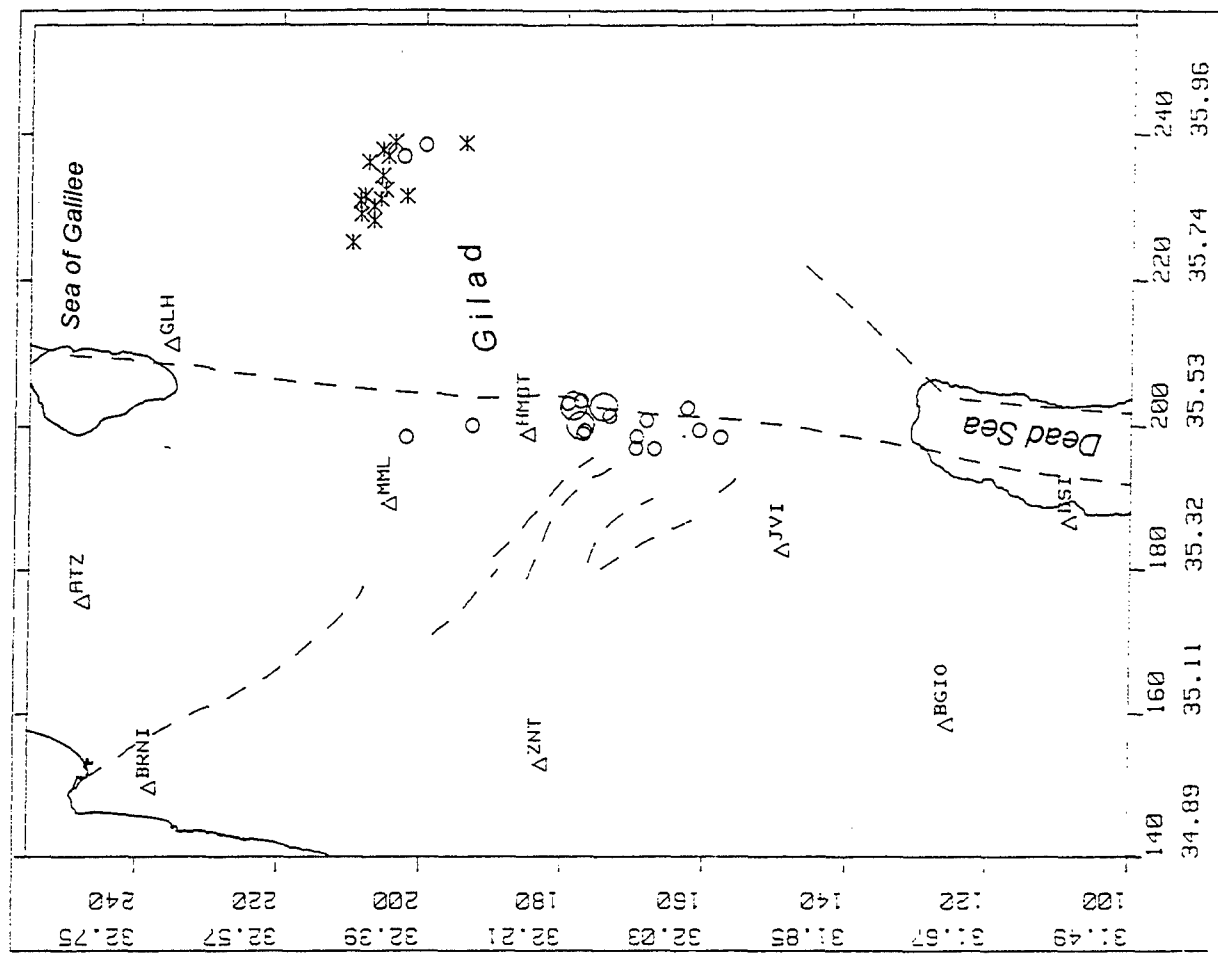
Table 6. Jordanian ripple-fired quarry blasts and single quarry blasts

| Ev. | Origin time (yr/mo/dy/hr/mn) | ML | X (km) | Y (km) | Depth (km) | Lat. (N) | Lon. (E) | Quarry/ Local area | Size (kg) |
|-----|------------------------------|-----|--------|--------|-----------|----------|----------|---------------------|-----------|
| | | | | Jordanian quarry blasts | | | | | |
| EJ1 | 9504021020 | 2.3 | 254.8 | −73.6 | 0 | 29.93 | 36.09 | Jordan/S.Ar. | 16500 |
| EJ2 | 9504040931 | 2.3 | 250.1 | −66.5 | 0 | 29.99 | 36.04 | Jordan/S.Ar. | 14750 |
| EJ3 | 9504240746 | 2.1 | 259.5 | −76.4 | 0 | 29.90 | 36.14 | Jordan/S.Ar. | 15900 |
| EJ4 | 9504250911 | 2.0 | 253.7 | −70.4 | 0 | 29.95 | 36.08 | Jordan/S.Ar. | 14800 |
| EJ5 | 9504300849 | 2.3 | 253.9 | −71.4 | 0 | 29.94 | 36.08 | Jordan/S.Ar. | 17000 |
| | | | | Single quarry blasts | | | | | |
| SB1 | 9505280842 | 1.8 | 192.5 | 205.6 | 0 | 32.44 | 35.46 | Revaya | 2180 |
| SB2 | 9506020917 | 2.3 | 191.0 | 206.8 | 0 | 32.46 | 35.44 | Revaya | 2840 |
| SB3 | 9506150709 | 1.7 | 192.4 | 206.6 | 0 | 32.45 | 35.46 | Revaya | 1946 |
| SB4 | 9505021026 | 2.0 | 155.6 | 62.3 | 0 | 31.15 | 35.06 | Har Nitzim | 2400 |
| SB5 | 9506011046 | 1.9 | 159.1 | 62.3 | 0 | 31.15 | 35.09 | Har Nitzim | 2200 |
| SB6 | 9601090952 | 1.4 | 155.8 | 61.3 | 0 | 31.14 | 35.06 | Har Nitzim | 1220 |
| SB7 | 9601161243 | 1.3 | 155.0 | 66.0 | 0 | 31.18 | 35.05 | Har Nitzim | 880 |
| SB8 | 9602041044 | 1.6 | 153.9 | 60.2 | 0 | 31.13 | 35.04 | Har Nitzim | 2400 |
| SB9 | 9603030908 | 1.7 | 154.9 | 61.3 | 0 | 31.14 | 35.05 | Har Nitzim | 2300 |
| SB10 | 9603241018 | 1.5 | 157.0 | 62.9 | 0 | 31.16 | 35.07 | Har Nitzim | 1900 |

Table 7. Seismic events in the Gilad region (Jordan),
and results of the velogram analysis.
(V = a + b*ln(R) fit. C = b + 0.33*a;
Preliminary filtering 1 - 10 Hz, Butterworth filter 21 coef.).

| Event | Origin time (yr/mo/dy/hr/mn) | ML | X (km) | Y (km) | H (km) | c (km/s) | c* (km/s) |
|---|---|---|---|---|---|---|---|
| | | | | | | | |

EXPLOSIONS

| Event | Origin time | ML | X (km) | Y (km) | H (km) | c (km/s) | c* (km/s) |
|---|---|---|---|---|---|---|---|
| ED1 | 9009201347 | 1.7 | 232.3 | 205.4 | 0 | 0.63 | |
| ED2 | 9103021348 | 1.9 | 238.7 | 194.2 | 0 | 0.54 | |
| ED3 | 9103211303 | 2.1 | 234.2 | 205.9 | 0 | 0.64 | |
| ED4 | 9106301052 | 0.0 | 225.0 | 210.0 | 0 | 0.91 | 0.62 |
| ED5 | 9112171531 | 0.0 | 231.0 | 206.0 | 0 | 0.59 | |
| ED6 | 9204061519 | 2.3 | 231.5 | 208.3 | 0 | 0.57 | |
| ED7 | 9204271430 | 0.0 | 236.1 | 207.8 | 0 | 0.60 | |
| ED8 | 9205051326 | 0.0 | 236.9 | 205.1 | 0 | 0.69 | 0.68 |
| ED9 | 9205271012 | 0.0 | 228.9 | 208.8 | 0 | 0.55 | |
| ED10 | 9205280910 | 0.0 | 238.9 | 204.1 | 0 | 0.56 | |
| ED11 | 9207080539 | 0.0 | 230.0 | 207.0 | 0 | 0.55 | |
| ED12 | 9207261256 | 0.0 | 228.0 | 207.0 | 0 | 0.38 | |
| ED13 | 9208101309 | 0.0 | 230.7 | 208.9 | 0 | 0.70 | 0.67 |
| ED14 | 9210201426 | 0.0 | 237.8 | 205.8 | 0 | 0.50 | |
| ED15 | 9301250926 | 0.0 | 231.4 | 202.4 | 0 | 0.59 | |

EARTHQUAKES

| Event | Origin time | ML | X (km) | Y (km) | H (km) | c (km/s) | c* (km/s) |
|---|---|---|---|---|---|---|---|
| QD1 | 9002110011 | 2.1 | 202.7 | 178.6 | 9 | 0.84 | |
| QD2 | 9002121343 | 1.9 | 198.4 | 202.2 | 12 | 1.10 | |
| QD3 | 9002122121 | 0.0 | 196.8 | 169.8 | 0 | 0.81 | |
| QD4 | 9002160530 | 1.6 | 203.4 | 177.6 | 12 | 0.76 | |
| QD5 | 9003212150 | 2.0 | 202.6 | 174.4 | 2 | 0.73 | |
| QD6 | 9006040047 | 0.2 | 200.0 | 192.9 | 7 | 0.85 | |
| QD7 | 9103131159 | 1.6 | 236.9 | 202.9 | 16 | 0.81 | |
| QD8 | 9104271058 | 1.1 | 196.7 | 167.2 | 0 | 0.70 | |
| QD9 | 9105072131 | 1.1 | 201.3 | 173.5 | 6 | 0.83 | |
| QD10 | 9105100127 | 1.3 | 200.7 | 168.3 | 12 | 0.82 | |
| QD11 | 9110162256 | 2.2 | 200.0 | 177.6 | 6 | 0.85 | |
| QD12 | 9109020226 | 1.4 | 198.3 | 158.0 | 16 | 0.72 | |
| QD13 | 9204051202 | 1.9 | 202.4 | 162.6 | 9 | 0.84 | |
| QD14 | 9208061619 | 1.3 | 199.3 | 160.9 | 0 | 0.69 | |
| QD15 | 9208080048 | 1.8 | 198.4 | 169.7 | 2 | 0.82 | |
| QD16 | 9210262004 | 1.4 | 238.5 | 199.9 | 12 | 0.97 | |
| QD17 | 9211010341 | 1.8 | 199.2 | 177.0 | 6 | 0.77 | |
| QD18 | 9211140957 | 1.4 | 198.8 | 177.2 | 5 | 0.77 | |
| QD19 | 9212051607 | 1.3 | 203.1 | 179.4 | 19 | 0.75 | |

## 2.8 GILAD DATASET OF QUARRY BLASTS AND EARTHQUAKES

The dataset includes 15 explosions and possible explosions and 19 earthquakes (classification according to the ISN bulletin) occurring in the Gilad region (see map in Fig. 7). All explosions are located in Jordan. Although we could not obtain ground-truth information for the blasts (conducted 3-4 years ago), this dataset was included in the analysis to provide a greater variety of geological environment. Locations of most of the blasts, presented in Table 7, are concentrated in a small area, possibly associated with the Gilad quarry (see Table 2, correct name and accurate coordinates of the quarry are unknown). The epicenter scatter can be explained by unfavorable mutual position of ISN stations and the quarry. Most of earthquakes are located along the Dead Sea transform between the Dead Sea and the Sea of Galilee, except for two which are located in the explosion cluster (Fig. 7), but were identified as earthquakes by an analyst in routine processing.

# 3. DISCRIMINATION METHODS USED IN STUDY AND TESTING ON THE GALILEE DATASET

## 3.1 SPECTRAL DISCRIMINANTS

### 3.1.1 Procedures and Parameters of Spectral Processing

We computed the Fourier spectra (FFT) of ground motions recorded by an ISN subnet, including 10 stations in the distance range 10-100 km (Fig. 2). For many events, due to noise, spikes and malfunctioning of a station, only some of these 10 stations provided seismograms suitable for the analysis. Computations are made for a time window of 20-30 sec. The analyzed window for an event is the same for all stations and includes the whole signal. Using this window we were able to avoid picking out separate wave phases (which is actually hardly practicable at these distances) and accumulate information about source (and possibly propagation) features being kept in all wave forms, thus enhancing resolving power of the considered discriminants. The spectra were instrument corrected and smoothed with a triangular operator (Hanning window) in a fixed 0.5 Hz moving window to provide equivalent spectral resolution for different stations. The log-log plotting mode of a single event spectra for a subnet of azimuthally distributed stations was used, facilitating clear identification of the coherent LFSM extrema for quarry blasts in the higher part of the frequency range.

### 3.1.2 Energy Spectral Ratio

It is commonly observed in Israel that seismograms of explosions are richer in low frequency energy as compared to earthquakes. The phenomenon is caused by the dominant surface waves generated by quarry blasts and associated with the regional crustal structure of widespread unconsolidated subsurface sediments. We utilized this effect in the spectral ratio, RE, of seismic energy in the low frequency range $(f_1, f_2)$ and the high-frequency range $(f_2, f_3)$ (Gitterman and Shapira, 1993):

$$R_E = \int_{f_1}^{f_2} |S(f)|^2 df \Big/ \int_{f_2}^{f_3} |S(f)|^2 df \tag{1}$$

where $|S(f)|$ is the smoothed FFT of ground velocity for the whole seismogram and the recording frequency range was divided for the analysis as $f_1 = 1$ Hz, $f_2 = 6$ Hz, $f_3 = 11$ Hz.

This energy spectral ratio, implying evident physical meaning, is similar to the ratios of average spectral amplitude (Bennett and Murphy, 1986) or power spectrum (Pulli, 1986). The ratios determined for a subnetwork of 10 ISN stations are presented in Fig. 8. A little overlap between quarry blasts and earthquakes is observed for specific stations (ADI, ATZ, MML, HRSH) (Fig. 8a). If the ratios for different events are averaged over several stations of the subnetwork covering a relatively broad azimuth and distance range (Fig. 8b), the resolving power is significantly enhanced and the two populations of seismic events are fully separated. Average ratio values are presented in Table 10. Several earthquakes (QG23-QG28) from a small area in Lake Kinneret (the Sea of Galilee), located exactly on the Dead Sea fault (Figs. 1 and 2), show anomalous high ratios (see Fig. 13b). In general, we can suggest that seismograms yielding an average ratio $R_E > 6.4$ are associated with quarry blasts. According this criterion, earthquakes QG23, QG25, QG28 and blasts EG3, EG8 are marginal events.
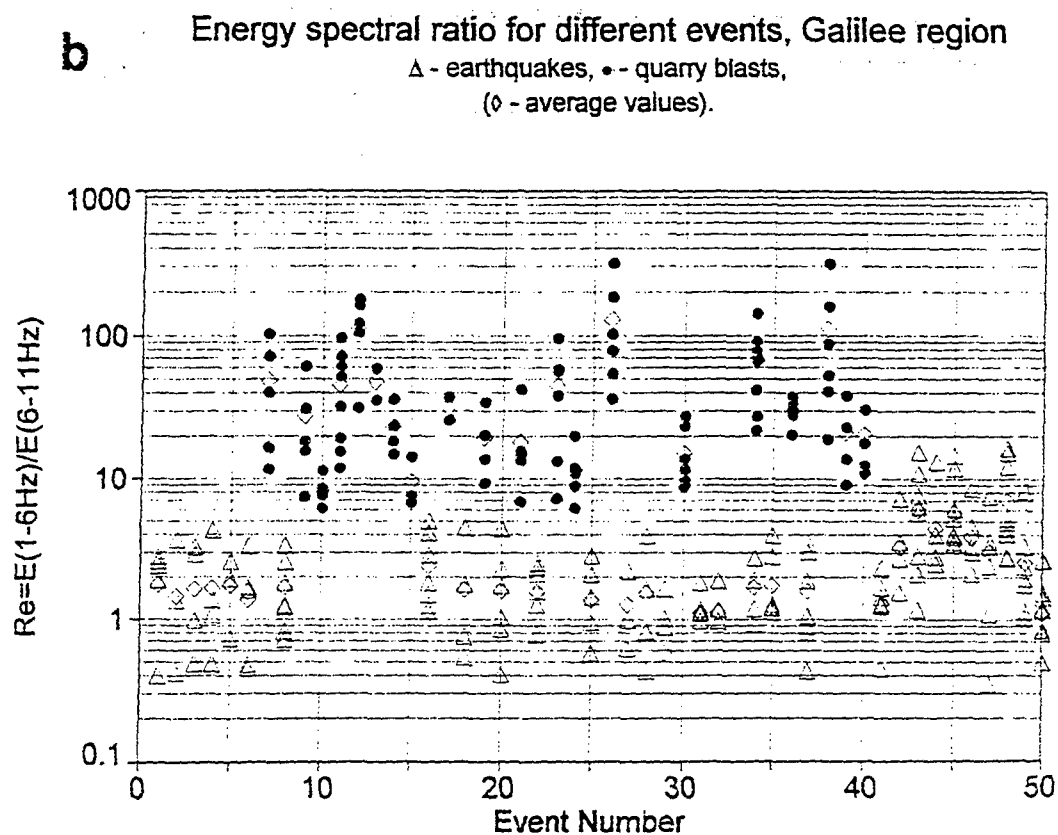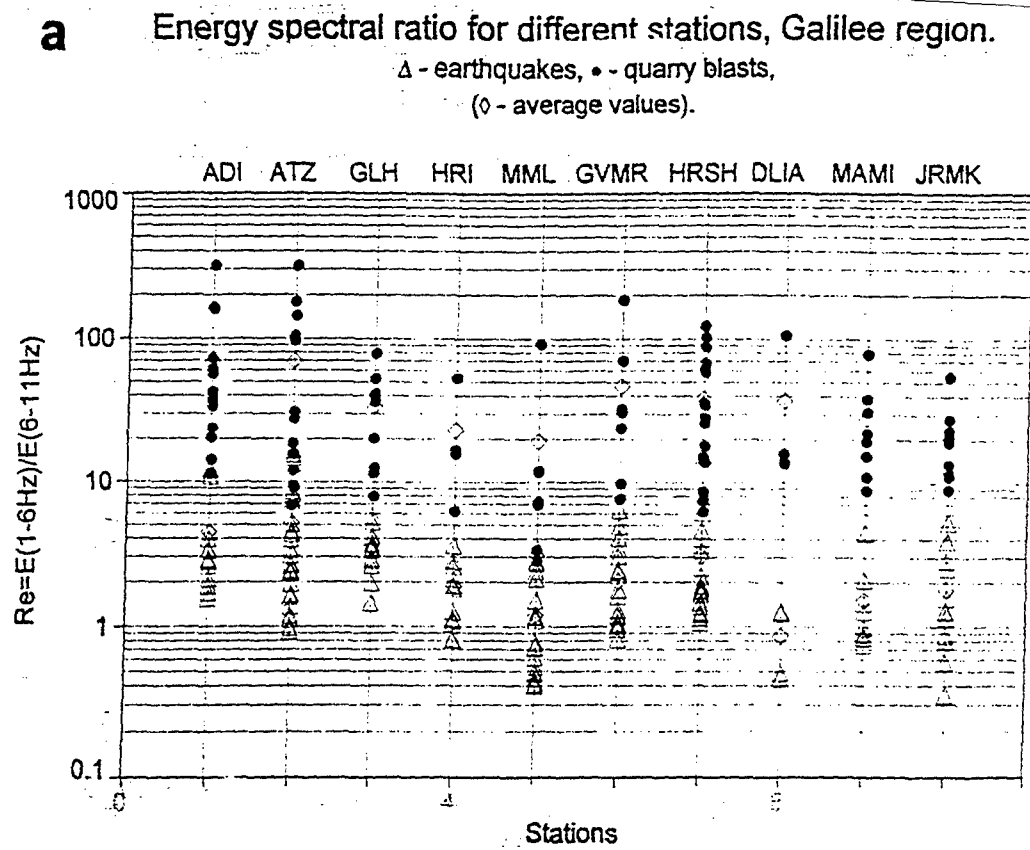
**a** Energy spectral ratio for different stations, Galilee region.
Δ - earthquakes, • - quarry blasts,
(◊ - average values).

ADI  ATZ  GLH  HRI  MML  GVMR  HRSH  DLIA  MAMI  JRMK

Re=E(1-6Hz)/E(6-11Hz)

Stations

**b** Energy spectral ratio for different events, Galilee region
Δ - earthquakes, • - quarry blasts,
(◊ - average values).

Re=E(1-6Hz)/E(6-11Hz)

Event Number

Figure 8. Energy spectral ratios for individual stations of the ISN subnetwork (a), and for different events (b). Diamonds show average values for each of two event populations.

24

### 3.1.3 Multidimensional Automatic Discrimination Procedures

During the period of this report we began investigating the Integrative Approach by application of Linear Discrimination function (Fisher) (LDF), Artificial Neural Network (ANN) and the King's cluster analysis procedure (CAP) to the data from the Galilee dataset. LDF is commonly used in the seismology statistical discrimination procedure based on the assumption that the X vectors of observational parameters generated by two stochastic (physical) mechanisms H1 and H2 (earthquakes and explosions), are described by a Gaussian distribution with equal covariance matrices, S, and different means, $M_i$. The optimal decision rule, based on log-likelihood ratio function $V(X)$, is as follows (Tsvang et al., 1993):

$$\{\text{assign X to } H_1, \text{ if } V(X) > 0 \text{ and assign X to } H_2, \text{ if } V(X) < 0\}$$

where $V(X) = F_1(X) - F_2(X) = 2(M_2 - M_1)^T S^{-1} X - M_1^T S^{-1} M_1 + M_2^T S^{-1} M_2$.

In practice, S and $M_i$ are unknown and estimated from the training set during the learning stage. The assumption that S1=S2 is rarely realized. However, the algorithm usually works well even if covariances S are different.

We used the ANN program, which was kindly provided and described by Dr. F. Dowla (LLNL) at our request. A multilayered feed-forward architecture of the network (Dowla et al., 1990, Dowla, 1995) is shown in Fig. 9. This network is a classic example of a supervised learning network applying a backpropagation learning algorithm to associate inputs with corresponding outputs for all or most of the events in a training set. This algorithm uses a gradient descent method to systematically modify the weights in the network so as to minimize the network output error.

The CAP is a modified, nearest neighbor, step-wise clustering procedure in which clusters with the closest centers of gravity are united at each step (King, 1967). Initially the number of clusters is equal to the number of data points. From step to step the number of clusters is reduced with one cluster comprising all the data points in the last step, number N. The algorithm separates the data points into several classes without any preliminary knowledge of their structure and is most useful for preliminary analysis of data.
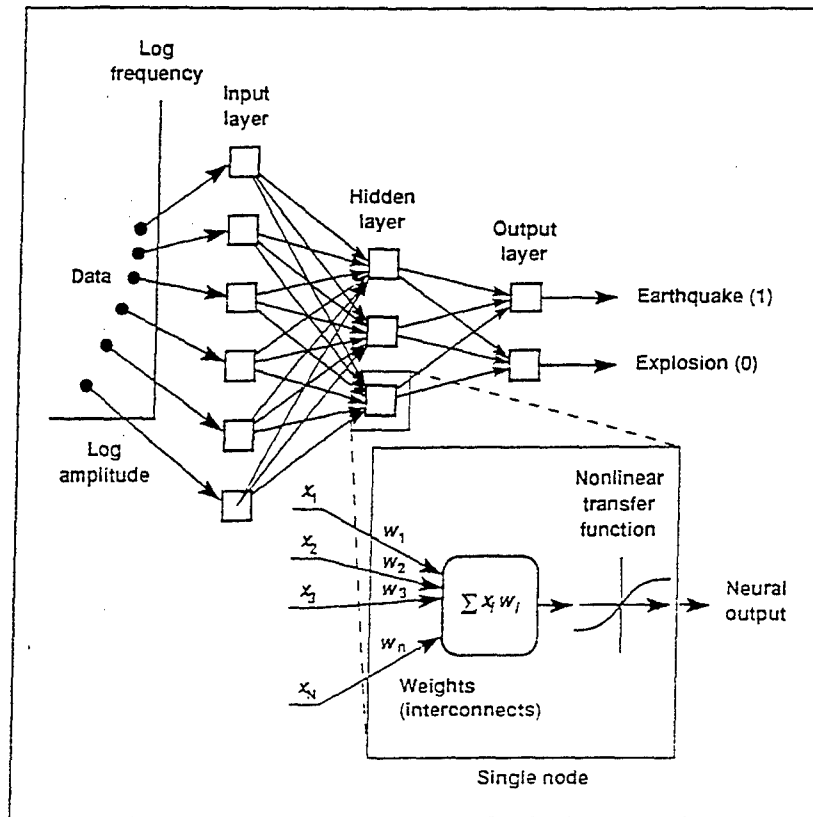
Figure 9. Architecture of the backpropagation neural network.

Classifier performance is often specified by the rate of mistakes: earthquakes, incorrectly specified as explosions plus explosions incorrectly specified as earthquakes. If a classifier is applied to the same data base which was used for training, the results are too optimistic and do not characterize its performance accurately. For the small database of 69 Galilee events, the leave-one-out method (Fukunaga and Hummels, 1989) can be applied. The method evaluates classifier performance by removing a single event from the database, learning on the remaining events and testing on that single event. The procedure is repeated for all the data points and the rate of mistakes is encountered which, in general assumptions, converge to the probability of mistake.

The training dataset was formed as follows: We selected smoothed spectra of event records as described above, divided the whole frequency band (1-11 Hz) into several equal intervals and computed the rms of spectral amplitude in each of them. The rms values were normalized to the maximum to eliminate dependence on event magnitude and distance and averaged over the 10 mentioned stations, forming the vector X. The one-leave-out procedure was then applied to test LDF and ANN performance on the Galilee dataset. The number and rate of mistakes is presented in Table 8. For the CAP we simply counted the number of wrong points assigned to the "earthquake" or "explosion" clusters.

The results of the test present an example of the optimal selection of the feature vector X and classification algorithms, providing a minimum mistake rate. According Table 8 both LDF and ANN show their best performance when the frequency interval (1-9 Hz) is divided into four bands, although ANN shows error-free performance in four and five bands cases, while LDF has one mistake at best. The CAP procedure lags behind (for the selected dataset).

In Fig. 10 the results of the leave-one-out test for the ANN and LDF are presented in the case of five spectral bands. Fig. 10b shows that there are only two explosions, wrongly assigned to earthquakes according positive values of LDF (see Eq. 2), but there are about 13 more marginal events. Fig. 10a shows error-free performance of the ANN with high reliability of the decisions obtained, except for event QG28.

Results of the application of the three procedures to every event from the Galilee dataset are presented in Table 10: CAP for the four spectral bands case (1-3, 3-5, 5-7 and 7-9 Hz) and LDF and ANN for the five spectral
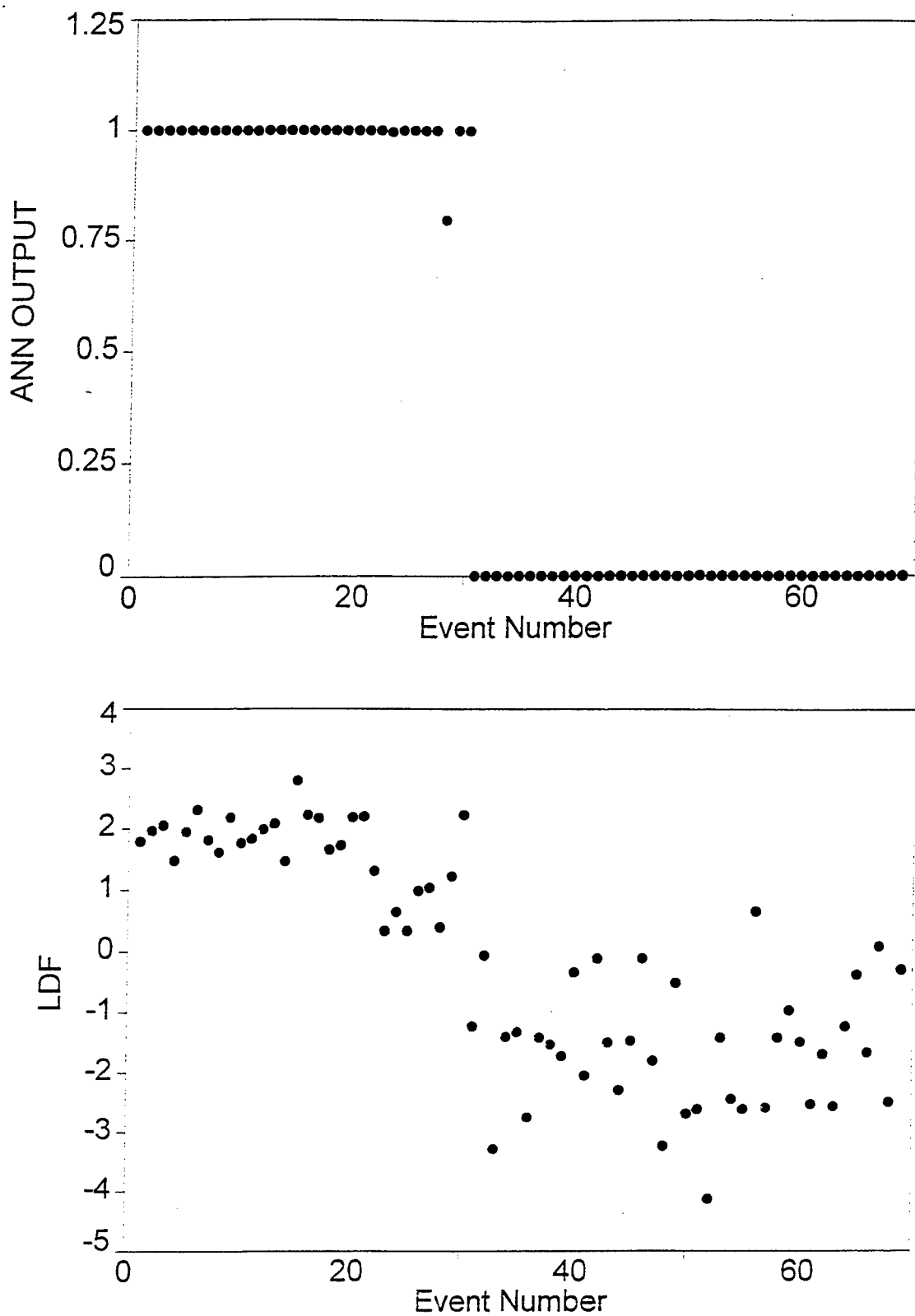
27

Figure 10. Testing of multidimensional discrimination procedures for the Galilee dataset
(1-30 - earthquakes, 31-69 - explosions): (a) ANN output, (b) LDF values.
Input is a vector of spectral r.m.s values in the 1-9 Hz range, divided into 5
equal intervals.

## TABLE 8

## NUMBER/RATE OF MISTAKES IN MULTIDIMENTIONAL AUTOMATIC DISCRIMINATION TEST PROCEDURE ON THE GALILEE DATASET

| NUMBER OF BANDS | FREQUENCY INTERVALS, Hz | PROCEDURE | | |
|---|---|---|---|---|
| | | LDF | CAP | ANN |
| 1 | 1-3 | 10/0.145 | 8/0.115 | 11/0.159 |
| 2 | 1-3, 3-5 | 8/0.116 | 2/0.029 | 10/0.145 |
| 3 | 1-3, 3-5, 5-7 | 3/0.043 | 3/0.043 | 1/0.014 |
| 4 | 1-3, 3-5, 5-7, 7-9 | 1/0.014 | 3/0.043 | 0/0 |
| 5 | 1-3, 3-5, 5-7, 7-9, 9-11 | 2/0.029 | 5/0.072 | 0/0 |
| 10 | 1-2, 2-3. 3-4, 4-5, 5-6, 6-7, 7-8, 8-9 9-10, 10-11 | 2/0.029 | 3/0.043 | 1/0.014 |

## TABLE 9

## AN AVERAGE CRUSTAL MODEL FOR ISRAEL AS USED IN THE STUDY

| N (km) | DEPTH (km) | THICKNESS (km/s) | P VELOCITY (km/s) | S VELOCITY (km/s) | DENSITY | QP (g/cm3) | QS |
|---|---|---|---|---|---|---|---|
| 1 | 2.00 | 2.00 | 4.00 | 2.31 | 1.93 | 100 | 50 |
| 2 | 3.00 | 1.00 | 4.50 | 2.60 | 2.09 | 120 | 60 |
| 3 | 8.00 | 5.00 | 5.70 | 3.29 | 2.48 | 200 | 100 |
| 4 | 13.00 | 5.00 | 6.00 | 3.46 | 2.58 | 400 | 200 |
| 5 | 20.00 | 7.00 | 6.30 | 3.64 | 2.68 | 600 | 300 |
| 6 | 28.00 | 8.00 | 6.50 | 3.75 | 2.75 | 1000 | 500 |
| 7 | halfspace | | 8.00 | 4.62 | 3.24 | 2000 | 1000 |

Tab. 10. Discrimination results for the Galilee dataset.

| Ev. | P/S | C,km/s | Re | smb. | cor. | smb. | cor. | CAP | LDF | ANN |
|---|---|---|---|---|---|---|---|---|---|---|
| F.band | 1-10 Hz | | | 1-11Hz | | 1 - 12 Hz | 1 - 7 Hz | 4bands | 5bands | |
| | | | | | *Quarry blasts* | | | | | |
| EG1 | 1.01 | 0.60 | 74.0 | 0.90 | 0.88 | 0.82 | 0.79 | 0 | -1.2 | 0. |
| EG2 | | 0.62 | 24.3 | 0.83 | 0.80 | 0.69 | 0.63 | 0 | -6.4E-2 | 1.6E-5 |
| EG3 | | 0.52 | 6.8 | 0.77 | 0.72 | 0.64 | 0.55 | 0 | -3.2 | 3.0E-6 |
| EG4 | 0.82 | 0.61 | 41.1 | 0.90 | 0.88 | 0.86 | 0.85 | 0 | -1.4 | 0. |
| EG5 | 0.83 | 0.62 | 121.7 | 0.92 | 0.91 | 0.88 | 0.86 | 0 | -1.3 | 0. |
| EG6 | | 0.65 | 25.3 | 0.85 | 0.82 | 0.75 | 0.70 | 0 | -2.7 | 0. |
| EG7 | - | 0.61 | 13.2 | 0.78 | 0.75 | 0.68 | 0.63 | 0 | -1.4 | 0. |
| EG8 | | 0.64 | 6.6 | 0.74 | 0.68 | 0.60 | 0.50 | 0 | -1.5 | 0. |
| EG9 | | 0.57 | 21.9 | 0.82 | 0.80 | 0.63 | 0.53 | 0 | -1.7 | 0. |
| EG10 | | 0.65 | 10.9 | 0.72 | 0.67 | 0.70 | 0.65 | 0 | -0.3 | 1.0E-6 |
| EG11 | | 0.58 | 15.5 | 0.82 | 0.79 | 0.72 | 0.66 | 0 | -2.0 | 0. |
| EG12 | 0.95 | 0.54 | 48.3 | 0.84 | 0.81 | 0.86 | 0.83 | 0 | -5.4E-03 | 0. |
| EG13 | 1.12 | 0.67 | 8.7 | 0.80 | 0.76 | 0.78 | 0.74 | 0 | -1.4 | 1.1E-05 |
| EG14 | | 0.61 | 45.9 | 0.91 | 0.89 | 0.91 | 0.89 | 0 | -2.2 | 0. |
| EG15 | 1.19 | 0.58 | 15.6 | 0.92 | 0.90 | 0.89 | 0.87 | 0 | -1.4 | 0. |
| EG16 | | 0.54 | 8.3 | 0.88 | 0.86 | | | 0 | -0.1 | 0. |
| EG17 | | 0.58 | 55.6 | 0.88 | 0.86 | 0.90 | 0.89 | 0 | -1.8 | 0. |
| EG18 | | 0.54 | 22.1 | 0.85 | 0.81 | 0.72 | 0.65 | 0 | -3.2 | 0. |
| EG19 | | 0.68 | 40.5 | 0.86 | 0.82 | | | 0 | -0.5 | 0. |
| EG20 | | 0.65 | 23.9 | 0.84 | 0.82 | | | 0 | -2.6 | 3.6E-04 |
| EG21 | | 0.66 | 75.5 | 0.88 | 0.86 | 0.85 | 0.82 | 0 | -2.6 | 1.2E-03 |
| EG22 | | 0.57 | 18.1 | 0.86 | 0.81 | 0.77 | 0.69 | 0 | -4.1 | 0. |
| EG23 | | 0.76 | 22.2 | 0.89 | 0.84 | | | 0 | -1.4 | 0. |
| EG24 | 0.98 | 0.57 | 27.3 | 0.88 | 0.86 | | | 0 | -2.4 | 1.4E-05 |
| EG25 | | 0.59 | 15.0 | 0.86 | 0.82 | 0.78 | 0.73 | 0 | -2.6 | 0. |
| EG26 | | 0.57 | 8.5 | 0.84 | 0.81 | | | 0 | 0.65 | 0. |
| EG27 | | 0.52 | 22.5 | 0.84 | 0.78 | | | 0 | -2.5 | 0. |
| EG28 | | 0.56 | 53.5 | 0.86 | 0.84 | | | 0 | -1.4 | 6.0E-06 |
| EG29 | | 0.67 | 12.2 | 0.86 | 0.83 | | | 0 | -0.9 | 0. |
| EG30 | | 0.60 | 7.3 | 0.73 | 0.68 | | | 0 | -1.4 | 1.2E-04 |
| EG31 | | 0.54 | 25.9 | 0.78 | 0.75 | | | 0 | -2.5 | 0. |
| EG32 | 0.54 | 0.57 | 103.0 | 0.92 | 0.90 | | | 0 | -1.6 | 0. |
| EG33 | | 0.63 | 20.2 | 0.79 | 0.74 | | | 1 | -2.5 | 0. |
| EG34 | | 0.55 | 48.0 | 0.88 | 0.86 | | | 0 | -1.2 | 1.4E-05 |
| EG35 | | 0.59 | 35.3 | 0.90 | 0.88 | | | 0 | -0.3 | 0. |
| EG36 | | 0.58 | 23.2 | 0.87 | 0.81 | | | 0 | -1.6 | 1.1E-05 |
| EG37 | | 0.56 | 11.0 | 0.85 | 0.78 | | | 0 | 9.03E-02 | 0. |
| EG38 | | 0.60 | 12.3 | 0.81 | 0.71 | | | 0 | -2.4 | 7.8E-06 |
| EG39 | | 0.59 | 25.8 | 0.86 | 0.83 | | | 0 | -0.2 | 1.1E-05 |
| | | | | | *Earthquake* | | | | | |
| QG1 | 0.31 | 0.78 | 1.4 | 0.32 | 0.19 | 0.49 | 0.38 | 1 | 1.79 | 1.00000 |
| QG2 | | 0.78 | 1.3 | 0.25 | 0.004 | 0.32 | 0.10 | 1 | 1.96 | 0.99968 |
| QG3 | | 0.74 | 1.5 | 0.21 | 0.009 | 0.32 | 0.14 | 1 | 2.05 | 1.00000 |
| QG4 | | 0.92 | 1.0 | 0.21 | 0.007 | 0.22 | 0.03 | 1 | 1.47 | 1.00000 |
| QG5 | 0.38 | 0.74 | 1.2 | 0.28 | 0.19 | 0.41 | 0.33 | 1 | 1.95 | 0.99977 |
| QG6 | | 0.71 | 1.0 | 0.19 | 0.03 | 0.21 | 0.05 | 1 | 2.31 | 0.99969 |
| QG7 | | 0.74 | 1.4 | 0.25 | 0.12 | 0.32 | 0.21 | 1 | 1.81 | 0.99920 |

| | | | | | | | | | | |
|------|------|------|-----|-------|--------|------|--------|---|------|---------|
| QG8  |      | 0.75 | 1.9 | 0.16 | 0.02   | 0.15 | 0.05   | 1 | 1.61 | 0.99994 |
| QG9  | 0.56 | 0.74 | 1.3 | 0.26 | 0.14   | 0.51 | 0.38   | 1 | 2.18 | 0.99926 |
| QG10 |      | 0.75 | 1.6 | 0.14 | -0.003 | 0.12 | -0.10  | 1 | 1.76 | 0.99913 |
| QG11 | 0.50 | 0.79 | 1.5 | 0.12 | -0.03  | 0.25 | 0.10   | 1 | 1.83 | 0.99879 |
| QG12 |      | 0.78 | 1.2 | 0.17 | -0.04  | 0.17 | -0.002 | 1 | 1.98 | 1.00000 |
| QG13 |      | 0.77 | 1.0 | 0.33 | 0.11   | 0.47 | 0.29   | 1 | 2.08 | 1.00000 |
| QG14 |      | 0.75 | 1.2 | 0.10 | -0.05  | 0.14 | -0.005 | 1 | 1.46 | 0.99999 |
| QG15 |      | 0.71 | 0.8 | 0.30 | 0.07   | 0.40 | 0.19   | 1 | 2.79 | 0.99995 |
| QG16 |      | 0.74 | 0.9 | 0.25 | 0.06   | 0.28 | 0.10   | 1 | 2.22 | 0.99995 |
| QG17 |      | 0.81 | 1.1 | 0.22 | -0.04  | 0.20 | -0.07  | 1 | 2.17 | 0.99975 |
| QG18 |      | 0.79 | 1.5 | 0.22 | -0.04  | 0.17 | -0.10  | 1 | 1.65 | 0.99985 |
| QG19 | 0.35 | 0.80 | 1.7 | 0.25 | 0.13   | 0.26 | 0.14   | 1 | 1.72 | 0.99992 |
| QG20 | 0.55 | 0.73 | 1.3 | 0.24 | 0.13   | 0.42 | 0.33   | 1 | 2.18 | 0.99970 |
| QG21 | 0.32 | 0.84 | 1.1 | 0.32 | 0.21   | 0.44 | 0.34   | 1 | 2.20 | 0.99999 |
| QG22 |      | 0.75 | 2.9 | 0.42 | 0.28   | 0.30 | 0.12   | 1 | 1.30 | 0.99980 |
| QG23 | 0.55 | 0.76 | 5.5 | 0.66 | 0.62   | 0.24 | 0.15   | 1 | 0.33 | 0.99637 |
| QG24 |      | 0.77 | 4.7 | 0.47 | 0.36   | 0.23 | 0.07   | 1 | 0.64 | 0.99997 |
| QG25 | 0.33 | 0.79 | 6.2 | 0.68 | 0.64   | 0.28 | 0.19   | 1 | 0.33 | 0.99999 |
| QG26 |      | 0.72 | 3.5 | 0.48 | 0.38   | 0.19 | 0.03   | 1 | 0.98 | 0.99902 |
| QG27 |      | 0.72 | 3.1 | 0.45 | 0.31   | 0.28 | 0.10   | 1 | 1.03 | 0.99974 |
| QG28 | 0.55 | 0.78 | 5.7 | 0.62 | 0.57   | 0.30 | 0.20   | 1 | 0.39 | 0.79460 |
| QG29 |      | 0.79 | 2.6 | 0.24 | 0.11   | 0.12 | -0.02  | 1 | 1.22 | 0.99966 |
| QG30 | 0.70 | 0.90 | 1.1 | 0.20 | 0.07   | 0.35 | 0.24   | 1 | 2.22 | 0.99942 |

bands case (1-3, 3-5, 5-7, 7-9 and 9-11 Hz). The values of LDF and the ANN output are shown as the result of the leave-one-out procedure; for the King's CAP, index 1 refers to the earthquakes cluster and 0 to the explosions cluster.

### 3.1.4 Spectral Coherency Statistics

The efficiency of the LFSM approach in identifying explosions with a low signal-to-noise ratio (SNR) was investigated. A number of quarry blasts recorded at remote stations with SNR<1 for P-waves and SNR≅1.5-2 for S and coda waves show clear spectral modulation patterns, presented by coherent minima (or nulls) and maxima (Fig. 11a,b). Any modulation and coherency in spectra of pre-signal noise is not observable (Fig. 11a). Spectral scallops depend heavily on ripple-firing parameters, e.g. the frequency of the first null, dominant in our frequency-limited recordings, is determined mainly by the duration of ripple-firing (Gitterman and van Eck, 1993; Barker et al., 1993). Similar plots for earthquakes demonstrate the irregular character of spectral shapes and minima for different azimuths (Fig. 12).

Coherency of spectral shapes for different stations can be quantitatively assessed by "semblance" and "cross-correlation" statistics commonly used in seismic prospecting for phase correlation of seismic traces in time domain (e.g. Neidell and Taner, 1971). After some modification (including spectra logarithming and subtraction of the average) the statistics can be written as:

$$\text{smb} = \frac{1}{N} \frac{\sum_{f_1}^{f_2} S1_i}{\sum_{f_1}^{f_2} S2_i} \qquad \text{cor} = \frac{1}{N-1} \frac{\sum_{f_1}^{f_2} (S1_i - S2_i)}{\sum_{f_1}^{f_2} S2_i} \qquad (3)$$

where

$$S1_i = \left[ \sum_{k=1}^{N} (S_{ki} - \bar{S}_k) \right]^2 \qquad S2_i = \sum_{k=1}^{N} (S_{ki} - \bar{S}_k)^2 \qquad (4)$$

32
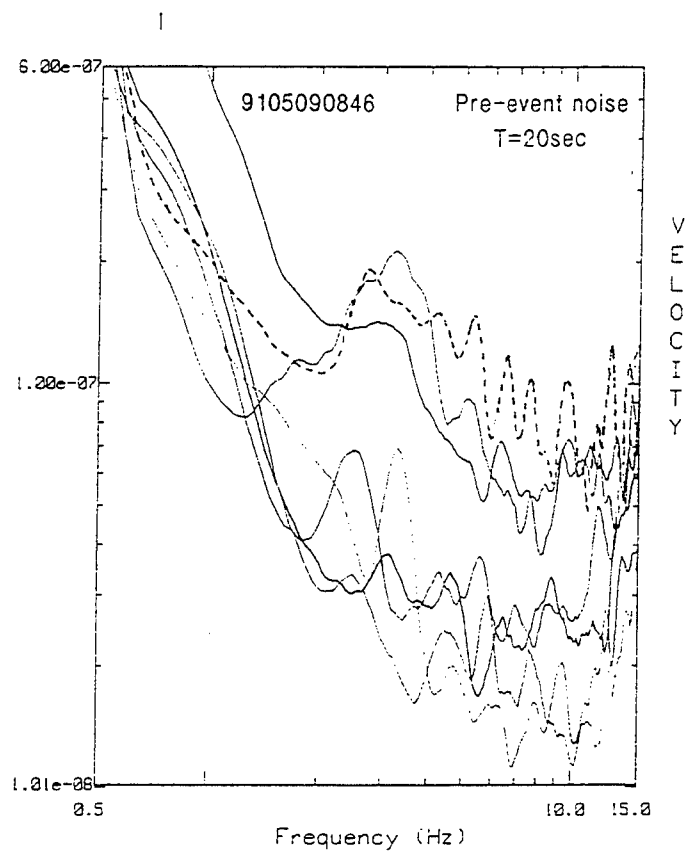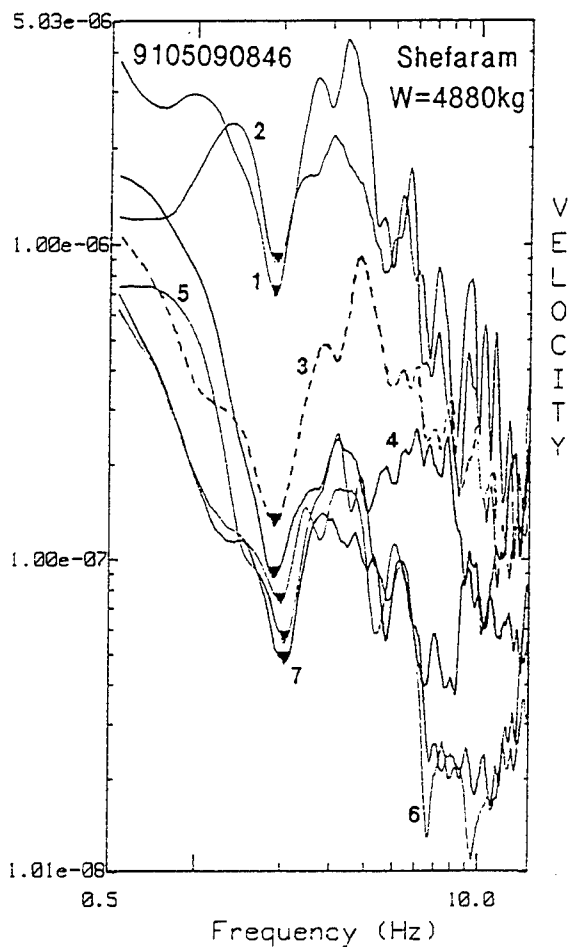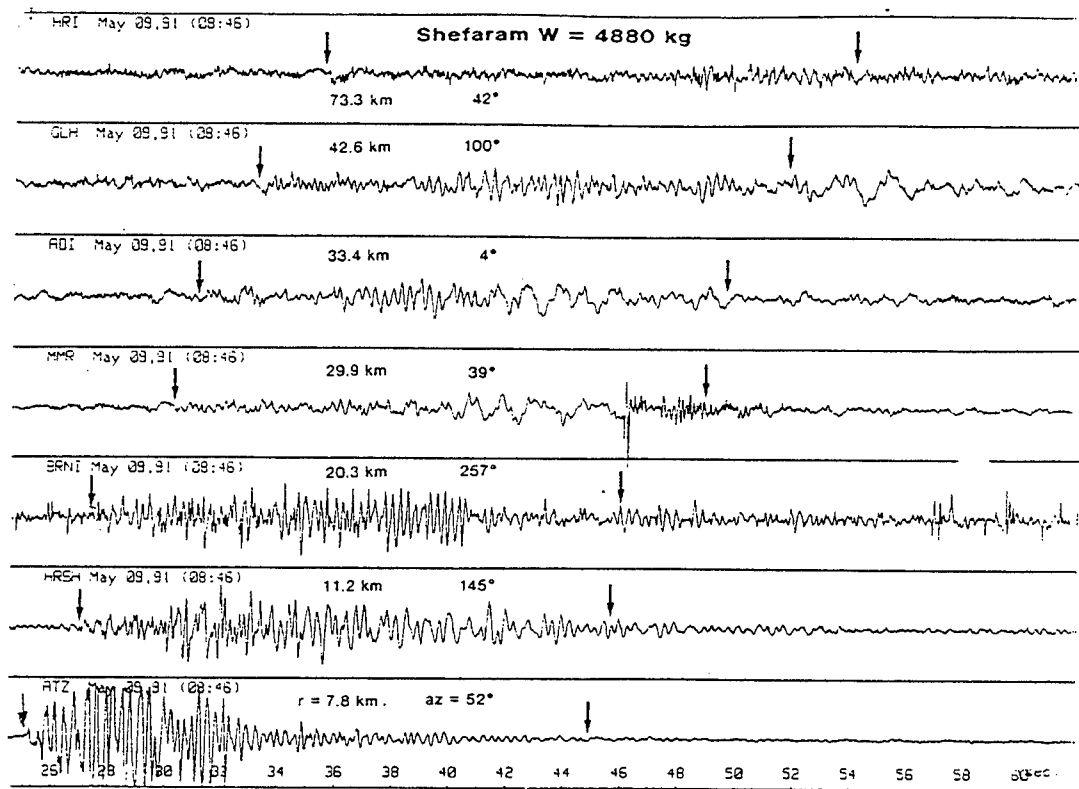
**Figure 11.** Example of distinct low frequency, azimuth and distance-independent spectral modulation for low SNR<2 recordings of two Galilee quarry blasts EG33 (a) and EG16 (b). FFT spectra are instrument corrected and smoothed by a triangle operator in the 0.5 Hz window.

# b



**Tamra, W = 4200 kg**

MML Feb 04,91 (08:52)
50.5 km   159°

MFMI Feb 04,91 (08:52)
40.4 km   190°

GVMR Feb 04,91 (08:52)
36.9 km   154°

BRN Feb 04,91 (08:52)
25.6 km   237°

ADI Feb 04,91 (08:52)
24 km   1°

JRMK Feb 04,91 (08:52)
22 km   50°

HRSH Feb 04,91 (08:52)   r = 19 km, az = 166°

30  32  34  36  38  40  42  44  46  48  50  52  54  56  58  60  62  (sec)

9102040852                    Tamra
                              W=4200kg

Figure 11b.

34
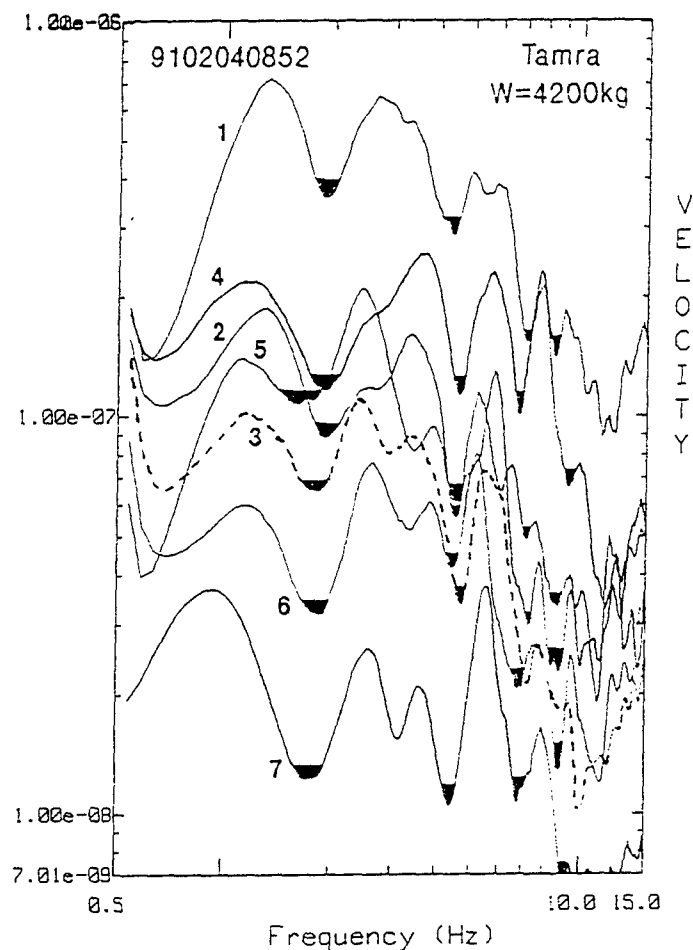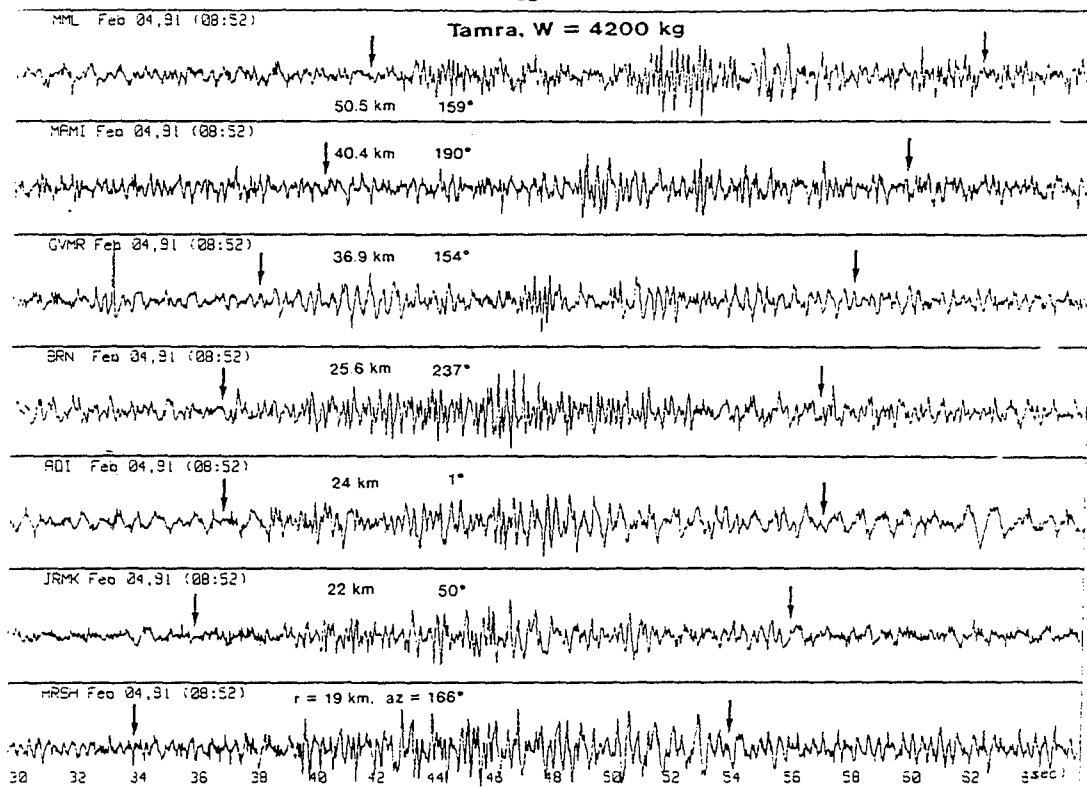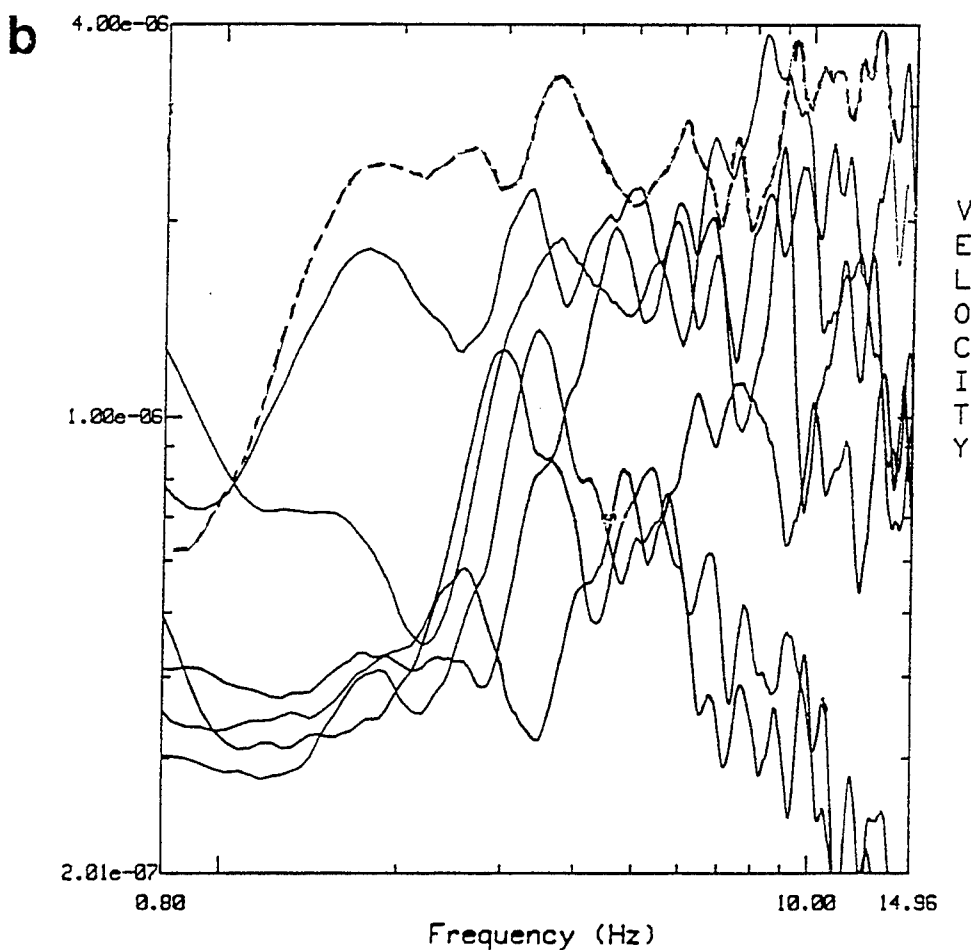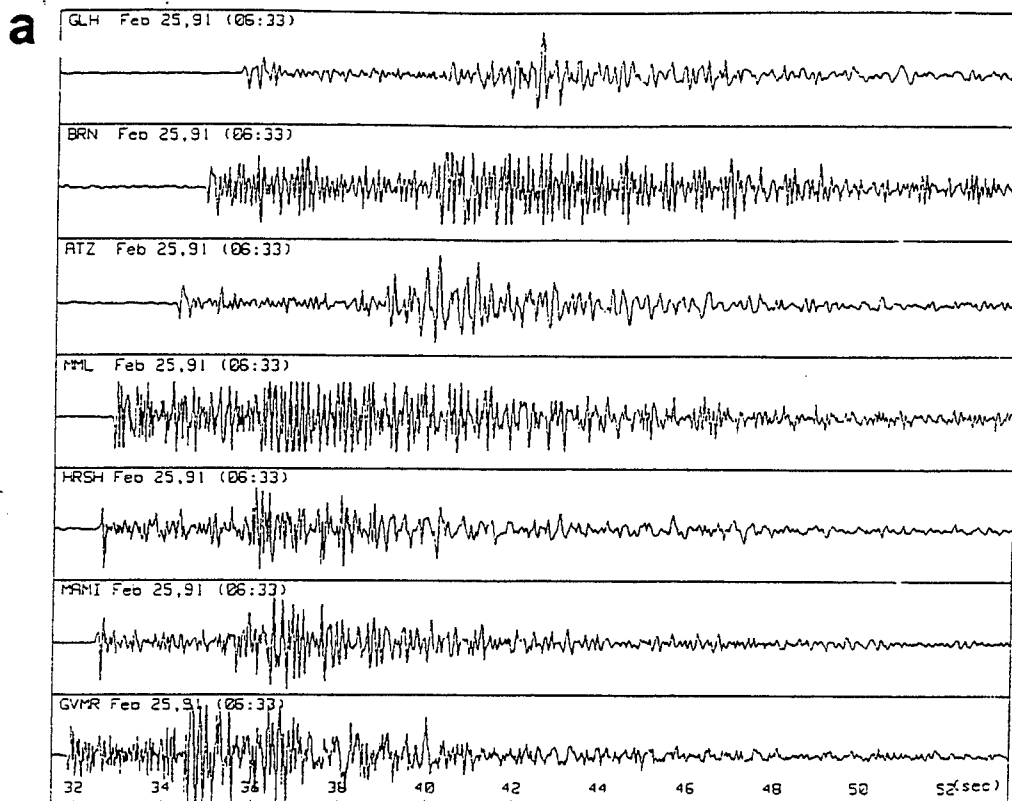
Figure 12. Example of the Galilee earthquake QG20 recordings (a) showing irregularity of spectral shapes and low frequency minima (nulls) for a broad azimuth range (66-354°) of ISN stations (b).

$S_{ki} = \log_{10} S_k(f_i)$ - log spectral amplitude at k station; $\overline{S_k}$ is the average spectral level; N is the number of stations and $[f_1, f_2]$ is the frequency range for calculation.

The correlation technique was applied to smoothed amplitude spectra of the selected subnetwork of 10 stations. We tried two spectral intervals for the analysis: 1-7 Hz and 1-12 Hz; the results are presented in Table 10. The statistics values obtained are higher for quarry blasts (0.7-0.9) than for earthquakes (0.1-0.4).

The statistics remain virtually unchanged if different windows of spectra smoothing are selected (0.25 Hz, 1 Hz). The semblance statistic shows a slightly higher resolving power than cross-correlation; in general, better discrimination results (better separation of earthquakes and explosions) are obtained when processing the whole signal spectra in the frequency range 1-12 Hz. As may be expected, a strong correlation between semblance and cross-correlation statistics is observed (see Fig. 13a), therefore, in the following, we consider them as one discriminant. For the same few earthquakes mentioned above as showing enlarged energy ratio values originating on the main fault at Lake Kinneret (Sea of Galilee), we obtained anomalous high semblance values of 0.4-0.65, the two sets of seismic events are, however, completely separate. The same result is observed on the plot of semblance versus energy ratio (Fig. 13b). It should be noted that the spectral range 1-7 Hz showed "normal" values of the statistics for the events from the Sea of Galilee (see Table 10).

Discussion

The high resolving power of the "semblance" discriminant lies in the nature of the seismic sources investigated. A ripple-fired blast may be considered a point source, therefore the interference pattern is uniform in different directions, resulting in the azimuth-independent SM and high "semblance" values. Frequencies of spectral minima for different stations caused by nulls of the interference function, have random small shifts (Fig. 11). It is maintained (Der and Baumgardt, 1995) that the Doppler effect could be responsible for this phenomenon which can even suppress the nulls (Blanford, 1995). We consider this azimuthal effect, caused by the spacing of individual shots in a quarry blast, as minor and that the shifts are determined mainly by the spectrum slope of a single shot explosion at a station site (Gitterman and van Eck, 1993).
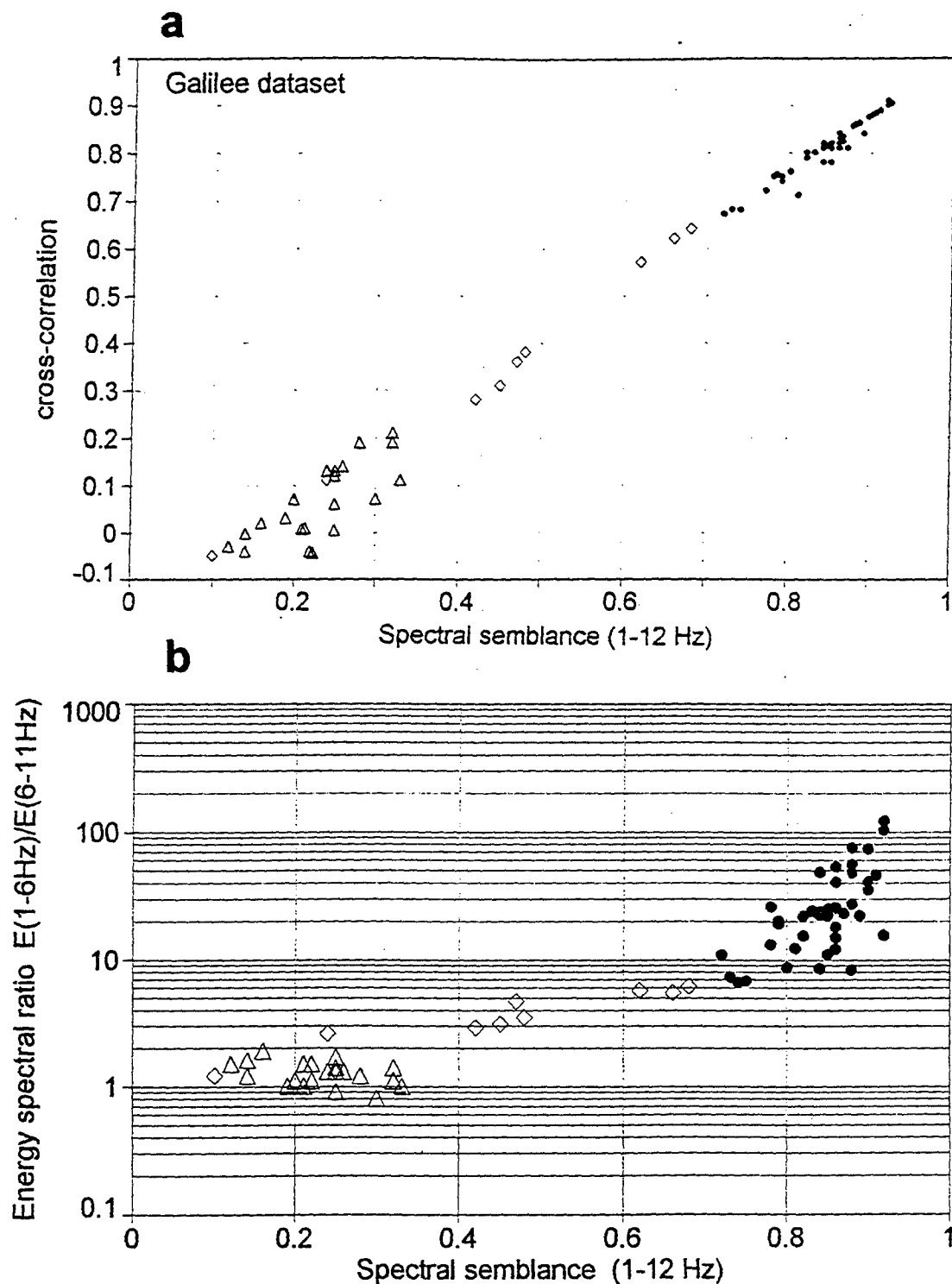
Figure 13. Discrimination results for the Galilee dataset: (a) cross-correlation versus semblance, (b) semblance versus energy ratio (Δ - earthquakes, • - quarry blasts, ◊ - earthquakes from the Sea of Galilee).

The Doppler effect could be relevant in the case of earthquakes which are actually line sources and the stochastic superposition of sub-events along the rupture also produces some kind of SM, "scalloped spectra" (Bakun et al., 1978); consequently the presence of a time-independent SM alone does not prove ripple-firing (Baumgardt and Zigler, 1988). Moreover, a time-independent SM can be acquired during propagation in the case of shallow earthquakes and the low velocity stratified media with sharp boundaries along the path (Hedlin et al., 1989). These detrimental effects can be misleading when observed at one station or at stations with similar azimuths (an array, for example), but this is negligible in the azimuth-invariant modulation patterns observed at regionally distributed stations of a RDSN. Supposedly due to the directivity effect, the interference pattern for an earthquake will be azimuth-dependent, i.e. maxima and minima in a spectrum will be shifted significantly in accordance with the direction to a station, therefore, for stations with broad azimuthal coverage, we observe visual non-coherence of spectra (Fig. 12) causing low semblance values.

The spectral discriminants show dependence on source region. Semblance values as well as energy spectral ratios for most earthquakes from the Sea of Galilee are greater than for the adjacent Galilee region, but provide separation from quarry blasts.

Our results provide a positive answer to questions such as: whether short delay (20-30 msec) ripple-fired events are capable of generating SM below 20 Hz and if this feature can be used for discrimination of distant regional (0-400km) events (Hedlin et al., 1995). The LFSM approach also solves the problem of disappearing high frequency (above 5 Hz), spectral scalloping in spectrograms of mine explosions in central Chile at distances greater than 100km (Beck and Wallace, 1995).

## 3.2 VELOGRAM ANALYSIS

This discrimination technique is based on velograms, determined by the Short Time Average (STA) transform of the original seismograms, using a group velocity sections instead of the conventional time section (Fig. 14). This approach is inspired on one hand by Kim et al. (1994), who used a group velocity section obtained over a short period seismic network to demonstrate the effect of inhomogeneous crust and, on the other hand, by Husebye and Ruud (1995) in which seismic network intensity curves (STA) were utilized in an automatic epicenter location procedure. The kinematic group velocity

38
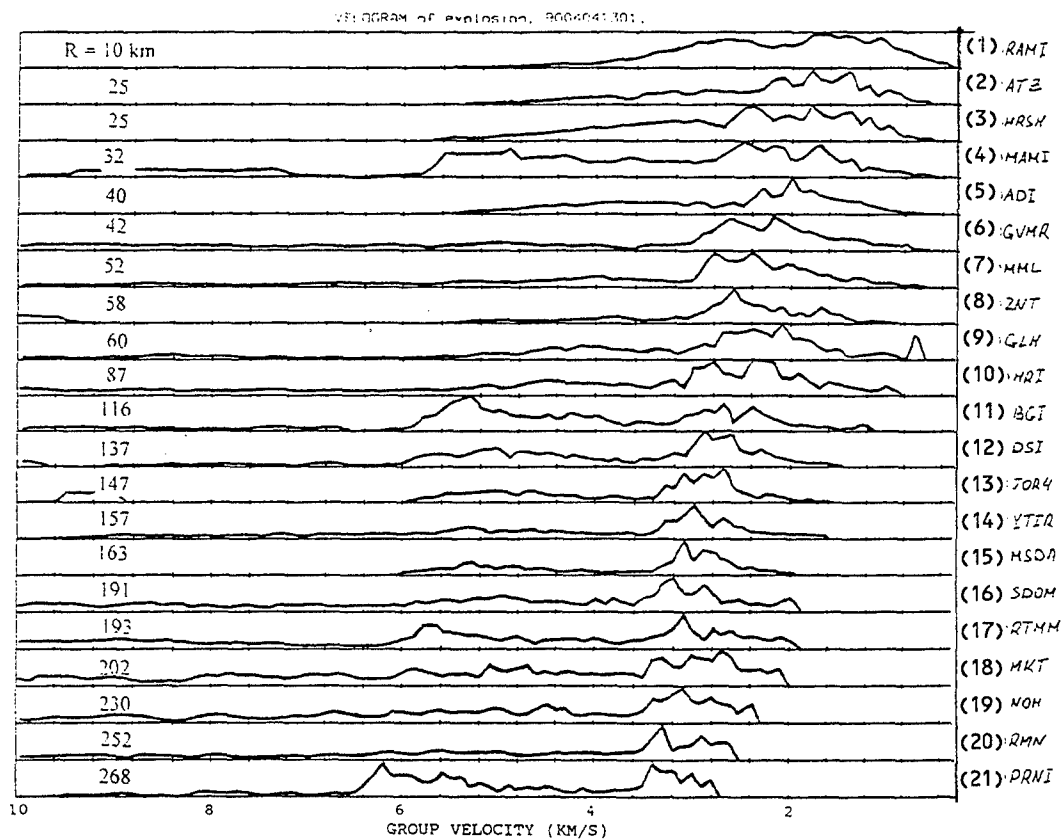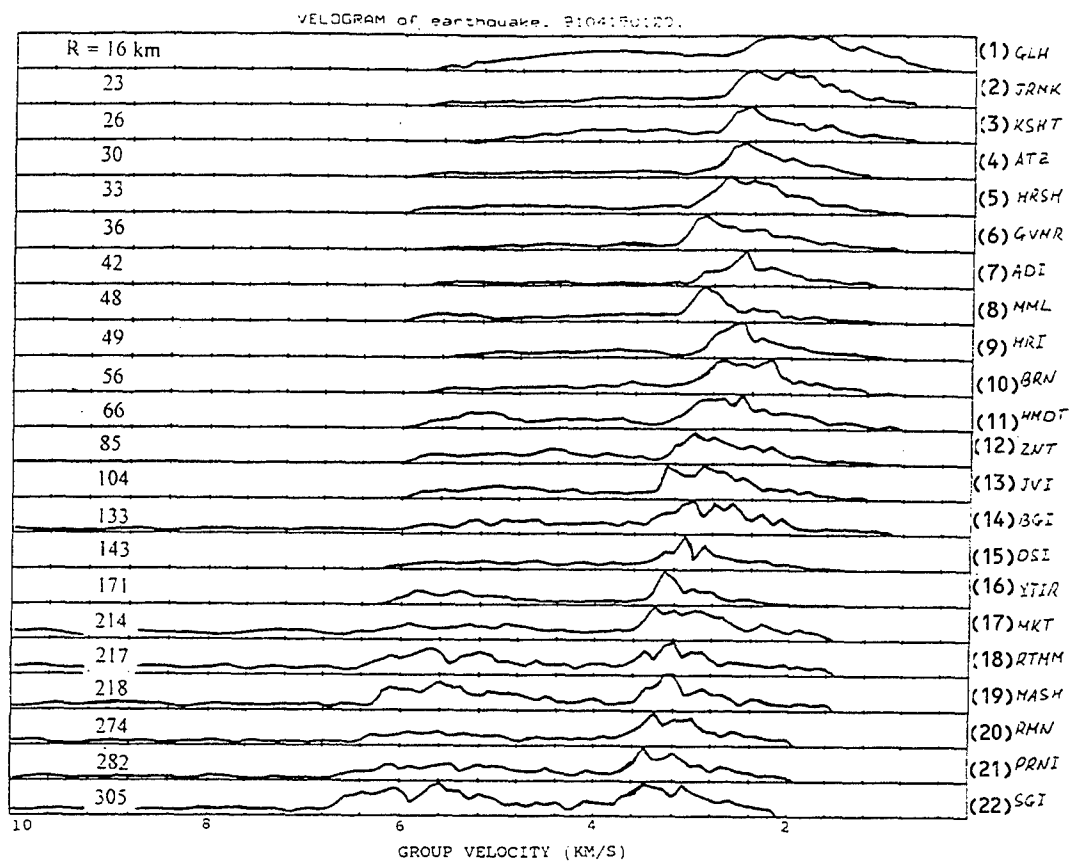
Figure 14. Velogram section for an earthquake Q (a) and an explosion X (b).

discriminator is compared with the conventional dynamic P/S discriminator which may also be obtained from velograms.

The processing scheme for each channel is illustrated in Fig. 15. In the first step, the STA is computed from digital seismograms; then, for the sequence of velocities $V_j = V_0 + j*dV$ $(j=1,...,J)$, the velogram $Q(V_j)$ is obtained from the STA as:

$$Q(V_j) = STA(R/V_j), \qquad (5)$$

where R is the distance from the source. In this study the window length for the STA was 1 sec, moving over seismograms with a 0.02 sec step equal to the digitizing interval. Time $T_j = R/V_j$ is the travel-time associated with the beginning of the moving window. Group velocity V was in the range of 0.1-1.0 km/s, computed in steps dV=0.1 km/s. For noise reduction, all the original seismograms were filtered in the frequency range 1-10 Hz using a Butterworth filter.

The velogram characterizes the distribution of seismic wave intensity versus group velocity. The intensity peaks in the study were characterized by maximum velogram values $P_{max}$ and $S_{max}$ (see Fig. 15) in group velocity intervals 4-8 km/s and 1-4 km/s, corresponding to P and S-Lg-Rg wave groups. The group velocities $V_{mp}$ and $V_{ms}$ corresponding to the peak values of $P_{max}$ and $S_{max}$, respectively were tested as possible discriminants.

It was found that $V_{mp}$ does not resolve events whereas $V_{ms}$ has a tendency to be slightly larger for earthquakes than for explosions over a wide range of distances, 10-200 km. This information may be accumulated using a set of observations at different distances. Thus, in the following steps we concentrated on the variations of $V_{ms}$ across the regional seismic network as a possible discriminant between earthquakes and explosions. The examples of the velogram section of an earthquake and a quarry blast obtained from the ISN short period seismograms are shown in Figs. 14a and 14b (see ISN stations locations in Fig. 2); a tendency of the wave intensity to shift with distance towards larger velocities and a slight lagging of the explosion S-wave intensity relative the earthquake are observed.

The value of $V_{ms}$ was calculated for each velogram corresponding to the specific distance, R. Examples of individual $V_{ms}(R)$ curves, extracted from the velograms presented in Fig. 14, are shown in Fig. 16. Fig. 16 shows that the curves $V_{ms}(R)$, as a first approximation, can be fitted by a function of the form:

(1)

(2)

TIME [min]

GROUP VELOCITY (KM/S)

S_max

P_max

V_mp

V_ms

(3)
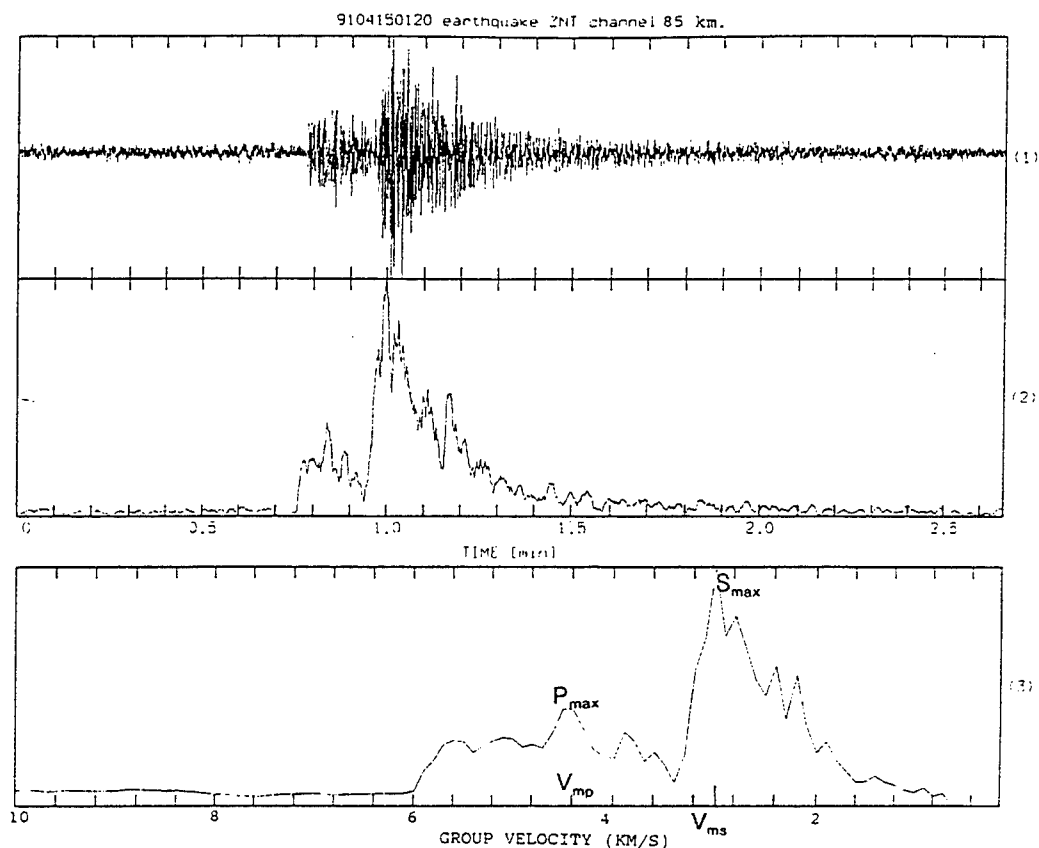
Figure 15. Velogram analysis.Example of data processing for an earthquake Q record at the station ZNT (85 km from the source): (1) band-pass (1-10 Hz) filtered digital seismogram; (2) 1-second length STA; (3) velogram.
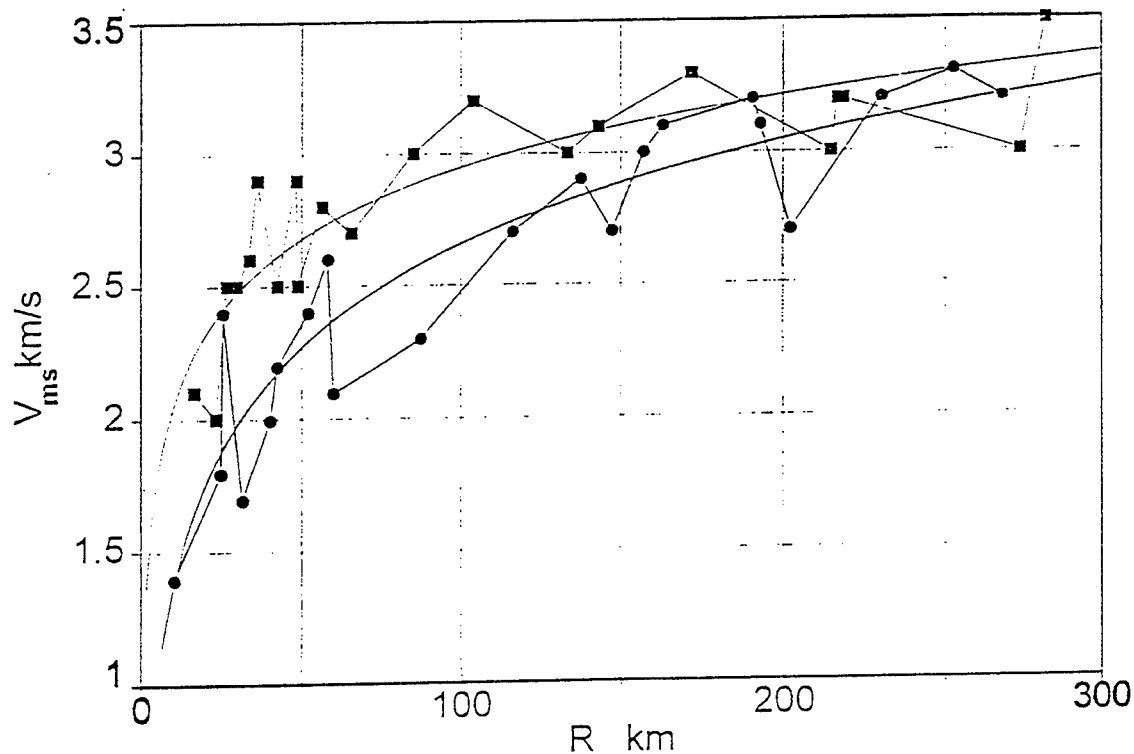
Figure 16. Velogram analysis. $V_{ms}$-distance curves for an earthquake Q (■) and an explosion X (●), and the corresponding least squares fit curves $V_{ms}=a+b*\ln(R)$. Q: a=1.16, b=0.389; X: a=0.793, b=0.487.

41

$$V_{ms} = a + b^* \ln(R) \qquad (6)$$

The fitted curves for an earthquake, Q, and an explosion, X, are shown in Fig. 16. The relationship expressed by Eq. (6) is general in form, but coefficients "a" and "b" differ for each event and can serve as a compact parametric characteristic of the event type provided by focal depth and mechanism. The coefficients are computed by least squares fitting for each of the analyzed events.

The results are presented in Fig. 17a, which shows separation of the two populations of seismic events and also demonstrates that:

1. there is a linear relationship between coefficients "a" and "b"; and

2. the slopes of the "b" versus "a" relationship are practically the same for earthquakes and explosions and equal to a first order approximation of 1/3.

Consequently, we propose that the populations of earthquakes and explosions can be distinguished by a single parameter:

$$C = b + 0.33^*a \qquad (7)$$

which, in this case, presents a simple linear discriminant function. The distribution of C values obtained from the analysis of velograms from all the events is presented in Fig. 17 (see also Table 10). Using the criterion C=0.69 we obtain almost complete separation between earthquakes and explosions. One mistake was accounted for by an extremely low magnitude explosion, absolutely invisible at distances R>28 km. For the interpretation of the discrimination results obtained from the velogram analysis, Dr. B. Ruud from the Seismological Department of Bergen University provided at our request 1-D modeling of the group of S and surface wave propagation in the crust for the two types of sources: close to the surface and deep. The crustal model (see Table 9) used in the study was obtained by averaging several models for Israel (Feigin and Shapira, 1994).

In Table 9, the S-velocities are computed from the P-velocities by assuming a Poisson ratio of 0.25. The densities are also computed from P-velocities using a version of Birch's law. The Q values are for a reference frequency of 1.0 Hz. The frequency dependence assumed for Q is: $Q(F)=Q(1.0)^*f^{0.5}$. The source is an explosion at different depths. According to the model some synthetic seismograms were computed with normal mode
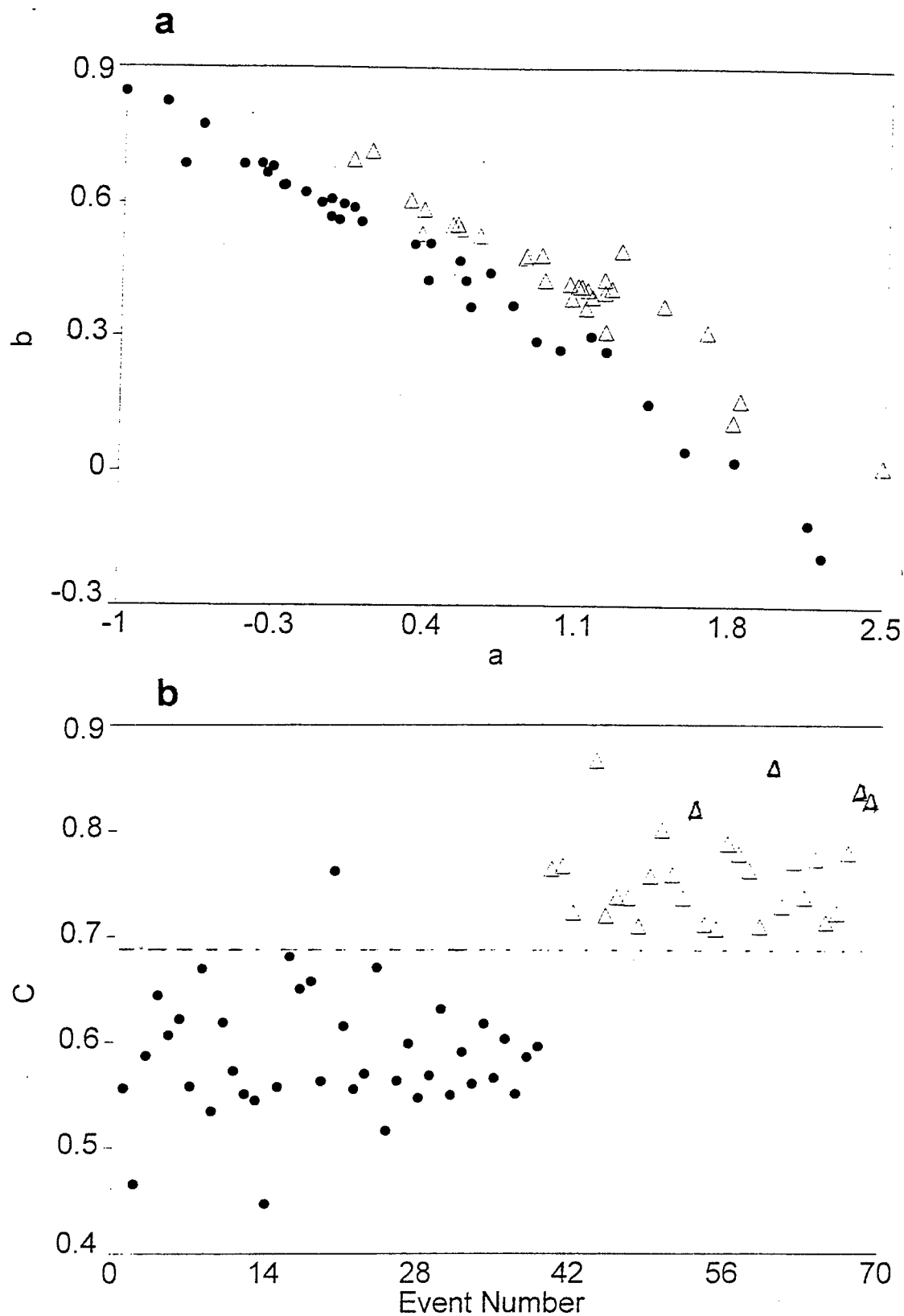
Figure 17. Velogram analysis. Galilee events. $V_{ms}(R)$ fit curve parameters for earthquakes ($\Delta$) and explosions ($\bullet$): (a) pairs (a,b); (b) c = a + 0.33b.

43

summation with the following results. When the source is in the sediments (upper 3km), the seismograms show two groups of S- and surface-waves propagating with quite different group velocities. The first group, which propagates mainly in the 3rd and 4th layers, has a velocity of 3.2-3.4 km/s and the second group, which propagates in the sediments, has a velocity of 2.1 km/s. At short distances the second group is dominant in amplitude while at longer distances, the first group. The relative amplitude of the two groups is strongly dependent on the Q values in the sediments. For sources below the sediments the second group of waves is virtually absent.

The modeling results agree with the velogram analysis of ISN records and confirm our assumption regarding the different kinematic properties of seismic waves generated by deep and shallow events in the layered media with a thick sedimentary layer. Moreover, they suggest which media factors would have a prime influence on the developed kinematic discriminant: the thickness and average velocity of the sedimentary layer, the velocity below the sediments and the Q values within the sediments (Dr. B. Ruud, personal communication).

### 3.3 P/S

Using the velograms of the ISN individual channels, we tested a dynamic P/S discriminant in which $P=P_{max}$ and $S=S_{max}$ (see example in Fig. 15). This statistic characterizes the ratio of velogram intensities in the specified group velocity intervals 4-8 km/s for P and 1-4 km/s for S. A tendency for that the P/S for explosions will be greater than that for earthquakes is expected. In practice, this appeared to be true for only a limited number of ISN stations and only for strong events with a good SNR at distances greater than 100km. Only 18 events of the data set fall into this category, i.e. 8 explosions and 11 earthquakes.

Fig. 18a shows the P/S ratios at various distances. No distinction between earthquakes and explosions may be observed here. Six stations for which this tendency was evident were selected, all of them at distances greater than 100km from the source. Fig. 18b shows the P/S ratios for these stations for various events. For each event P/S values were averaged over the various stations (see Table 10). From Fig. 18c we can see that, except for one or two events, the average P/S ratio enables us to distinguish between earthquakes and explosions.

The combined P/S and C criteria (P/S are average values) for the 18 events are shown in Fig. 19. The joint (P/S,C) parameter vector evidently
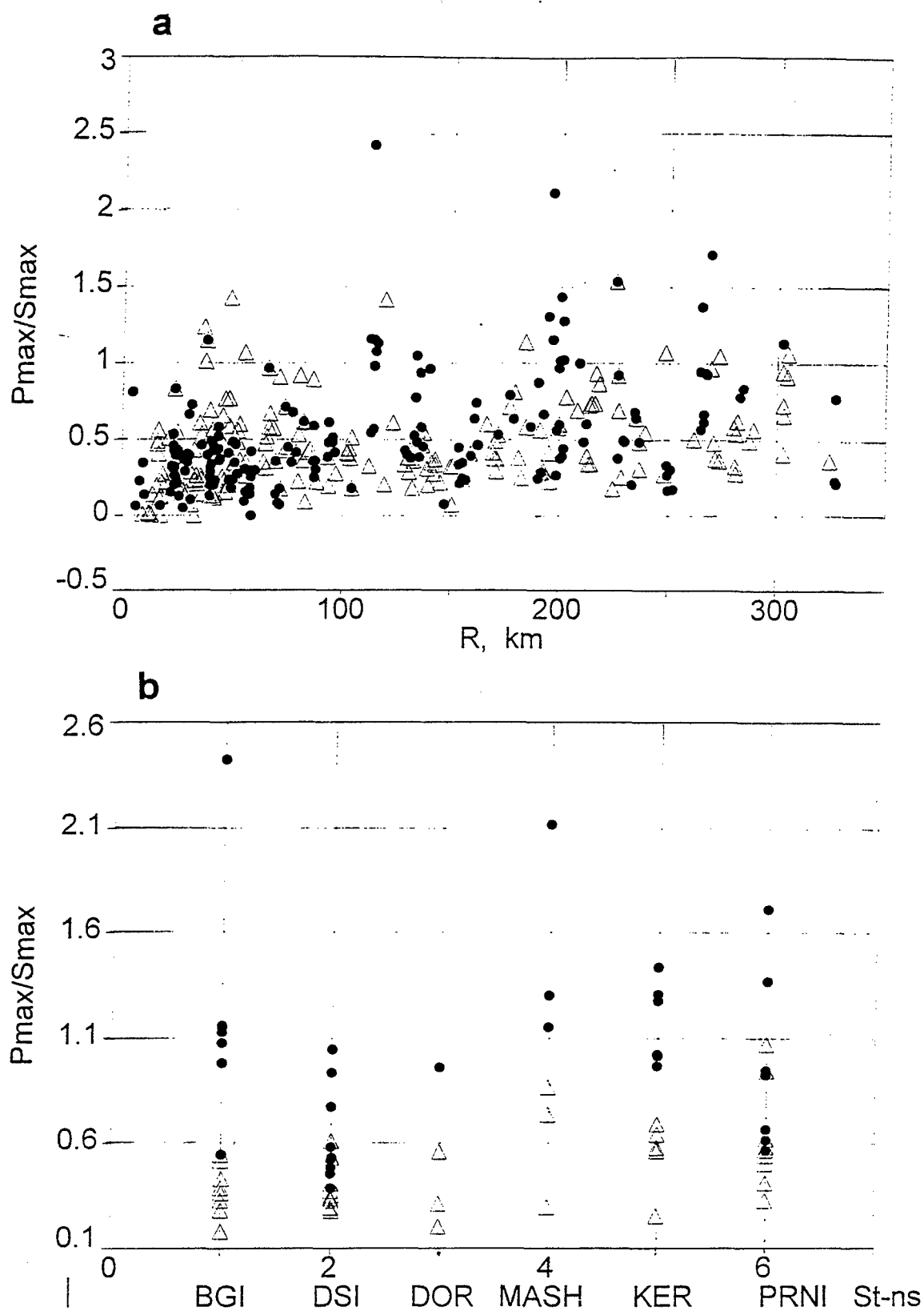
Figure 18. Velogram $P_{max}/S_{max}$ for the Galilee strong events: 11 earthquakes ($\Delta$) and 8 explosions ($\bullet$): (a) distance dependency; (b) for selected stations; (c) averages ($+$) for selected stations.

45

**c**



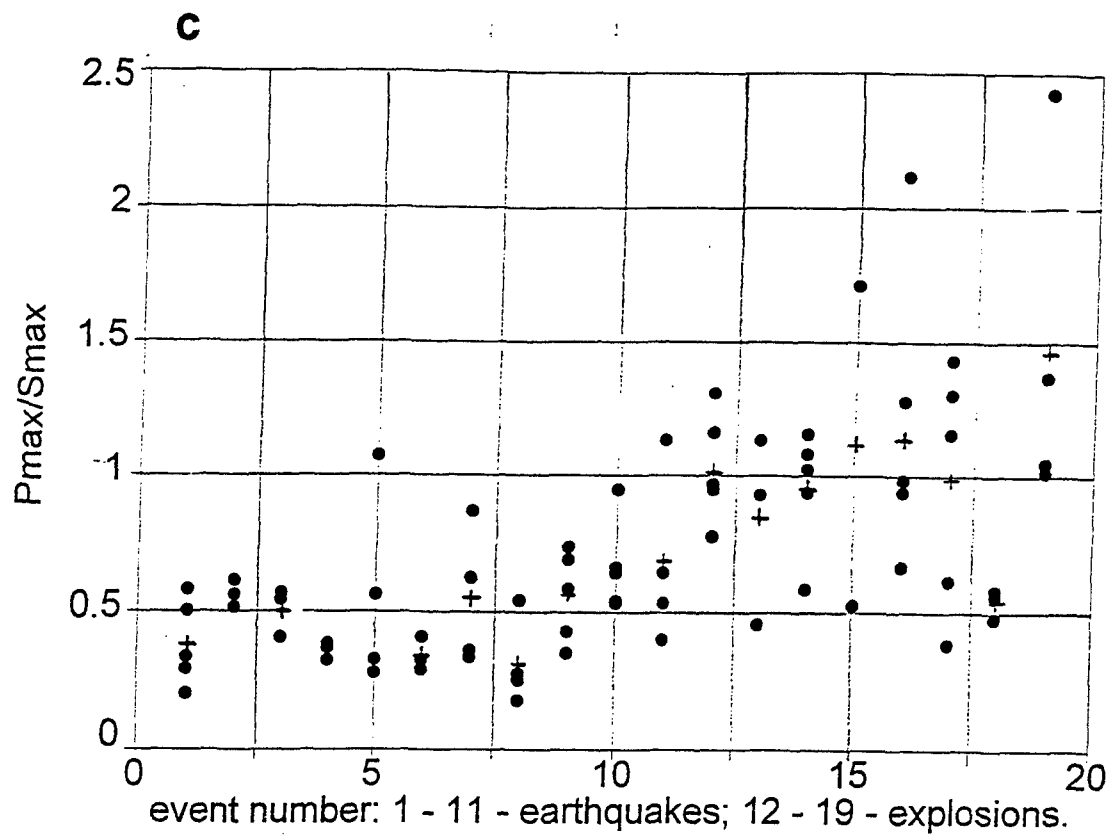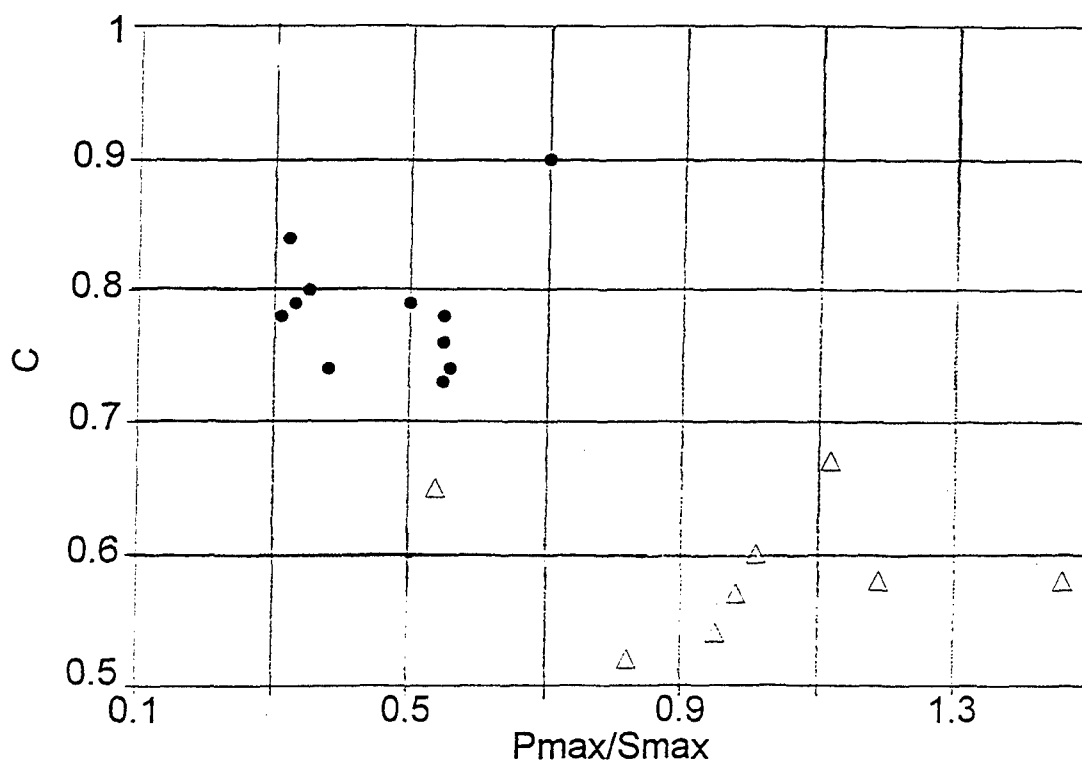event number: 1 - 11 - earthquakes; 12 - 19 - explosions.

Figure 18 (Continued)



Figure 19. Joint (P/S, C) discriminator for a subset of relatively strong Galilee events: 8 explosions (•) and 11 earthquakes (Δ).

enhances the resolution power of the individual discriminants, however, the applicability and reliability of the dynamic P/S discriminant is much less than that of the kinematic parameter C.


## 3.4 CODA WAVE

Su et al.(1991) have used records of only 2 short period stations. Supposing that any real effect should be enhanced by averaging over the dense ISN, we tested this discriminant in our region using the Galilee dataset. The first order body-wave scattering model of the coda waves (Aki and Chouet, 1975) was applied:

$$A(f|t) = A_0(f)*exp(-2\pi ft/Q(f))/t \qquad (8)$$

where the lapse time $t>20$ sec. The envelope $A(f|t)$ was estimated by the seismogram rms computed in a moving window 1.8 sec long. $Q(f)$ and $A_0(f)$ estimators were obtained as a linear fit to the logarithm of the $RMS(t)$ in the 34 sec window. The records from the ISN stations were taken at distances up to 35km to ensure a coda wave window that starts usually at lapse times equal to twice the S-wave travel time. The important difference from Su et al. (1991) is that our dataset has average magnitudes 1.85 and 1.65, while they had 2.6 and 2.3 for earthquakes and explosions correspondingly, and, consequently, better (on average) SNR.

We controlled SNR by measuring rms in the 5 sec window, beginning at 10 seconds before P-wave arrival for noise and at lapse time 20 sec for the signal. Seismograms were band-pass filtered by the Butterworth filter. Figs. 20a through 20d show the results of $Q_0=Q/f$ measurements versus SNR for the frequencies $f=1.5$, 3, 6 and 10 Hz correspondingly - centers of frequency bands: 1-2, 2-4, 4-8 and 8-12 Hz. All values of $Q_0$ larger than 300 were zeroed.

From Fig. 20 we see that both event populations are indistinguishable for all of the frequency bands. The general feature is that very randomly scattered $Q_0$ estimates are large (on average) for SNR<10 and for a larger SNR the estimates are stabilized at a lower level, the same for both populations. For a fixed magnitude, explosions usually have a larger SNR at low frequencies (1-2 Hz). This may cause on average a smaller Q for explosions than for earthquakes (Fig. 20a) and may be interpreted erroneously as a discrimination result. $Q_0$ obtained in the range 50-80 for
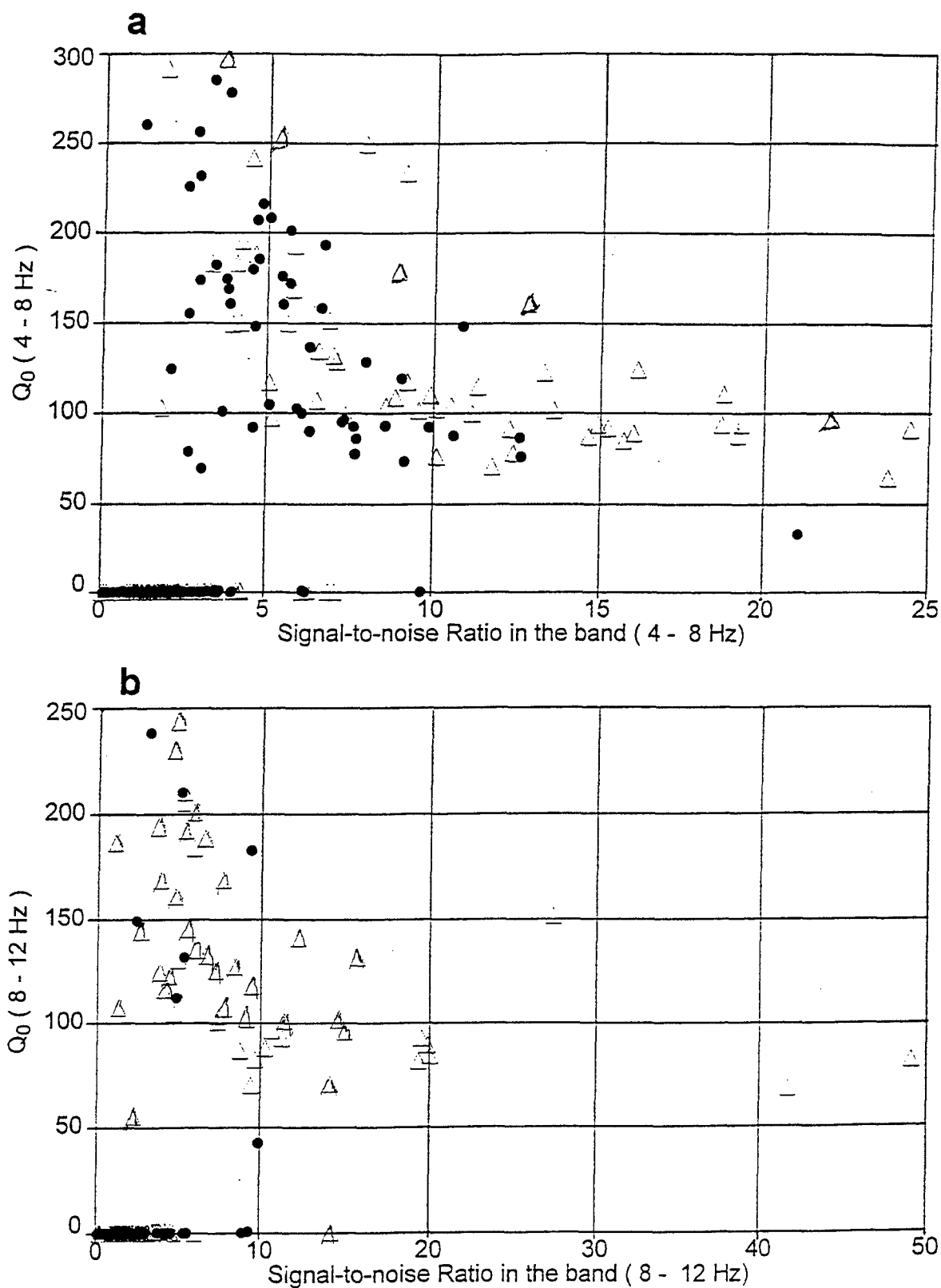
Figure 20. Coda analysis. Galilee events.Results of $Q_0$ = Q(f)/f measurements versus
SNR for the frequencies f = 1.5 (a), 3 (b), 6 (c) and 10 (d) Hz
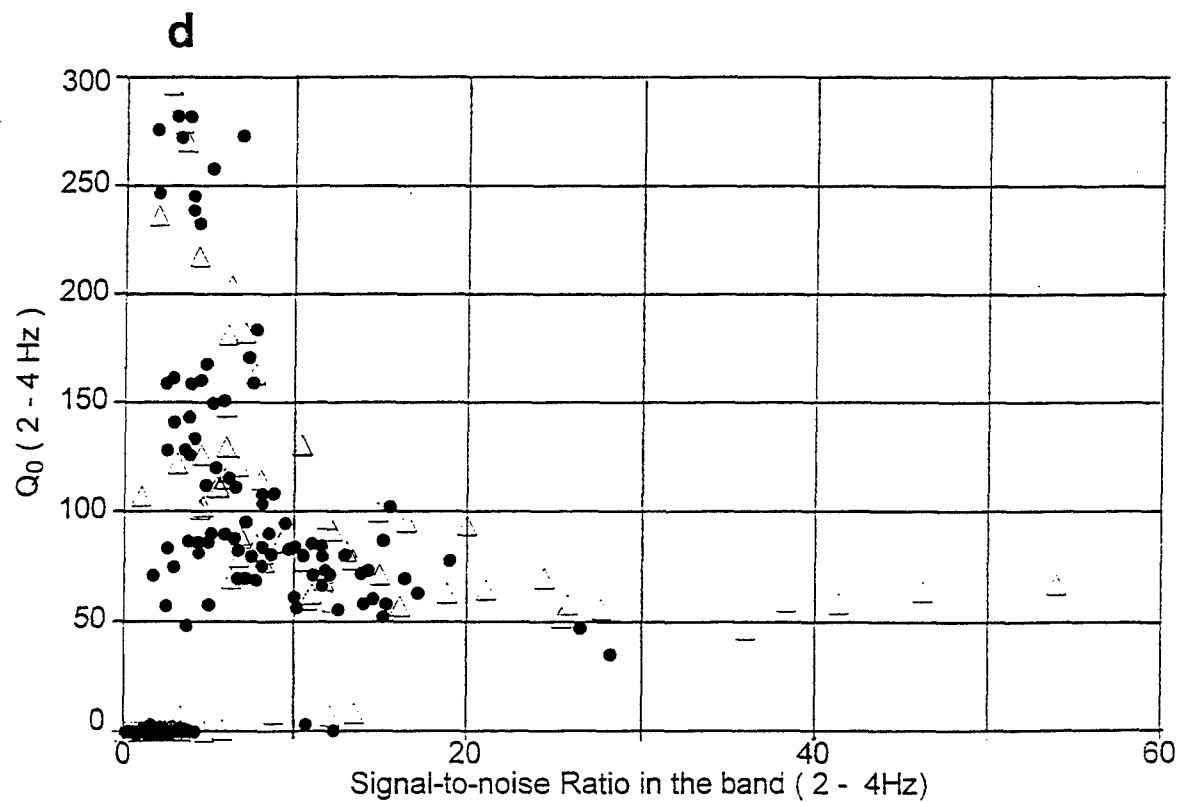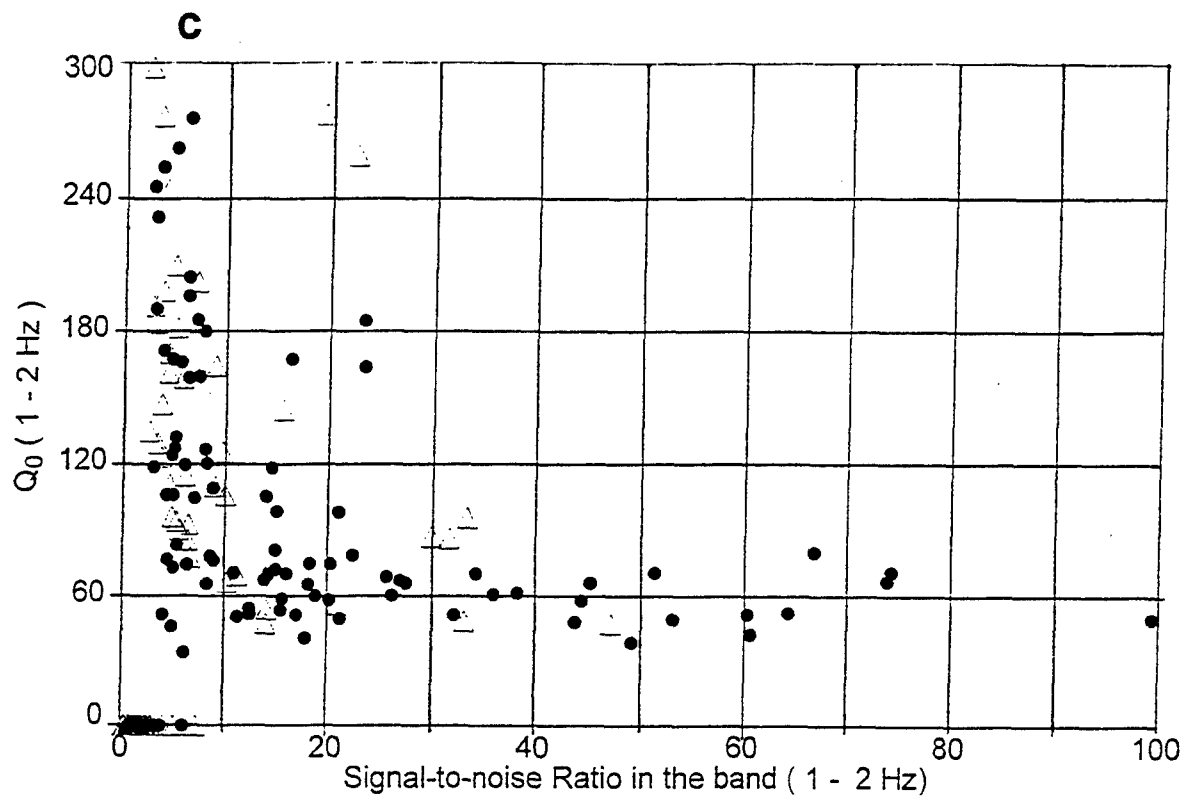(Δ - earthquakes, • - explosions).

**c**

**d**

Figure 20 (Continued)

the larger SNR represents values usually obtained for continental measurements (see, for example, van Eck, 1988).

Parameter $A_0(f)$, mentioned above, measures time-independent spectral amplitudes of coda carrying spectral peculiarities of the source. In van Eck (1988) and Hartse (1995), it is reported that coda spectra of explosions are richer in lower frequency energy as compared to earthquakes. Fig. 21 shows ratio $R = A_0(1.5\ Hz)/A_0(10\ Hz)$ measured for a data set of 28 earthquakes and 30 explosions at different stations; the event populations are highly overlapped being, on average, higher for explosions than for earthquakes. Averaging of R over a set of stations would improve the result, though false values will remain. As shown in the previous section, the spectral ratio of low-to-high frequency energy measured for the whole signal and averaged for a subset of stations appeared to be much more efficient in our study.

Discussion: The explosions usually have dominant surface waves propagating at the upper crust layer with high attenuation which should result in a low Q measured for coda at low frequencies. However, for the given Galilee dataset, Q values did not provide separation for the two populations, even for sufficiently strong events. It is possible that our region has a smaller surface wave attenuation than in the work of Su et al. (1991). Analysis showed that the method is very sensitive to the SNR and, even for regions where it does work, it cannot be applied to weak and/or remote seismic events with SNR<10.

## 3.5 DISCUSSION OF RESULTS

The results of the application of all the discriminants described above (except for coda discriminants which failed) to the Galilee dataset (see map in Fig. 2 and Table 1) are presented in Table 10.

All the discriminants show high resolving power. There is only one misclassification by the "C" criterion, event EG23 with C=0.76; one misclassification in King's CAP, event EG33 and 2 events, EG26 and EG37, have incorrectly positive LDF value for explosions. The rest: $R_E$, semblance and ANN output, showed a 100% success rate, without overlapping in the earthquake and explosion populations.

Note that the above mentioned earthquakes from the Kinneret region (e.g. QG23, QG25, QG28) and explosions (EG3, EG8), characterized as marginal events according the spectral ratio $R_E$, "semblance" and "cross-correlation" criteria in the 1-12 Hz band, are reliably identified by the rest of the
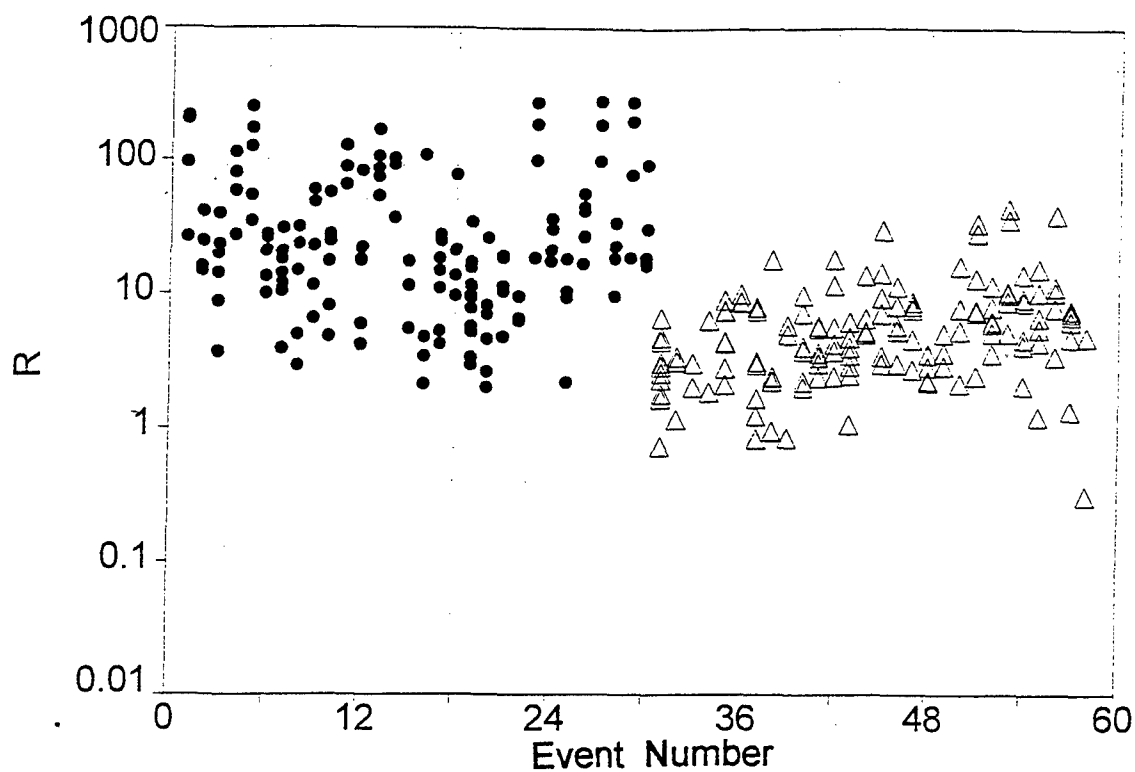
50

Figure 21. Ratio of coda spectral amplitudes R = $A_0$(1.5 Hz)/ $A_0$(10 Hz) measured for the Galilee data set of 28 earthquakes (Δ) and 30 explosions (•) at different stations.

discriminants. Hence, mutual application of the different discriminants evidently increases identification resolving power.

Successful discrimination can be attributed mostly to the dominance of low frequency S and surface waves for the very shallow events due to propagation effects in thick sediments present in the region and the ripple-firing phenomenon manifested in that frequency band. Though signal and noise spectra overlap a great deal around 1 Hz (see Fig. 11a), the discriminants showed high robustness even for very weak events with $M_L < 1.0$ (see Table 1) and a poor SNR for most of the stations.

# 4. APPLICATION OF SPECTRAL RATIO, SEMBLANCE AND VELOGRAM DISCRIMINATION PROCEDURES TO THE SOUTHERN DATASET

Three of the described discriminants were tested on earthquakes and quarry blasts from the southern Dead Sea basin and Negev desert (see map, Fig. 3 and Table 3); values of discriminating parameters are presented in Table 11.

Spectra were calculated for 10 selected ISN stations shown on the map (the distance range 10-150km). Velogram analysis was conducted in a broader range: 10-250km. Examples of typical blast and earthquake recordings and appropriate spectra are presented in Figs. 22 and 23. For most quarry blasts a very clear deep spectral modulation is observed as evidence of high regularity of blasting patterns at the Negev phosphate quarries (see also the remark in Section 5.2). A new feature (compared to the Galilee events), a distinct Rg wave group (see Fig. 22), may be observed on many seismograms of blasts.

The results of joint application of the two spectral discriminants (ratio and semblance/cross-correlation) are shown on Fig. 24, demonstrating almost full separation of the two classes of seismic events. There is only one (of 42 events) evident outlier, earthquake QS9 with an anomalously high average ratio $R_E = 10.6$, smb=0.82 and cor=0.78 and one marginal event QS15 (smb=0.64 and cor=0.60).

Results of velogram analysis are shown on Fig. 25. Two outliers are encountered: earthquake QS10 and blast ES2 (see Table 11). Considering all three discriminants jointly and using the majority voting rule (Wuster, 1993), events QS10, ES2 and QS15 can be correctly classified. The only outlier, nocturnal event QS9, is located in the southern Dead Sea basin near
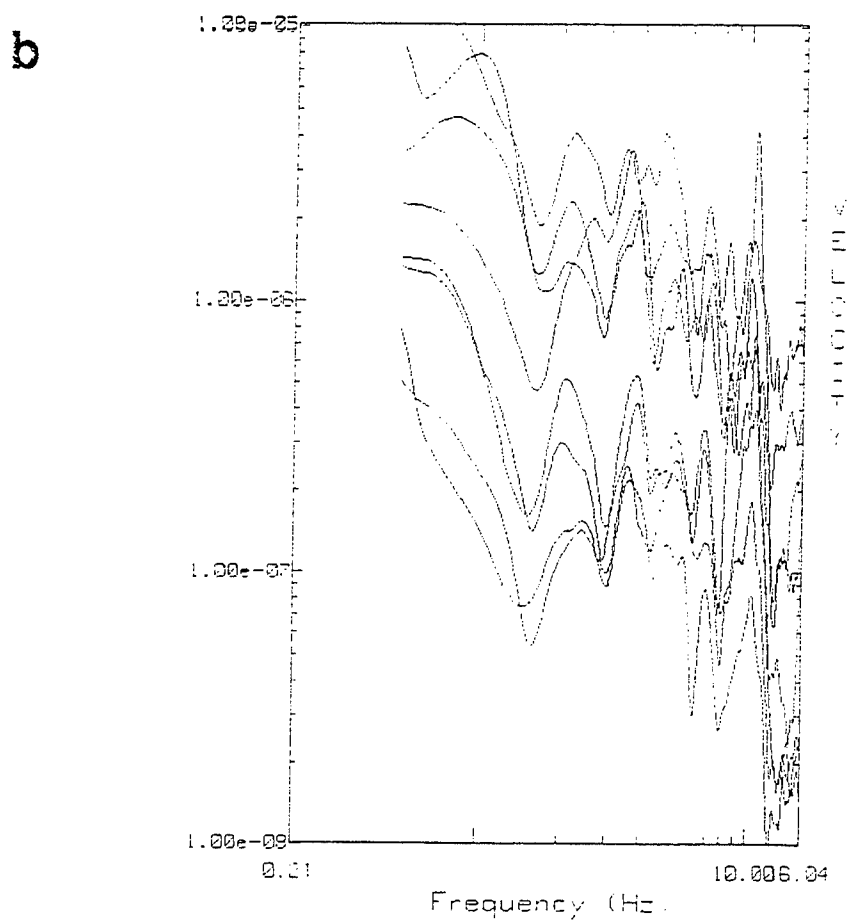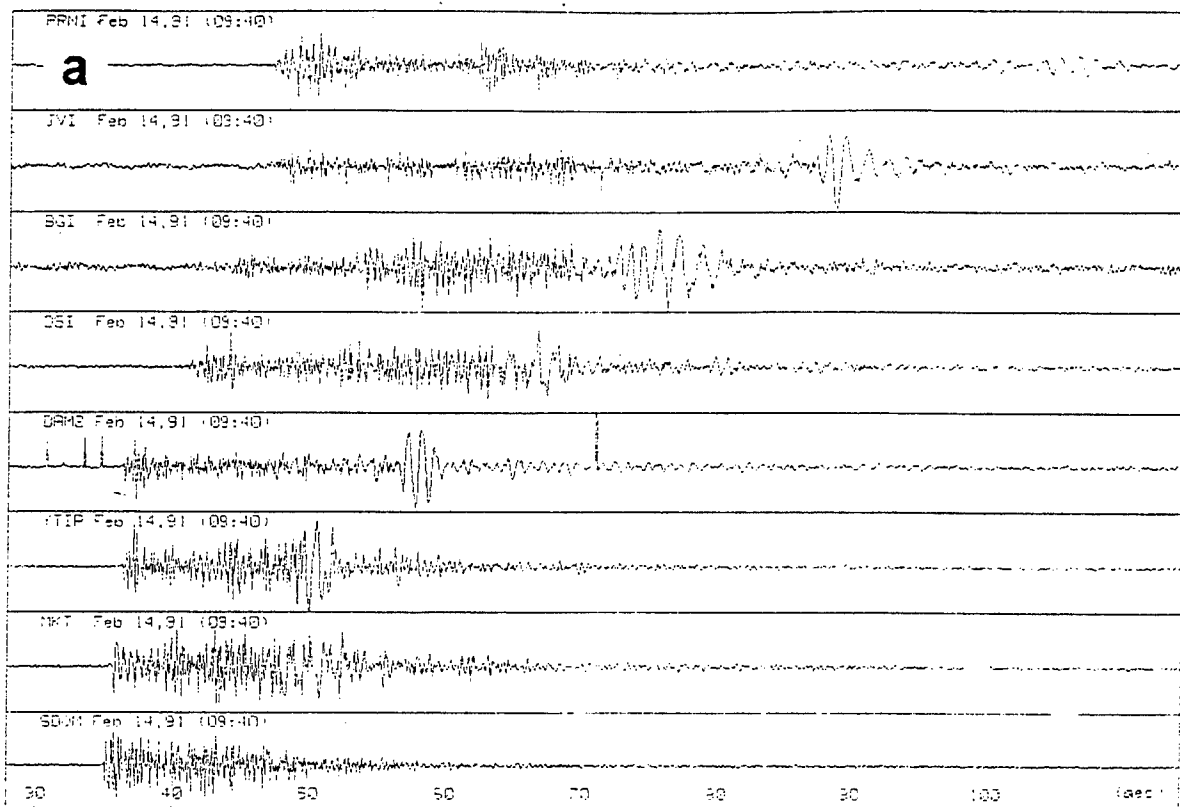
Figure 22. Example of recordings from the Negev quarry blast ES6 (a)
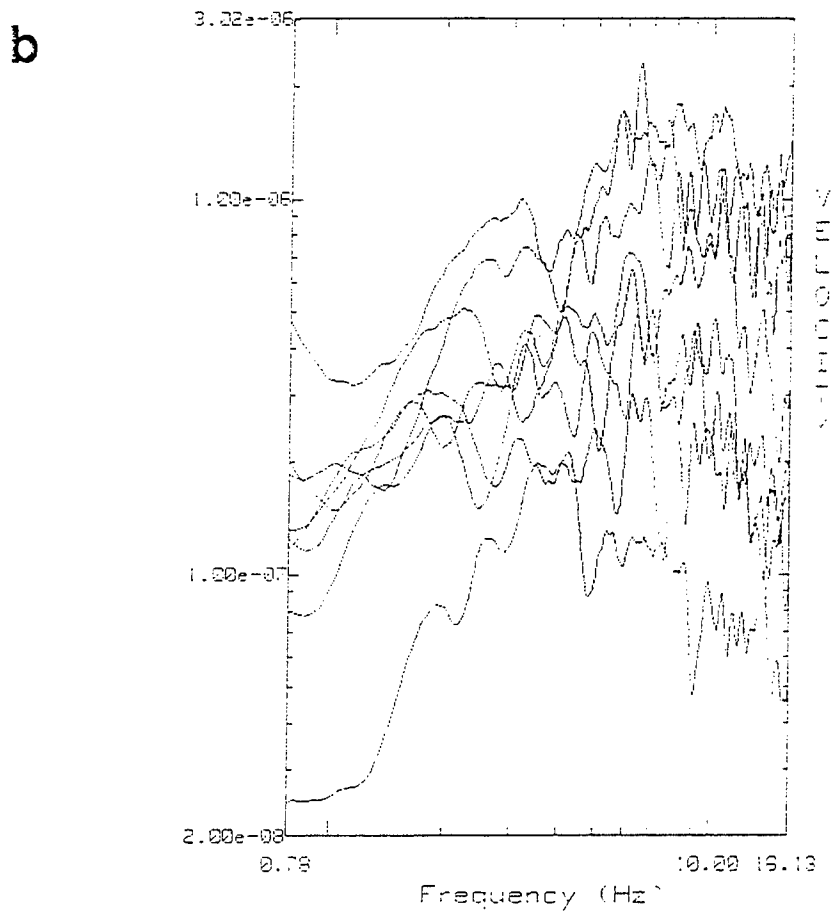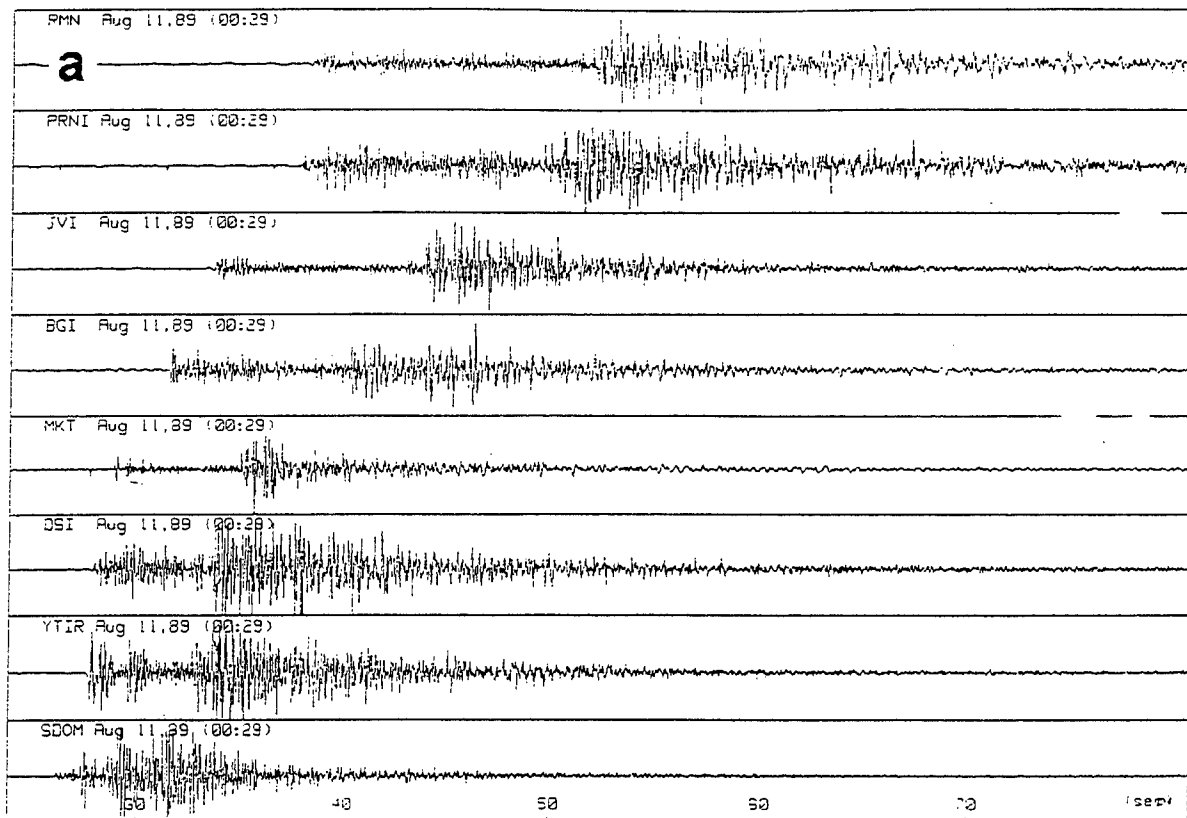showing very clear spectral modulation (b).

53

Figure 23. Example of recordings from the Dead Sea earthquake QS3 (a) showing non-coherency of spectral shapes (b).
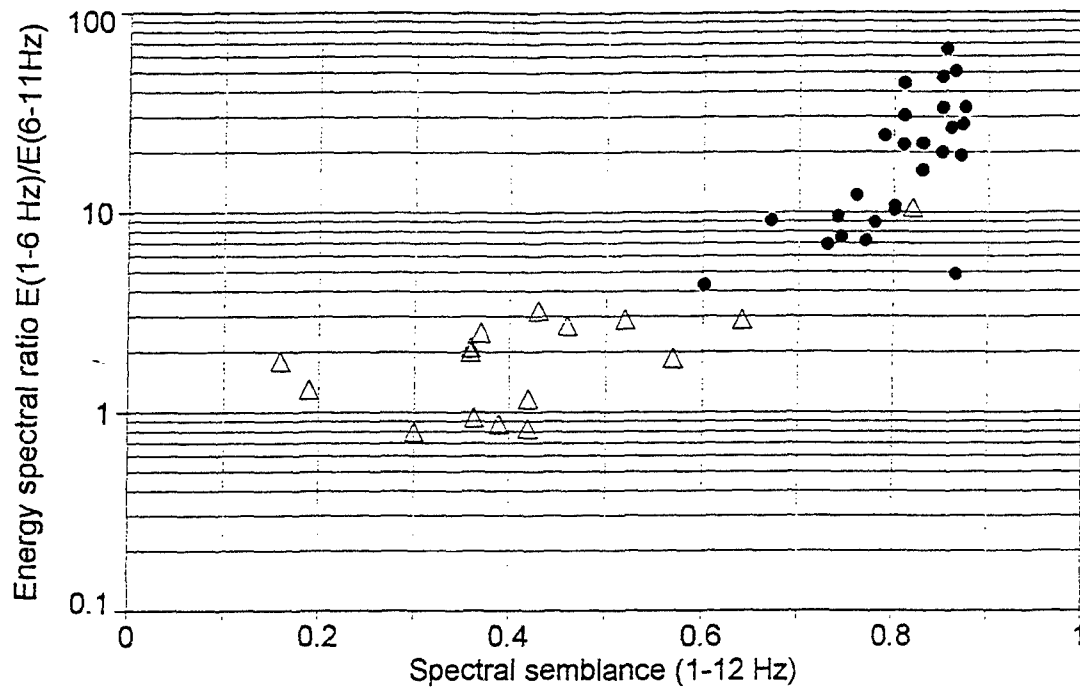
Dead Sea/Negev dataset



Figure 24. Discrimination results for the Southern dataset: semblance versus energy ratio (Δ - earthquakes, • - quarry blasts).
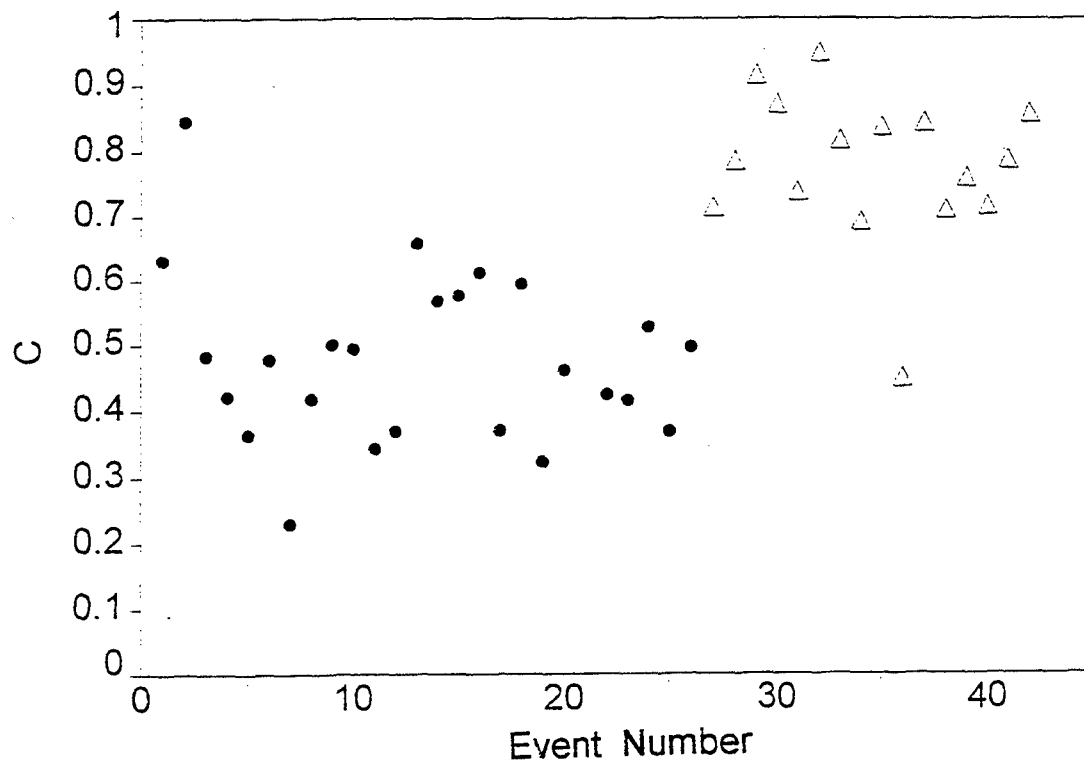


Figure 25. Velogram analysis. Dead Sea/Negev region. Discrimination parameter "C" for 16 earthquakes (Δ) and 26 explosions (•).

Table 11. Discrimination resuts for the Southern dataset.

| Ev. | C,km/s | Re | cor. sembl. | |
|-----|--------|------|------|------|
| | 1-10Hz | 1-11Hz | 1-12Hz | |

### Quarry blasts

| Ev. | C,km/s | Re | cor. | sembl. |
|-----|--------|------|------|------|
| ES1 | 0.63 | 19.3 | 0.85 | 0.87 |
| ES2 | 0.84 | 10.3 | 0.80 | 0.80 |
| ES3 | 0.48 | 8.9 | 0.75 | 0.78 |
| ES4 | 0.42 | 12.2 | 0.73 | 0.76 |
| ES5 | 0.36 | 10.7 | 0.77 | 0.80 |
| ES6 | 0.48 | 4.3 | 0.56 | 0.60 |
| ES7 | 0.23 | 47.4 | 0.83 | 0.85 |
| ES8 | 0.42 | 20.0 | 0.82 | 0.85 |
| ES9 | 0.50 | 9.5 | 0.71 | 0.74 |
| ES10 | 0.49 | 4.9 | 0.8 | 0.86 |
| ES11 | 0.34 | 65.3 | 0.83 | 0.85 |
| ES12 | 0.37 | 33.6 | 0.85 | 0.87 |
| ES13 | 0.66 | 7.5 | 0.71 | 0.74 |
| ES14 | 0.57 | 26.5 | 0.84 | 0.86 |
| ES15 | 0.58 | 22.1 | 0.8 | 0.83 |
| ES16 | 0.61 | 21.8 | 0.77 | 0.81 |
| ES17 | 0.37 | 50.7 | 0.84 | 0.86 |
| ES18 | 0.59 | 6.9 | 0.7 | 0.73 |
| ES19 | 0.32 | 30.4 | 0.79 | 0.81 |
| ES20 | 0.46 | 9.1 | 0.63 | 0.67 |
| ES21 | -0.67 | 44.0 | 0.78 | 0.81 |
| ES22 | 0.42 | 16.3 | 0.81 | 0.83 |
| ES23 | 0.42 | 33.2 | 0.81 | 0.85 |
| ES24 | 0.53 | 24.2 | 0.74 | 0.79 |
| ES25 | 0.37 | 27.6 | 0.85 | 0.87 |
| ES26 | 0.50 | 7.2 | 0.75 | 0.77 |

### Earthquakes

| Ev. | C,km/s | Re | cor. | sembl. |
|-----|--------|------|------|------|
| QS1 | 0.71 | 2.1 | 0.28 | 0.36 |
| QS2 | 0.78 | 2.5 | 0.29 | 0.37 |
| QS3 | 0.91 | 0.83 | 0.35 | 0.42 |
| QS4 | 0.87 | 1.3 | 0.06 | 0.19 |
| QS5 | 0.74 | 0.94 | 0.28 | 0.36 |
| QS6 | 0.94 | 1.85 | 0.51 | 0.57 |
| QS7 | 0.82 | 1.16 | 0.34 | 0.42 |
| QS8 | 0.69 | 0.87 | 0.29 | 0.39 |
| QS9 | 0.84 | 10.6 | 0.78 | 0.82 |
| QS10 | 0.45 | 3.2 | 0.29 | 0.43 |
| QS11 | 0.84 | 2.9 | 0.47 | 0.52 |
| QS12 | 0.72 | 2.7 | 0.41 | 0.46 |
| QS13 | 0.76 | 0.8 | 0.2 | 0.3 |
| QS14 | 0.72 | 2.0 | 0.29 | 0.36 |
| QS15 | 0.79 | 2.9 | 0.60 | 0.64 |
| QS16 | 0.86 | 1.8 | 0.04 | 0.16 |

the shore (see map, Fig. 3) and lies at depth H=0.0±1.4km (mislocation estimates are also very small, dX,dY<1km). An attempt to improve location did not change the result. Possibly, the very shallow source of this earthquake led to low-frequency spectral content of the seismograms and, hence, caused anomaly values of spectral discriminants.

# 5. APPLICATION OF SPECTRAL RATIO AND SEMBLANCE TO MEDITERRANEAN AND DEAD SEA UNDERWATER EXPLOSIONS, JORDANIAN QUARRY BLASTS AND SINGLE QUARRY BLASTS

Only spectral discriminants were applied to distinctive man-made events:

a) UWE in the Mediterranean (illegal fishing therefore no ground-truth information); and

b) a set of single UWEs in the Dead Sea for seismic profiling, single blasts at Israeli quarries Revaya and Har Nitzim and ripple fired blasts at a Jordanian quarry (all with ground-truth information) (see maps in Figs. 3, 5 and 6 and Tables 3-6).

## 5.1 UWE

Detonations in deep water produce seismic waves bearing spectral features caused by a source (bubbling phenomenon) and path propagation effect (reverberations). Gitterman and Shapira (1994) gave a detailed description of low-frequency azimuth-invariant spectral modulation observed from ISN recordings of UWE off the coast of the Levant and similar to ripple firing. They also showed that source-effect interference is significant, but of a different physical nature, i.e. interference of gas bubble oscillations which are produced by the interaction of the expanding volume of explosion-generated gases and hydraulic pressure.

This bubbling effect produces a complete harmonic series of spectral maxima (unlike odd harmonic series due to the vertical reverberation in the water layer near the source) with a fundamental frequency $f_{1b}$, which is characterized by the detonation depth, d(m) and the explosive yield, W (kg of TNT) (see, for example, Willis, 1963):

$$f_{1b} = (d+10)^{5/6}/(2.1W^{1/3}); \quad f_{nb} = nf_{1b}, \quad n = 1,2, \ldots \qquad (9)$$

57

Remarkable examples of spectral maxima series up to the fifth order due to the bubbling phenomenon were presented by Gitterman and Shapira (1994) for UWE in the Tyre region, with high coherency of spectral shapes at different ISN stations. These effects, not observed in the case of earthquakes (occurring off the coast) can be utilized in the semblance discrimination procedure. Here we present only one example of an UWE (see Fig. 26), showing long trains of low-frequency surface waves on seismograms owing to bubbling and reverberations (and causing overestimation of local magnitudes).

Similar wave trains are observed on seismograms of experimental Dead Sea explosions (see example for the largest explosion, EU1 on Fig. 27). Bubbling actually affects all types of recorded seismic waves throughout the whole seismogram, however it is better manifested in the initial body-wave portion (P and P-coda) of the seismogram, which is virtually free from reverberations and low-velocity channelling effects: Fig. 27b shows a complete harmonic series (3, 6 and 9 Hz) due to the bubbling effect. Spectra of the whole signal are much more complicated and mixed with reverberations maxima (Fig. 27c), however low-frequency SM minima (4.5 and 7.5 Hz), corresponding to the bubbling interference, are sharpened and expressed more distinctly.

Using ground truth information (Table 5) and taking into account the high density of salt water in the Dead Sea ($r=1.4$ $gr/cm^3$) (correction to greater depth), we estimated from Eq. 9 the bubbling fundamental frequency for the explosion EU1, $f_{1b} \approx 3.2$ Hz, corresponding well to the observed value $f_{1b} \approx 3.0$ Hz (Fig. 27b). (Without going into detail, we would like to note that this $f_{1b}$ value is possibly very close to the reverberation fundamental frequency $f_{1r} = V_0/4H$, for the sound velocity in the Dead Sea $V_0 \approx 1600-1700$ m/sec and an average water depth $H \approx 150-250$m, causing merging of the two first maxima of bubbling and reverberation).

The average energy spectral ratio and spectral coherency statistics were applied to selected off-shore events from the Tyre region and single explosions in the Dead Sea for seismic profiling; results are shown on Fig. 28.
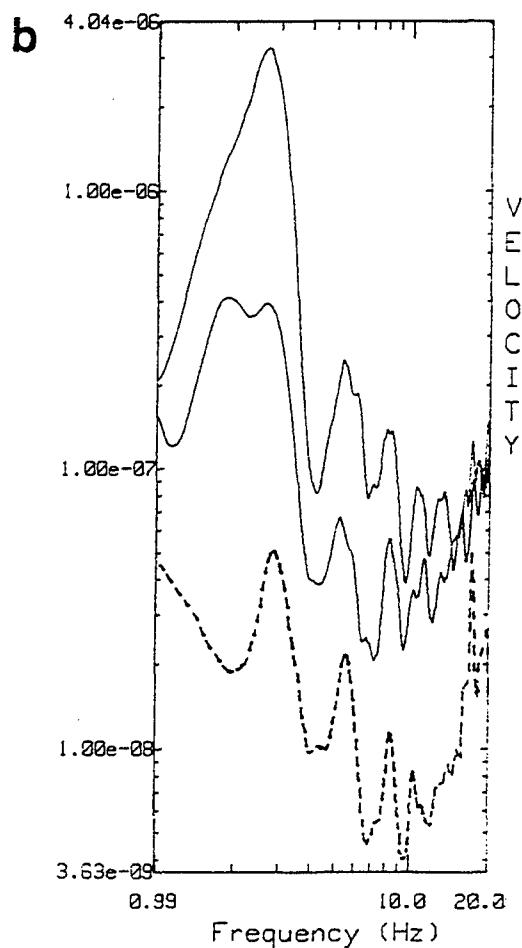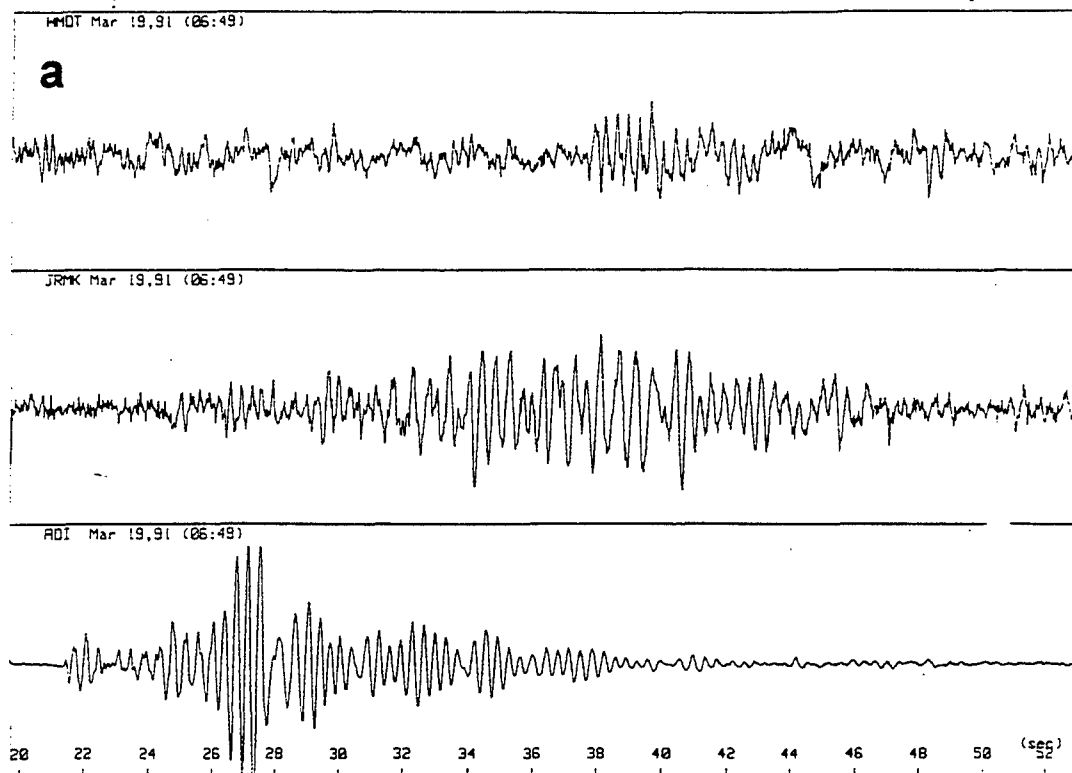
Figure 26. Example of underwater explosion recordings from the Tyre region (EU7) (a) showing a complete harmonic series in the spectra of the whole signal (b).
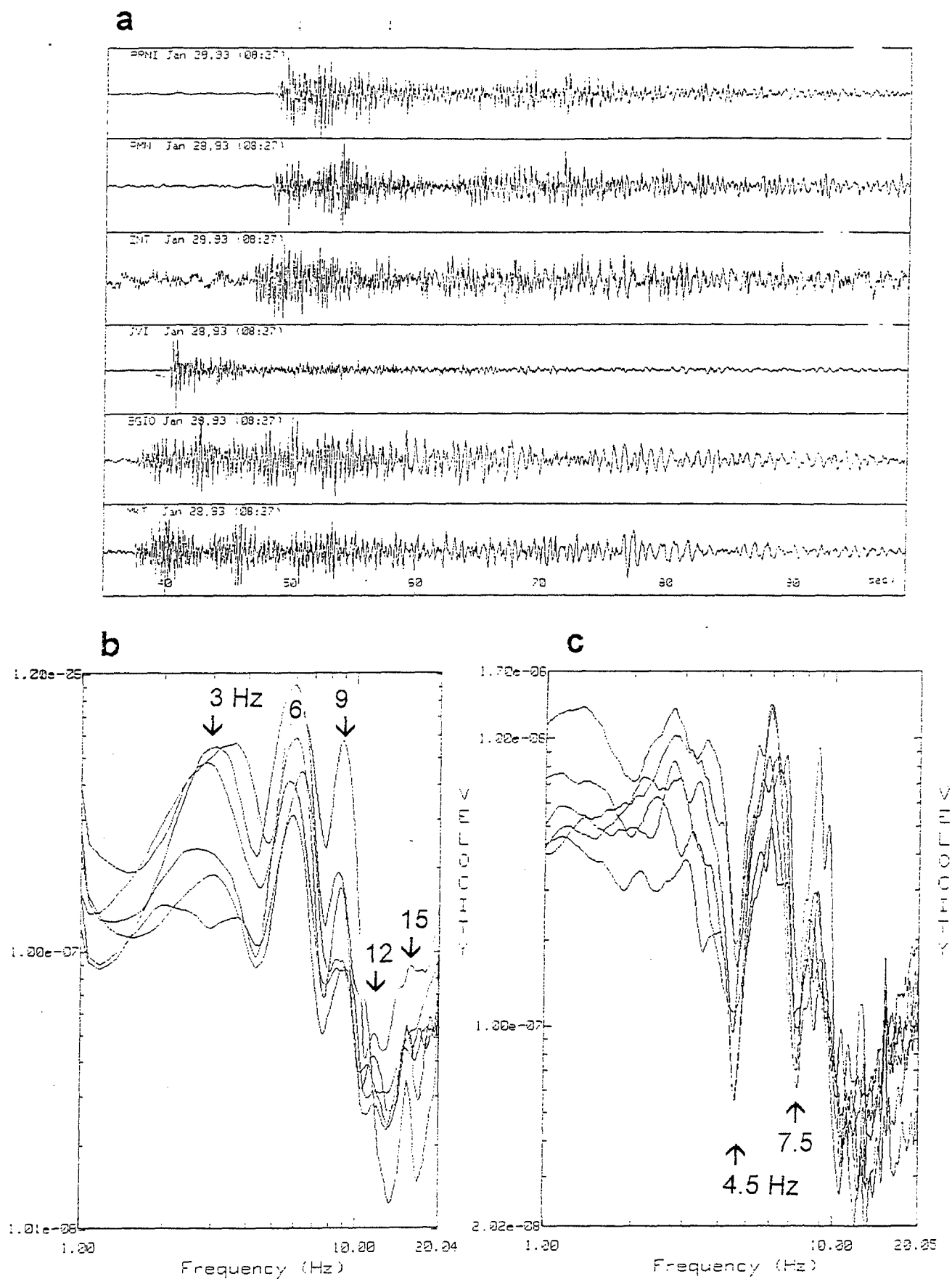
Figure 27. Example of the Dead Sea experimental underwater explosion EX1 with charge weight W = 304 kg: (a) recordings; (b) spectra of the first 8 sec of P and P-coda waves; (c) spectra of the whole signal (about 60 sec).
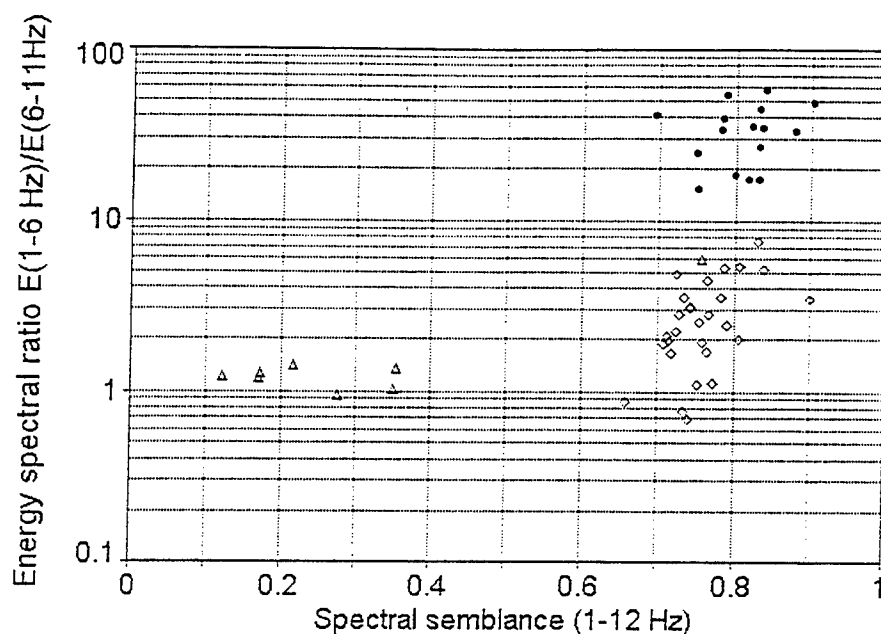
60

**Figure** 28. Discrimination results for the Tyre region seismic events and Dead Sea experimental underwater explosions: semblance versus energy ratio ($\Delta$ - earthquakes. • - Mediterranean UWE. ◊ - Dead Sea UWE).
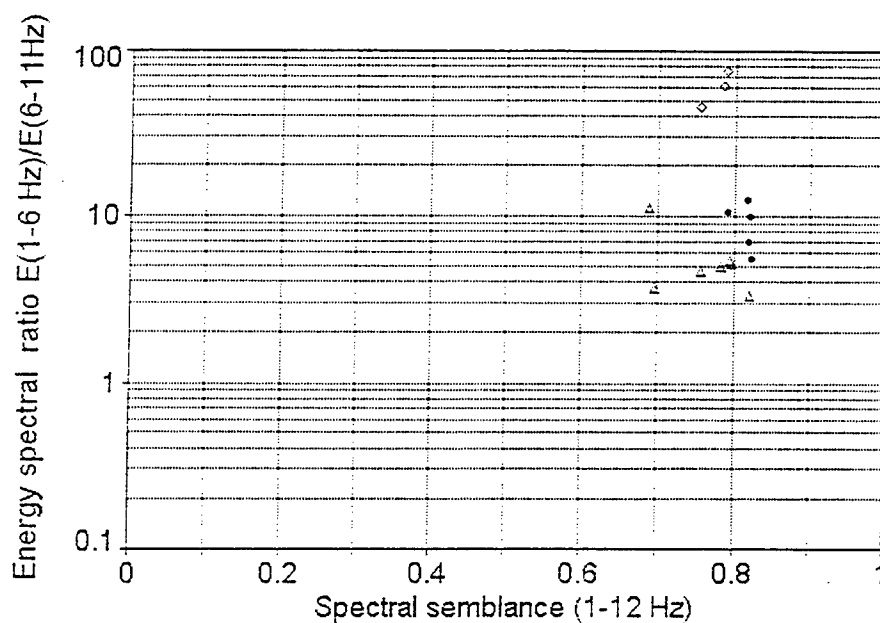


**Figure** 29. Discrimination results (semblance versus energy ratio) for Jordanian ripple-fired quarry blasts (•), single quarry blasts at Har Hitzim ($\Delta$) and Revaya (◊).

## 5.2 QUARRY BLASTS

Seismograms and spectra of one of the ripple-fired blasts (EJ1) from a Jordanian quarry (see Table 6) are shown in Fig. 30. We do not have detailed information regarding patterns of blasting practice, but we may assume a high regularity of shot parameters along the bench owing to very deep spectral minima (nulls). Variance (deviation) of delays and delayed charge weights (in groups of shot holes) causes a reduction in modulation depth or smoothing of sharp spectral troughs and peaks (Gitterman and van Eck, 1993).

The average energy spectral ratio and spectral coherency statistics were calculated for the Jordanian quarry blasts and selected single blasts from two Israel quarries (see Table 6); results are shown in Fig. 29 and Table 12. For comparison, we also took several south earthquakes located relatively close to the blasts (Table 6).

Seismograms and spectra of two single blasts from two Israeli quarries (see Table 6) are shown in Fig. 31: an obvious difference in waves forms and spectral contents for the two examples is observed. More detailed analysis of spectral and kinematic features of single quarry blasts affecting discrimination performance, will be carried out in the subsequent stage of the project. The single blasts database will, if necessary, be enlarged and additional analysis, relating to "yield-magnitude" and "amplitude (energy)-scaled distance" relationships is assumed.

## 5.3 DISCRIMINATION RESULTS

Values of spectral discriminating parameters are presented in Table 12. The values for Jordanian quarry ripple-fired blasts are close to those estimated for the Galilee and Negev regions (see Figs. 13 and 24). The spectral ratio for Har Nitzim quarry single blasts is low, unlike that for Revaya quarry blasts. This may be explained by the quite different character of wave groups and frequencies, as clearly demonstrated in Fig. 31, caused by the uppermost local geology near the quarries.

The semblance and cross-correlation values for single blasts are lower than for ripple fired blasts but higher than for earthquakes. A possible explanation is that single shot spectra do not possess interference modulation caused by delays, but are, in actual fact, point sources and radiated waves have a weak azimuthal dependence, unlike line sources of earthquakes subjected to the directivity effect (see Section 3.1.4). Apart from the left hand side of a single blast spectra (at different stations)

Table 12. Discrimination results for the Jordanian
and single quarry blasts.

| Event | Ratio Re 1 - 11 Hz | sembl. 1 - 12 Hz | correl. |
|-------|------|------|------|
| | | | |
| **Jordanian quarry blasts** | | | |
| | | | |
| EJ1 | 9.8 | 0.82 | 0.78 |
| EJ2 | 10.4 | 0.79 | 0.76 |
| EJ3 | 12.4 | 0.82 | 0.80 |
| EJ4 | 5.5 | 0.82 | 0.79 |
| EJ5 | 6.9 | 0.82 | 0.79 |
| | | | |
| **Single quarry blasts** | | | |
| | | | |
| SB1 | 60.7 | 0.784 | 0.712 |
| SB2 | 74.8 | 0.789 | 0.747 |
| SB3 | 45.9 | 0.755 | 0.673 |
| SB4 | 4.9 | 0.782 | 0.728 |
| SB5 | 5.1 | 0.797 | 0.729 |
| SB6 | 4.6 | 0.757 | 0.696 |
| SB7 | 11.2 | 0.688 | 0.584 |
| SB8 | 5.4 | 0.794 | 0.726 |
| SB9 | 3.3 | 0.820 | 0.730 |
| SB10 | 3.7 | 0.697 | 0.596 |
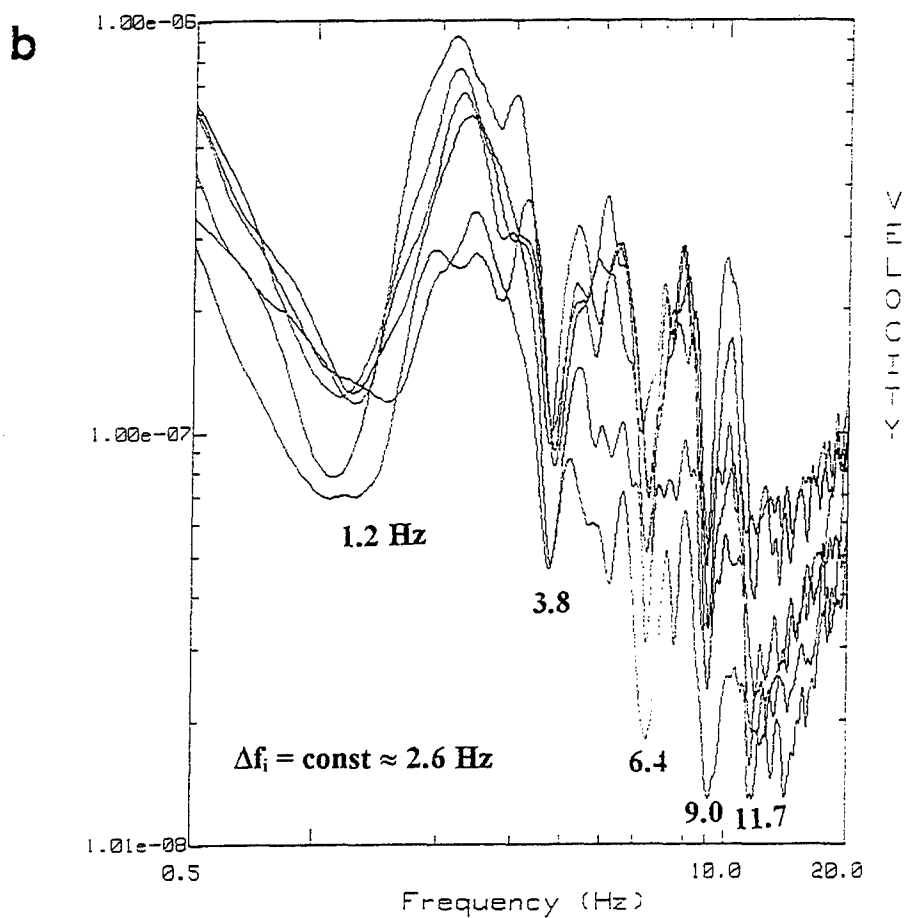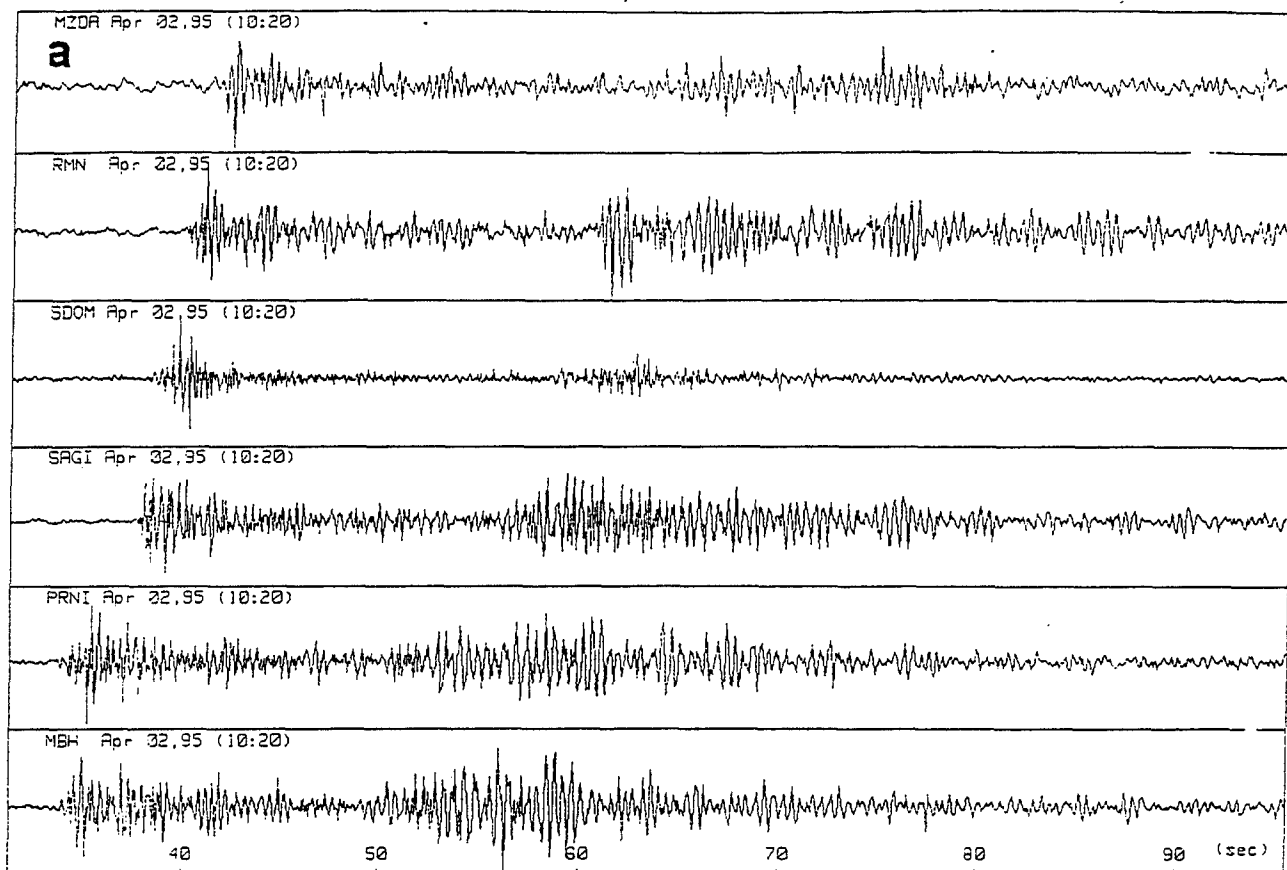
Figure 30. Seismograms (a) and spectra (b) of the ripple-fired blast EJ1 from a Jordanian quarry (distance range 114-168 km, azimuth range 260°-340°, t ≈ 60 sec).
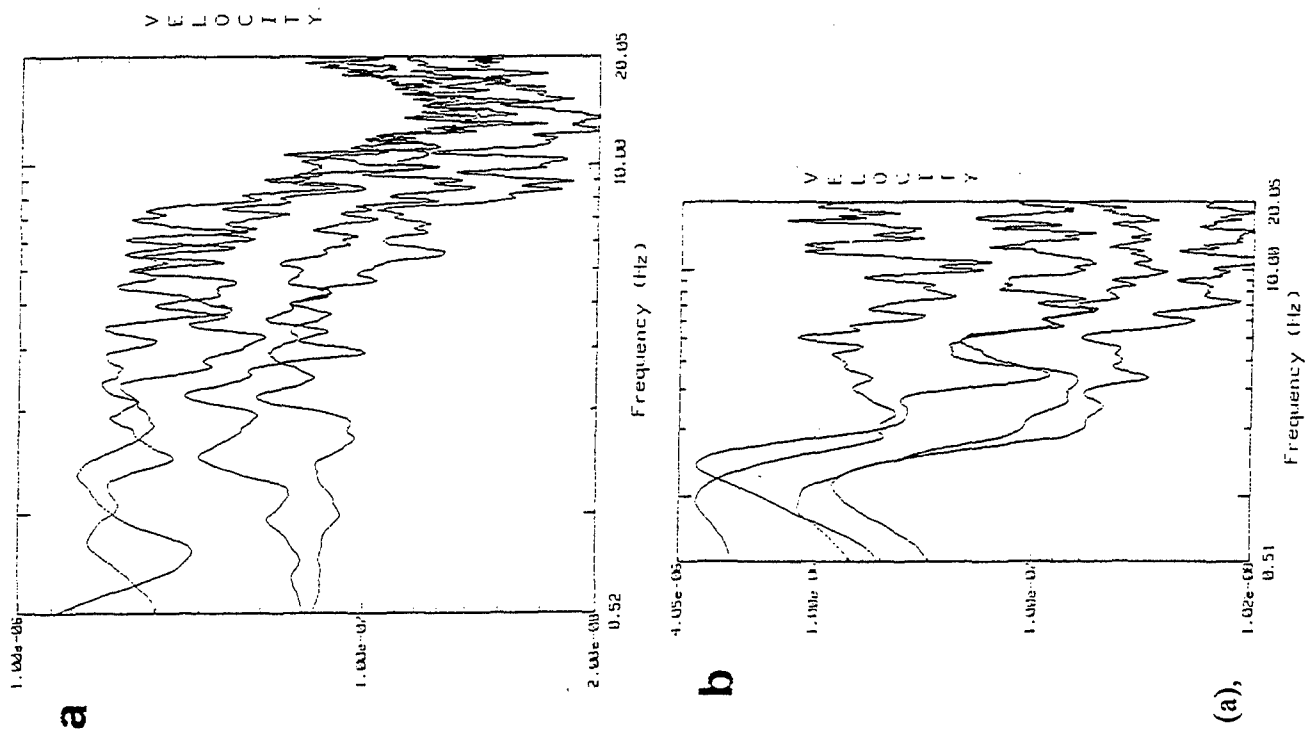
Figure 31. Seismograms and spectra of single quarry blasts SB5 (Har Nitzim) (a), and SB2 (Revaya) (b).

show some coherency due to low frequency surface waves (Fig. 31) and make a significant contribution to semblance and cross-correlation statistics.

## 6. APPLICATION OF VELOGRAM ANALYSIS TO THE GILAD DATASET

The velogram technique previously described was applied to the data set of the Gilad region (see Section 2.8), consisting of 15 presumed explosions and 19 earthquakes. The results of computation of the "C" discriminator are shown in Table 7 and Fig. 32a. Initially, three events, ED4, ED8 and ED13, from the presumed explosions population were classified as earthquakes with C values equal to 0.91, 0.69 and 0.70, correspondingly, according the C=0.69 criteria chosen above. No errors were encountered in the earthquakes set. Suspicious events QD7 and QD13, close to the explosion locations cluster, were reliably estimated as earthquakes with a C value equal to 0.81 and 0.97, correspondingly. The time and spectral domain visual analysis of the events agrees with that conclusion.

Returning to the three wrongly classified explosions, we found that mistakes encountered can be easily corrected provided some simple additional criteria are introduced. On Fig. 33a shows $V_m(R)$ curves of the three explosions. The curve for event ED4 has a large anomaly value of S group velocity $V_m=3.9$ km/s at a distance of 29km, owing to significant interference (unusual for both earthquakes and explosions) of P-wave coda with S-wave train. In the case of ED13, the value $V_m=2.1$ km/s is too small both for earthquakes and explosions at a distance of 193km. In the third case (event ED8), we deal with a relatively low $V_m=2.7$ km/s at a distance of 180km.

If a kind of appropriate distance-dependent confidence interval (as additional criteria) is chosen, the anomaly points may be ignored. Excluding the mentioned points (stations) from velograms of the corresponding events, we obtained corrected $V_m(R)$ curves (Fig. 33b) and C values, presented in the C* column of Table 7. After correction, events ED4 and ED13 fit the criteria with C values of 0.62 and 0.67 and event ED8 is of marginal character. The final results are shown also in Fig. 32b.
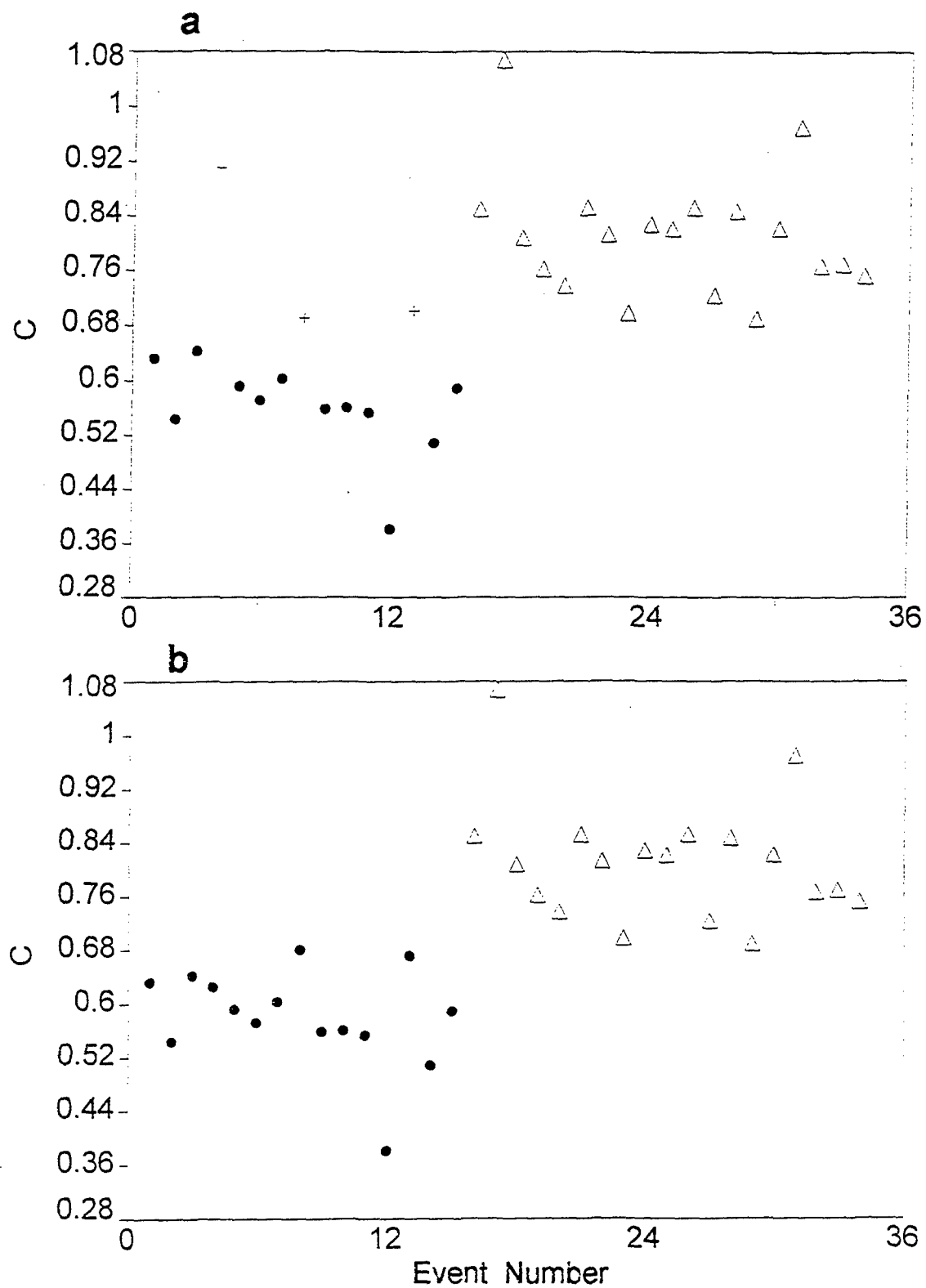
Figure 32. Velogram analysis. Gilad region. Discrimination parameter "C" for 19 earthquakes ($\Delta$) and 15 explosions ($\bullet$), before (a) and after (b) correction. Three misclassified explosions ($\div$) are shown.
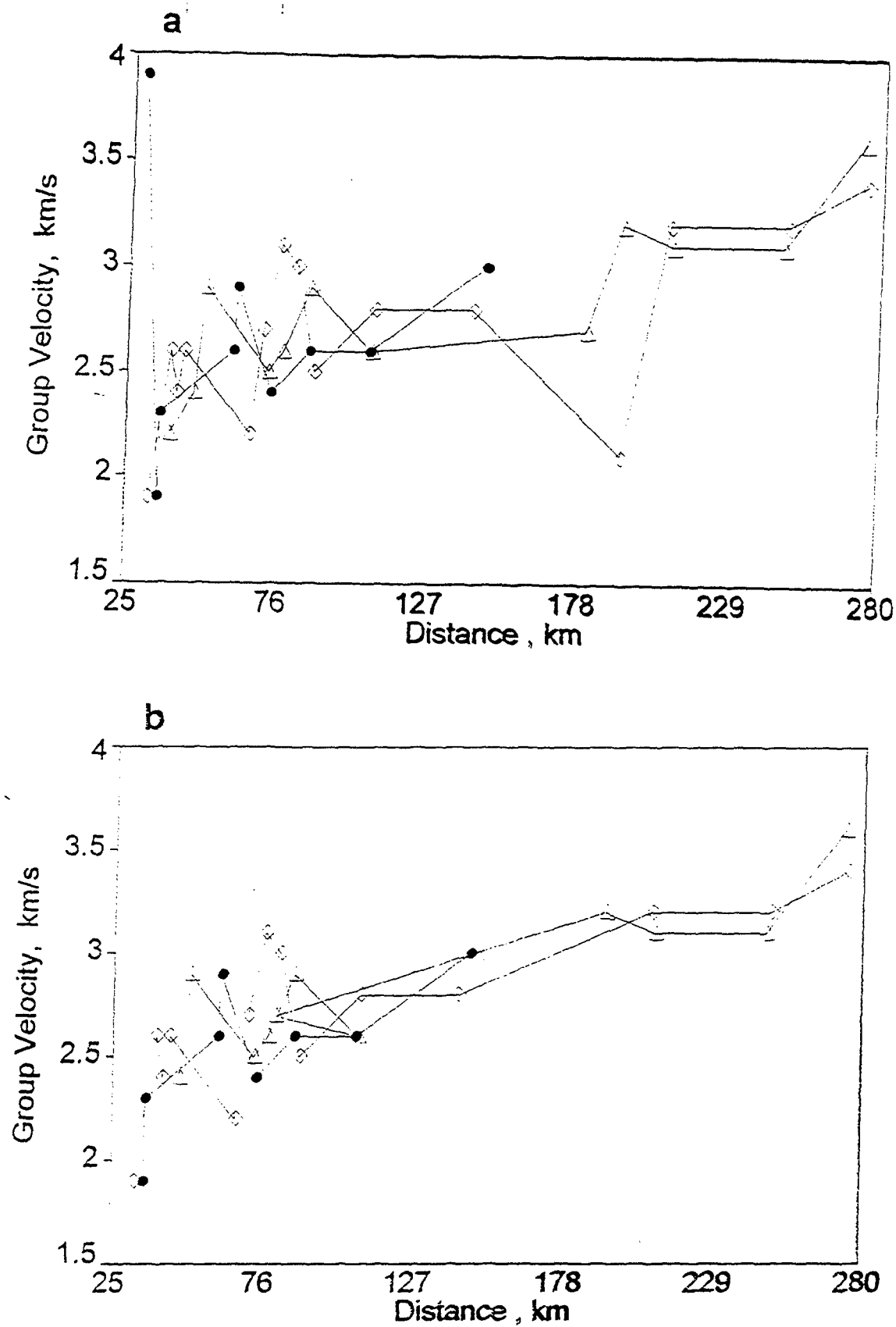
Figure 33. Velogram analysis. Gilad region. $V_m(R)$ curves of the 3 initially misclassified Gilad explosions, before (a) and after (b) correction.

# 7. INVESTIGATION OF A SIMPLIFIED SMALL APERTURE SEISMIC ARRAY.

A simplified small aperture (2km), short period seismic array consisting of 13 stations and three concentric circles was deployed in the Negev in June 1995 (Fig. 34). Preliminary results show good improvement of the signal-to-noise ratio and stable detection of week regional events (Fig. 35) using the standard beamforming technique. However, results previously obtained from an experimental micro-array we tested in the Galilee, show that the classic algorithms do not provide sufficient accuracy in resolving the azimuth and apparent velocities (Malitzky and Shapira, 1994a,b). Small variations (0.2-0.5 sec) of the start time or window length selected for F-K analysis can lead to 8-10 variations in the arrival azimuth determinations (Fig. 36 and 37).

It should be noted that we are aiming for an accuracy of less than 5° (standard deviation) in azimuth determination. These results lead us to seek another approach. We are continuing to develop and examine an interactive process based on phase correlation analysis (Gelchinsky and Krauklis, 1964, Gelchinsky et al., 1985). To reduce hardware costs, we have invested a great deal of effort in developing software for personal computers.

It has been demonstrated that behavior of the phase correlation function is very sensitive for detection of week seismic signals in the case of relatively high noise level (Fig. 38). Preliminary results show that the new procedure provides enhanced azimuth determinations with an accuracy of ±1° and precise identification (better than 0.1 sec) of the first P and S arrivals (Fig. 39 and 40) (Malitzky and Shapira, 1995).

The operation and maintenance of the micro-array was financed by IPRG. Unfortunately, owing to significant budgetary cuts, the IPRG Seismology Division had to dismantle the micro-array. We hope to obtain the necessary funds, possibly during 1997, to re-install the micro-array at a different location and continue this investigation.

$$R = R_{min} * \alpha^n \qquad ,n=0,1,2$$
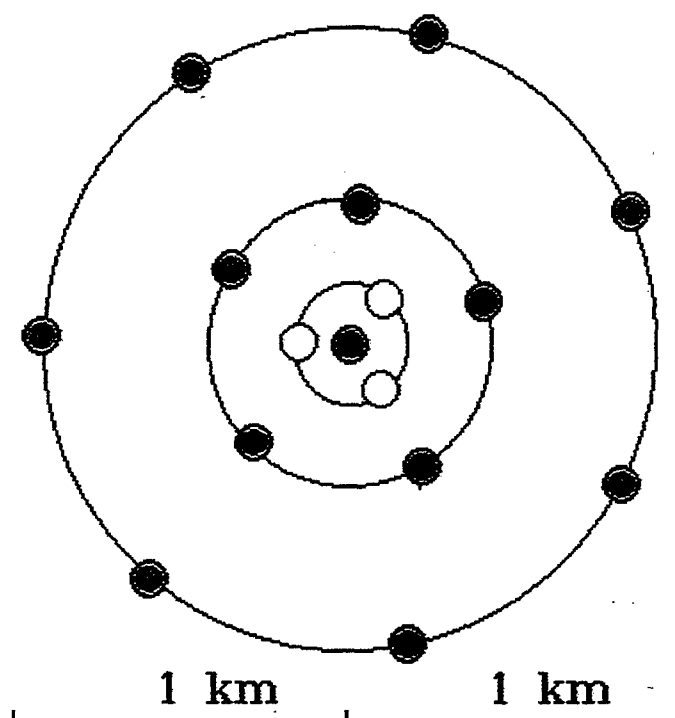
$$R_{min} = 199 \text{ m}$$

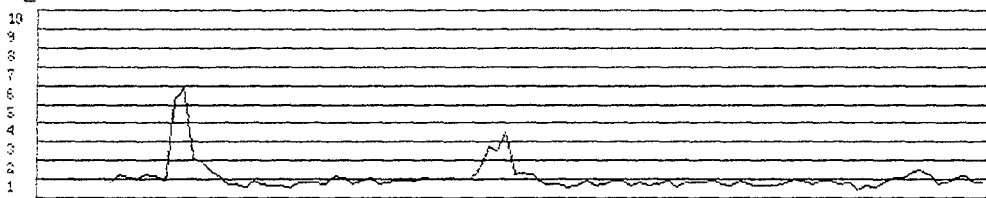$$\alpha = 2.15$$

Figure 34. Israeli Regional Experimental Seismic Array configuration.

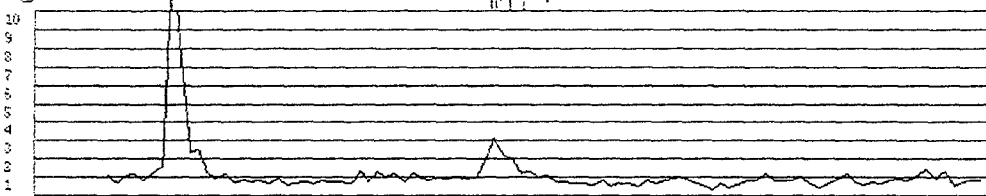SINGLE CHANNEL                                        EVENT:13-05 19:36
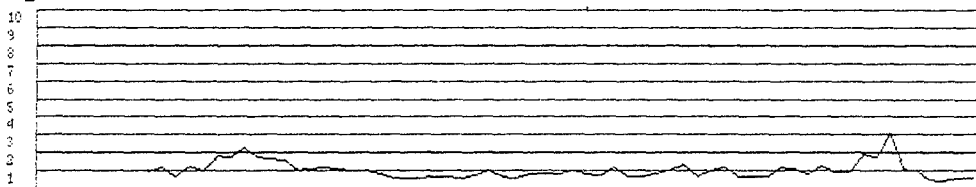
signal/noise

BEAM

signal/noise

A . Cyprus , $M_L$=2.2, $\Delta$=500 km.
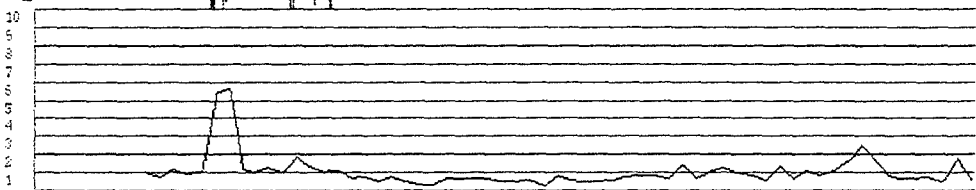
SINGLE CHANNEL                                        EVENT:06-05 09:18
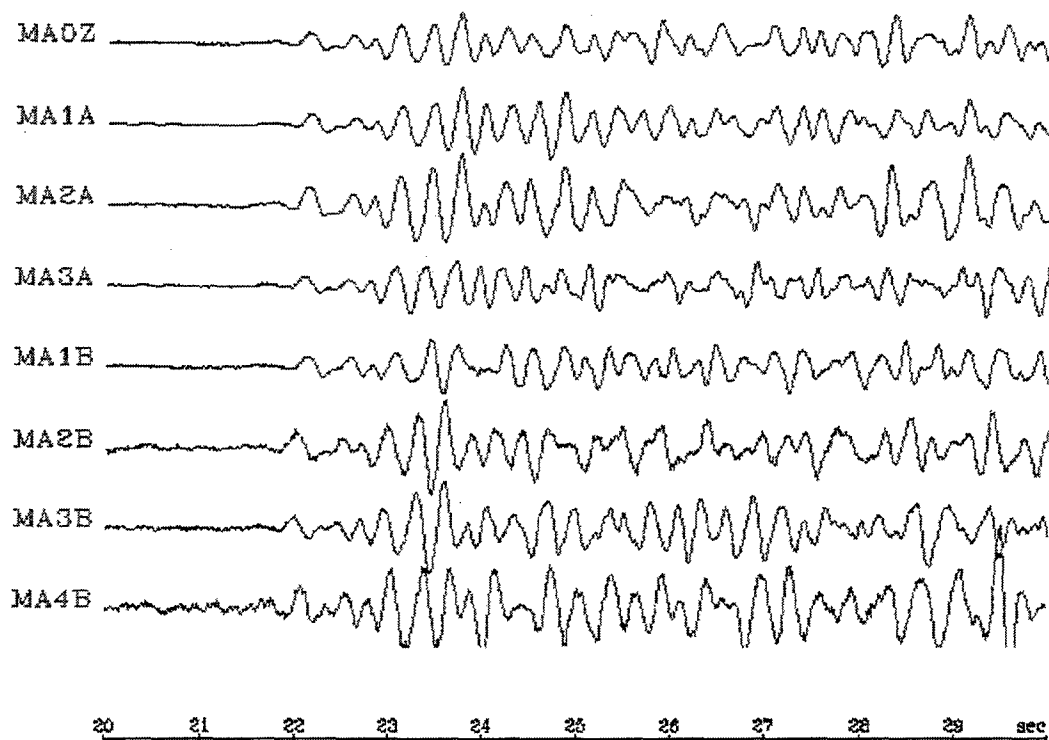
signal/noise

BEAM

signal/noise

B. Explosion near Beiruth, $M_L$=2.2, $\Delta$=350 km.

Figure 35.        Signal-to-noise improvement using array technique.

71

MAOZ

MA1A

MA2A

MA3A

MA1B

MA2B

MA3B

MA4B

F-k RESULTs

1: 21.3-23.3sec

Az= 188.1

Vapp= 7.1

3: 21.7-23.7sec

Az = 188.1

Vapp= 7.1

2: 21.5-23.5sec

Az = 180.0
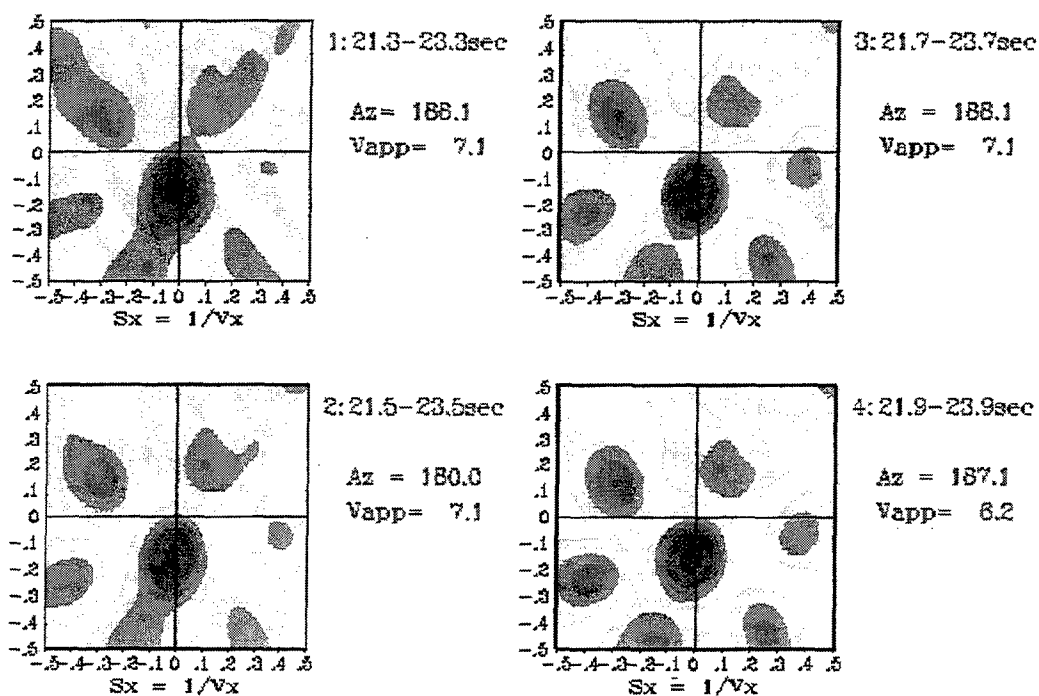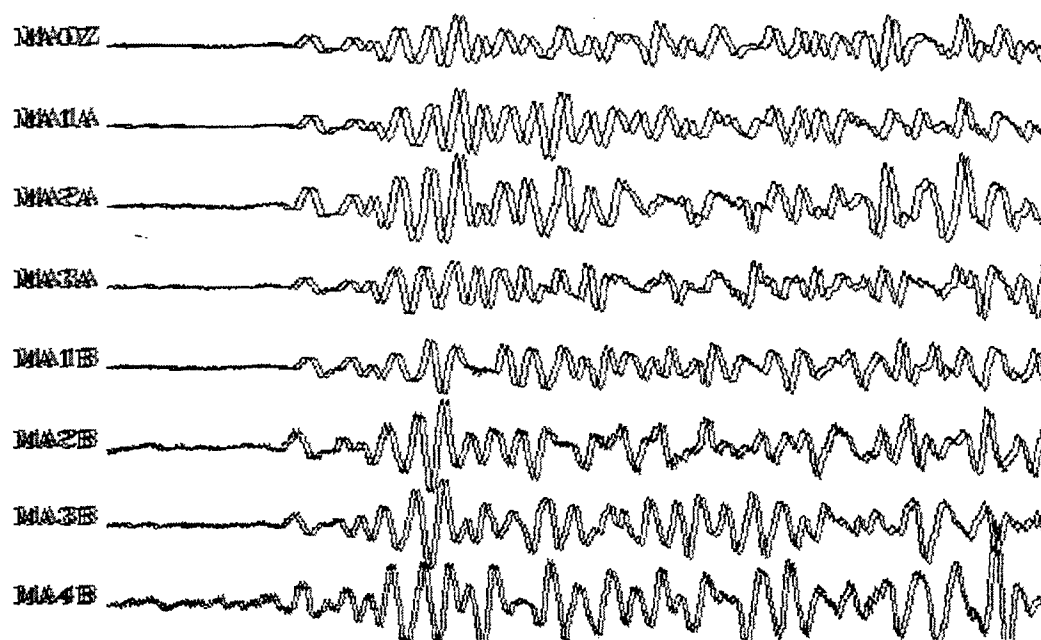
Vapp= 7.1

4: 21.9-23.9sec

Az = 187.1

Vapp= 6.2

Figure 36. F-k diagrams calculated for time windows of different positions.

Oct 16, 1993  20:51  100 sps

Gulf off Elat  mb=4.5

MA0Z

MA1A

MA2A

MA3A

MA1B

MA2B

MA3B

MA4B

20  21  22  23  24  25  26  27  28  29  30
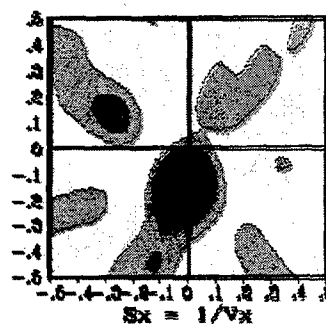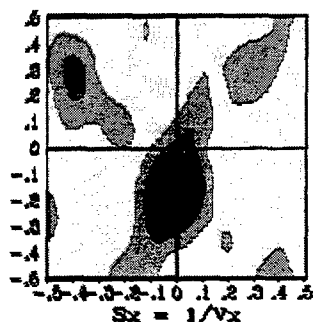
F-k RESULTs
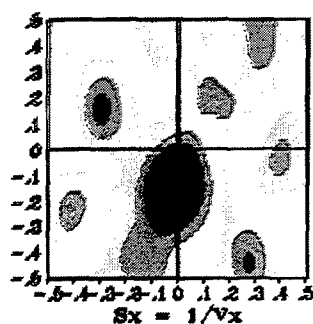
1:21.8-22.3sec
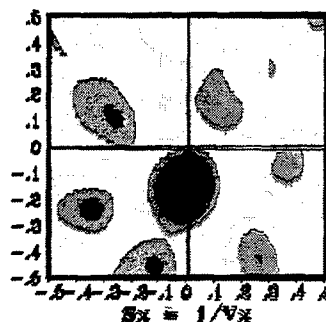
Az= 180.0
Vapp= 7.1

3:21.8-23.3sec

Az = 188.1
Vapp= 7.1

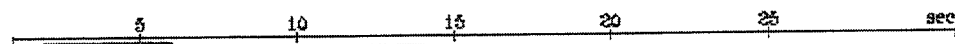2:21.8-22.8sec

Az = 180.0
Vapp= 7.1

4:21.8-23.8sec

Az = 180.0
Vapp= 8.2

Sx = 1/Vx

Figure 37. F-k diagrams calculated for time windows of different lengths.

73

Gulf of Elat  mb=4.3

MAOZ

MA1A

MA2A

MA3A

MA1B

MA2B

MA3B

MA4B

MA5B

```
        5        10       15       20       25      sec
```
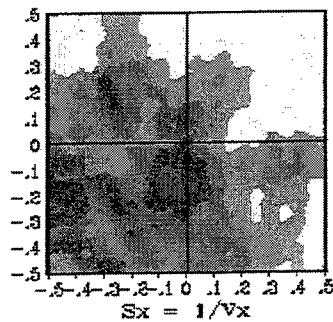
PHASE CORRELATION ANALYSIS

1: 2.0- 6.0sec

Az= 241.9
Vapp= 2.9

Sx = 1/Vx

3: 14.0-18.0sec

Az = 180.0
Vapp= 6.2

Sx = 1/Vx
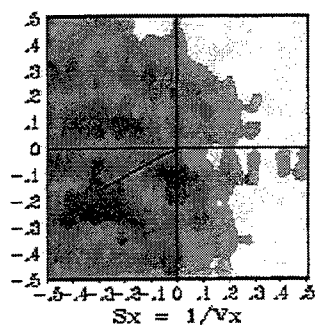
2: 10.0-14.0sec

Az = 241.9
Vapp= 2.9

Sx = 1/Vx

4: 22.0-26.0sec

Az = 186.3
Vapp= 5.5

Sx = 1/Vx
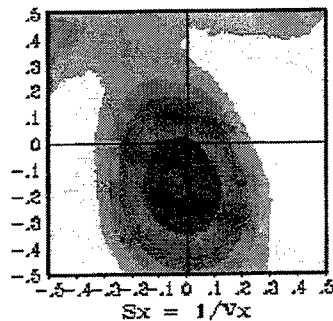
Figure 38. Phase correlation diagrams calculated for the seismic noise (1,2) and
seismic signal (3,4) domains.
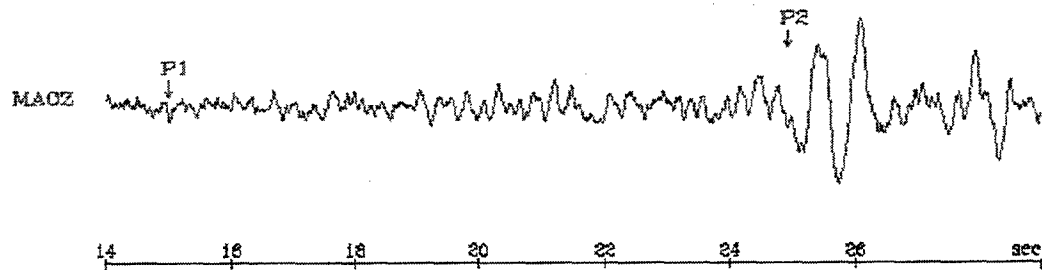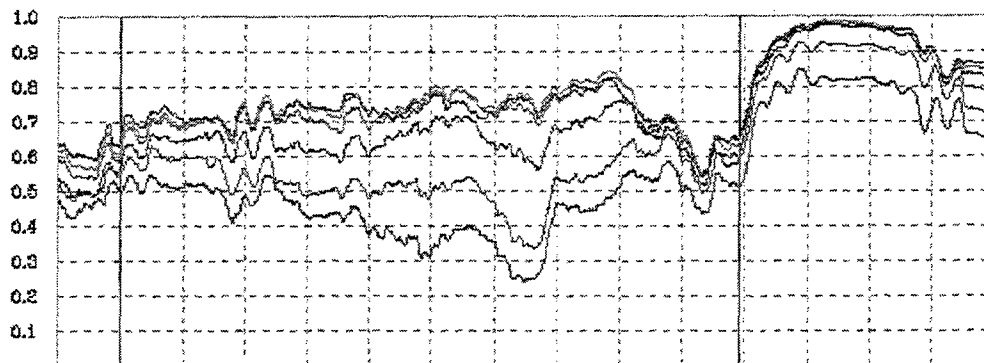
P2

P1

MAOZ

14      16      18      20      22      24      26      sec

## Phase correlation

1.0
0.9
0.8
0.7
0.6
0.5
0.4
0.3
0.2
0.1

P−wave groups:          S−wave groups:

5.5 km/sec              3.1 km/sec

6.2 km/sec              3.6 km/sec

7.95 km/sec             4.45 km/sec

## PHASE CORRELATION ANALYSIS

.5
.4
.3
.2
.1
0
-.1
-.2
-.3
-.4
-.5
-.5 -.4 -.3 -.2 -.1 0 .1 .2 .3 .4 .5
Sx = 1/Vx
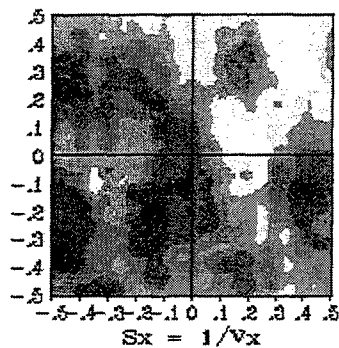
P1:

15.0−15.3sec

Az= 189.5

Vapp=  6.2

.5
.4
.3
.2
.1
0
-.1
-.2
-.3
-.4
-.5
-.5 -.4 -.3 -.2 -.1 0 .1 .2 .3 .4 .5
Sx = 1/Vx
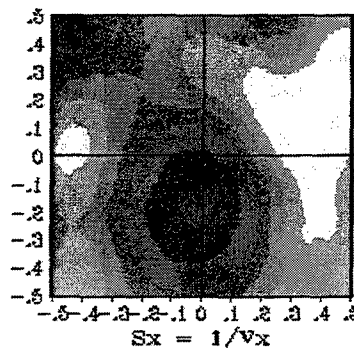
P2:

24.9−25.3sec

Az = 187.1

Vapp=  6.2

Figure 39. Arrival azimuth and apparent velocity determined for P1- and P2-onsets from
the phase correlation diagrams.
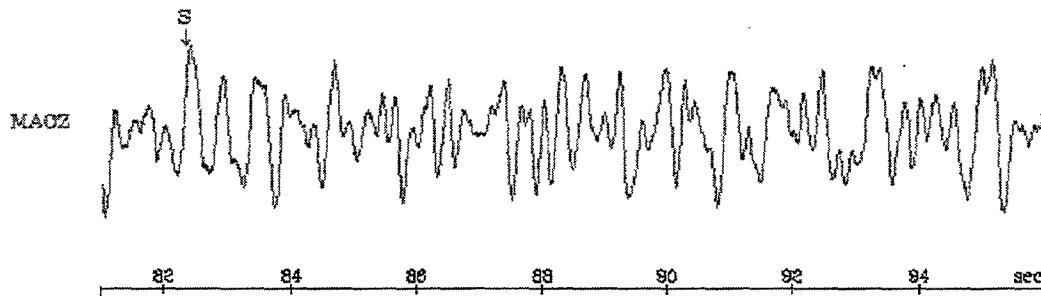
75

Nov 3. 1993 19:07 100 sps
Gulf of Elat mb=4.3

S

MAOZ

82    84    86    88    90    92    94    sec

Phase correlation

1.0
0.9
0.8
0.7
0.6
0.5
0.4
0.3
0.2
0.1
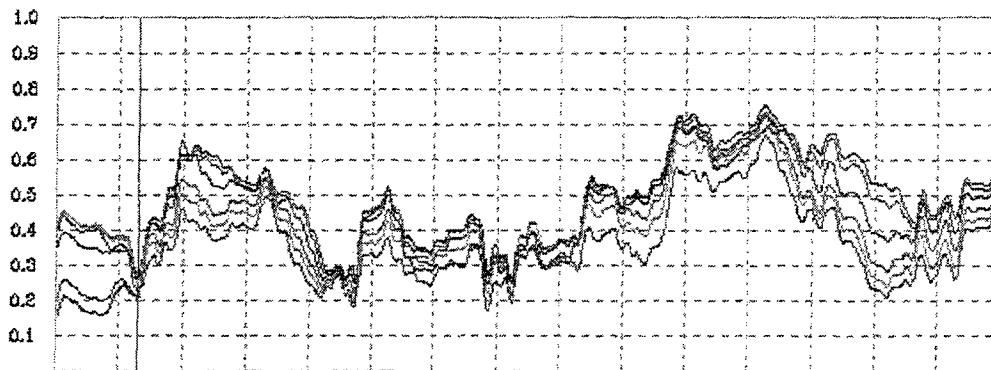
P—wave groups:        S—wave groups:
5.5 km/sec            3.1 km/sec
6.2 km/sec            3.6 km/sec
7.95 km/sec           4.45 km/sec

PHASE CORRELATION ANALYSIS
(S—wave)

82.3—83.0sec
Az= 188.7
Vapp= 3.8 km/sec

Sx = 1/Vx

Figure 40. Arrival azimuth and apparent velocity determined for S-onset from
the phase correlation diagrams.

76

# 8. DISCUSSION AND CONCLUSIONS

The ISN regional seismograms and their corresponding spectra show three main features which were utilized for the construction of formal discriminants:

a) As a rule earthquakes are much richer in high frequency (>6 Hz) -energy than explosions.

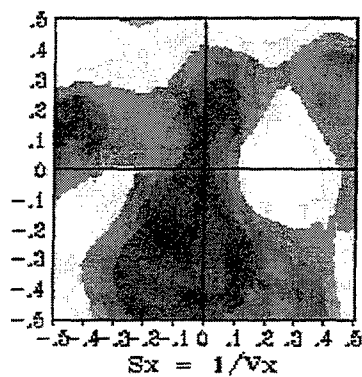b) There is a clear train of low frequency Rg waves following body waves phases on the explosion seismograms.

c) Smoothed spectra from explosions showed distinct minima and maxima, coherent for the ISN stations, located at different azimuths and distances.

At least the first two of the above may be attributed to:

1. Low frequency S and surface waves generated by shallow seismic events (mainly quarry blasts) and associated with the regional crustal structure of widespread unconsolidated subsurface sediments; and

2. low frequency reverberations generated by underwater explosions in the sea water layer.

The third feature is related more to the ripple-firing effect combined with symmetric radiation diagram which is characteristic to the explosion (actually, point) source.

Based on these observations, new discriminants having a large resolving power for Israel and surrounding areas were constructed:

a) The seismic energy spectral ratio ($R_E$) between the low frequency (1-6 Hz) and the high frequency (6-11 Hz) bands.

b) Group velocity statistics based on velogram analysis, characterizing kinematic properties of the S and surface wave phases.

c) Spectral "semblance" and "cross-correlation" statistics measuring the coherency of smoothed spectra at different ISN stations.

77

The discriminants were tested on a large amount of data, 73 earthquakes and 139 explosions with ground truth information for quarry blasts and experimental single underwater shots from the different areas within the region. The statistics constructed efficiently utilized the advantage of the ISN as a Regional Dense Seismic Network (RDSN).

Ratio $R_E$ for individual ISN stations, though efficient, showed overlapping of the earthquake and explosion populations due to path and site effects. Being averaged over a subnetwork of the ISN stations, its resolving power was enhanced and the two populations were separated with a 99% success rate for 173 events (excluding single quarry blasts, see Section 5).

The group velocity, very variable for individual stations, was fitted by the parametric function of distance in the range 10-350km. The "C" discriminant derived from estimates of the function parameters provided a 97% success rate for almost 140 events.

The spectral semblance statistics, utilizing azimuthal invariance of explosion spectra, appeared to be extremely efficient with a 99% success rate for 183 events.

We also tested the P/S type discriminant, derived from velograms, which worked only for some of the remote (R>100km) stations and, when applied to the Galilee data set, was not as reliable as the discriminants mentioned above. Coda Q discriminant, albeit very promising, failed completely in our investigation, showing severe dependency on the signal-to-noise ratio.

The study based on the searching for physically approved discriminants, was complemented by testing of the multivariate procedures using the Integrative Approach. Three of them, CAP, LDF and ANN, were applied to the averaged rms of the Galilee events spectra in different frequency bands with a 99%, 99% and 100% success rate, correspondingly.

From observations and testing of discriminants we may conclude that much of the information related to identification of earthquakes and explosions in Israel is concentrated in the seismograms spectra and may be effectively extracted using the RDSN discriminants developed.

An important question is the transportability of spectral (and maybe velogram) discriminants to another region with a different geology-tectonic environment. Hence we propose to examine this on Norwegian data (recorded by the Bergen University Network) which were collected during a visit by Drs. V. Pinsky and Y. Gitterman to Bergen University.

As stated above, further investigations associated with a seismic micro-array will depend on the availability of funds, but we are optimistic.

# REFERENCES

Alexander, S.S., Hsu, R.C., Karl, S.L., Gupta, I.N. and Salzberg, D.H., 1995. New techniques for estimating source depth and other diagnostic source characteristics of shallow events from regional observations of P, Lg and Rg signals, Proceedings of 17th Seismic Research Symposium on Monitoring a CTBT, AZ, 821-830. PL-TR-95-2108, ADA310037

Almagor, G. and Hall, J.K., 1984. Bathymetric chart of the Mediterranean coast of Israel, Geol. Surv. Israel Bull., 77.

Bakun, W.H., Stewart, R.M. and Bufe, C.G., 1978. Directivity in the high frequency radiation of small earthquakes, Bull. Seis. Soc. Am., 68:1253-1263.

Barker, T.G., McLaughlin, K.C. and Stevens, J.L., 1993. Numeral simulation of quarry blast sources, SSS-TR-93-13859, S-Cubed, La Jolla, CA.

Baumgardt, D.R., 1993. Seismic waveform feature analysis and discrimination of the December 31, 1992 Novaya Zemlya event, in: The Novaya Zemlya event of December 31, 1992 and Seismic Identification Issues, 15th Annual Seismic Research Symposium, ARPA Rep., 30pp. PL-TR-93-2160, ADA271458

Baumgardt, D.R. and Zigler, K.A., 1988. Spectral evidence of source multiplicity in explosions: application to regional discrimination of earthquakes and explosions, Bull. Seis. Soc. Am., 78:1773-1795.

Baumgardt, D.R. and Young, G.B., 1990. Regional seismic waveform discrimination and CS-based event identification using regional arrays, Bull. Seis. Soc. Am., 80, Part B, 1910-1934

Bennett, T.J. and Murphy, J.R., 1986. Analysis of seismic discrimination capabilities using regional data from Western United States events, Bull. Seis. Soc. Am., 76:1069-1086.

Bennett, T.J., Barker, B.W., McLaughlin, K.L. and Murphy, J.R., 1989. Regional discrimination of quarry blasts, earthquakes and underground nuclear explosions, Final Report, GL-TR-89-0114, S-Cubed, La Jolla, California. ADA223148

Blanford, R.R., 1995. Regional seismic event discrimination, in: E.S. Husebye and A.M. Dainty (Eds.) Monitoring a Comprehensive Test Ban Treaty, NATO ASI Series, Series E: Applied Sciences - Vol. 303, 689-719.

Beck, S.L. and Wallace, T.C., 1995. Broadband seismic recordings of mining explosions and earthquakes in South America, Proceedings of 17th Seismic Research Symposium on Monitoring a CTBT, AZ, 157-163. PL-TR-95-2108, ADA310037

Der, Z.A. and Baumgardt, D.R., 1995. Source finiteness, signal decorrelation, spectral scalloping and identification of multiple delayed explosions, Proceedings of 17th Seismic Research Symposium on Monitoring a CTBT, Scottsdale, AZ, 723-732. PL-TR-95-2108, ADA310037

Dowla, F., 1995. Neural networks in seismic discrimination, in: E.S. Husebye and A.M. Dainty (Eds.) Monitoring a Comprehensive Test Ban Treaty, NATO ASI Series, Series E: Applied Sciences - Vol. 303, 777-790.

Dowla, F., Taylor, S. and Anderson,R., 1990. Seismic discrimination with artificial neural networks: preliminary results with regional spectral data, BSSA, 80:1346-1373.

Dysart, P.S. and Pully, J.J., 1990. Regional seismic event classification at the NORESS array: seismological measurements and the use of trained neural networks, Bull. Seis. Soc. Am., 80, Part B, 1910-1934.

Feigin, G. and Shapira, A., 1994. A unified crustal model for calculating travel times of seismic waves across the Israel Seismic Network, IPRG Report Z1/567/79(107).

Fukunaga, K. and Hummels, D.M., 1989. Leave-one-out procedure for nonparametric error estimates, IEEE Trans. Pattern. Anal. and Machine Intel., 11:421-423.

Gelchinsky, B. and Krauklis, ??., 1964. On a Particular Computer Algorithms in Regard to the Process of Seismic-Wave Correlation, Questions of Dynamic Theory of Propagation of Seismic Waves, 7:115-123 (in Russian).

Gelchinsky, B., Landa, E. and Shtivelman, V., 1985. Algorithms of Phase and Group Correlation. Geophysics, 50:596-608.

Gitterman, Y. and van Eck, T., 1993. Spectra of quarry blasts and microearthquakes recorded at local distances in Israel, Bull. Seis. Soc. Am., 83:1799-1812.

Gitterman, Y. and Shapira, A., 1994. Spectral characteristics of seismic events off the coast of the Levant, Geophys. J. Int., 116:485-497.

Gitterman, Y. and Shapira, A., 1993. Spectral discrimination of underwater explosions, Isr. J. Earth Sci., 42:37-44.

Goldstein, P., 1995. Slopes of P- to S- wave spectral ratios - a broadband regional discriminant and a physical model, Geophys. Res. Lett., 22:3147-3150.

Hartse, H.E., Phillips, W.S., Fehler, M.C. and Hause, L.S., 1995. Single-station spectral discrimination using coda waves, Bull. Seis. Soc. Am., 85:1464-1474.

Hedlin, M., Minster, J.G. and Orcutt, J.A., 1989. The time-frequency characteristics of quarry blasts and calibration explosions recorded in Kazakhstan, USSR, Geophys. J. Int., 99:109-121.

Hedlin, M.A.H., Minster, J.B. and Orcutt, J.A., 1990. An automatic means to discriminate between earthquakes and quarry blasts, Bull. Seis. Soc. Am., 80, Part B, 2143-2160.

Hedlin, M., Vernon, F., Minster, J.G. and Orcutt, J.A., 1995. Regional small-event identification using seismic networks and arrays, Proceedings of 17th Seismic Research Symposium on Monitoring a CTBT, Scottsdale, AZ, 875-884. PL-TR-95-2108, ADA 310037

Husebye, E.S. and Ruud, B.O., 1995. Waveform synthetics in 3D and fully automatic event locations. Proceedings of 17th Seismic Research Symposium on Monitoring a CTBT, AZ, 389-400. PL-TR-95-2108, ADA 310037

Jarpe, S.P., Moran, B., Goldstein, P. and Glenn, L.A., 1996. Implications of mining practices in an open-pit gold mine for monitoring of a Comprehensive Test Ban Treaty, LLNL report UCRL-ID-123017, 35pp.

Kafka, A.L., 1990. Rg as a depth discriminator for earthquakes and explosions: a case study in New England, Bull. Seism. Soc. Am., 80:373-395.

Kim, W.Y., Simpson, D.W. and Richards, P.G., 1994. High-frequency spectra of regional phases from earthquakes and chemical explosions, Bull. Seis. Soc. Am., 84:1365-1386.

King, B.F., 1967. Step-wise clustering procedures. Journal of the American Statistical Association, 62:86-101.

Malitzky, A. and Shapira, A., 1994. Latest results of the experimental seismic antenna on Mt. Tur'an, Israel, Geol. Survey of Israel, Annual Meeting.

Malitzky, A. and Shapira, A., 1994. Application of correlation algorithms for a new seismic antenna in Israel, ESC, Athens.

Malitzky, A. and Shapira, A., 1995. Application of a seismic antenna technique in Israel, Geol. Surv. Israel, Annual Meeting.

Neidell, N.S. and Taner, M.T., 1971. Semblance and other coherency measures for multichannel data, Geophysics, 36:482-497.

Pomeroy, P.W., Best, J.W. and McEvilly, Th.V., 1982. Test ban treaty verification with regional data - a review, Bull. Seis. Soc. Am., 72, No. 6, S89-S129.

Pulli, J.J., 1986. Expanded use of computers in regional seismic data analysis, in: Technical Report C86-06, Center for Seismic Studies, Arlington, Virginia, 2.29-2.38.

Pulli, J.J., 1995. Extracting and processing signal parameters for regional seismic event identification, in: E.S. Husebye and A.M. Dainty (Eds.), Monitoring a CTBT, NATO ASI Series, Series E: Vol. 303, 741-754.

Shapira, A., 1988. Magnitude scales for regional earthquakes monitored in Israel, Isr. J. Earth Sci., Vol. 37, 17-22.

Shapira, A. and Avirav, V., 1990. ISDA - Israeli Seismic Data Acquisiton System, User's Guide, Version I, IPRG Report Z1/567/79(76).

Su, F., Aki, K. and Biswas, N.N., 1991. Discriminating quarry blasts from earthquakes using coda waves, Bull. Seis. Soc. Am., 81:162-178.

Suteau-Henson, A. and Bache, T.C., 1988. Spectral characteristics of regional phases recorded at NORESS, Bull. Seis. Soc. Am., 708-725.

Taylor, S.R., Sherman, N.W. and Denny, M.D., 1988. Spectral discrimination between NTS explosions and Western United States earthquakes at regional distances, Bull. Seis. Soc. Am., 78:1563-1579.

Taylor, S.R., Denny, M.D., Vergino, E.S. and Glaser, R.E., 1989. Regional discrimination between NTS explosions and western U.S. earthquakes, Bull. Seism. Soc. Am., 79:1142-1176.

Tsvang, S.L., Pinsky, V.I. and Husebye, E.S., 1993. Enhanced seismic source discrimination using NORESS recordings from Eurasian events, Geophys. J. Int., 112:1-14.

van Eck, T., 1988. Attenuation of coda waves in the Dead Sea region, Bull. Seis. Soc. Am., 78:770-779.

Walter, W.R., Mayeda, K.M. and Patton, H.J., 1995. Phase and spectral ratio discrimination between NTS earthquakes and Explosions, Part I: Empirical Observations, Bull. Seis. Soc. Am., 85:1050-1067.

Walter, W.R., Hunter, S.L. and Glenn, L.A., 1996. Preliminary report on LLNL mine seismicity deployment at the Twentymile Coal Mine. CTBT Seismic Monitoring Project Task S7.2, Deliverable #2, UCRL-ID-122800.

Wuster, J., 1993. Discrimination of chemical explosions and earthquakes in central Europe - a case study, Bull. Seis. Soc. Am., 83:1184-1212.

Willis, D.E., 1963. Seismic measurements of large underwater shots, Bull. Seis. Soc. Am., 53:789.

# Appendix A.

Date : July 16, 1995
TO  : Dr. Shapira     Seismology Division     Fax : 972-3-5502925
From : Abdel-Qader Amrat     Seismology Division     Fax : 962-6-827970

Concerning your fax dated June 26, 1995, requesting some information on 20-30 quarry blasts, please find herewith the information you need in your study of discrimination of seismic sources.
I wish that cooperation with you will develop in the future.

Yours sincerely,

Abdel-Qader Amrat

| DATE | TIME hour /min | LATITUDE degree | LONGITUDE degree | GELATINE Kg | NITRITE Kg |
|---|---|---|---|---|---|
| 01 11.91 | 14.00 | 31 09.20 | 36 09.17 | 725 | 12700 |
| 14 11.91 | 14:00 | 31 09.65 | 36 08.87 | 650 | 12500 |
| 16 11.91 | 14:00 | 31 09.65 | 36 08.87 | 750 | 15300 |
| 18 11.91 | 14:00 | 31 09.65 | 36 08.87 | 750 | 13500 |
| 21 11.91 | 14:00 | 31 09.65 | 36 08.87 | 800 | 15300 |
| 01 06.92 | 14:00 | 31 09.80 | 36 09.16 | 850 | 17000 |
| 02 06.92 | 14:00 | 31 09.80 | 36 09.16 | 675 | 16500 |
| 04 07 92 | 14:00 | 31 09.35 | 36 09.30 | 725 | 15000 |
| 07 07 92 | 14:00 | 31 09.35 | 36 09.30 | 575 | 12700 |
| 31 07 92 | 14:00 | 31 10.55 | 36 09.35 | 525 | 12700 |
| 10 03.93 | 14:00 | 31 09.67 | 36 09.25 | 525 | 13850 |
| 11 03.93 | 14:00 | 31 09.67 | 36 09.25 | 475 | 15450 |
| 16 03.93 | 14:00 | 31 09.67 | 36 09.25 | 550 | 13100 |
| 21 03.93 | 14:00 | 31 09.10 | 36 09.35 | 500 | 12500 |
| 31 03 93 | 14:00 | 31 09.75 | 36 09.15 | 900 | 22000 |
| 09 03.94 | 14:15 | 31 08.70 | 36 09.55 | 675 | 11000 |
| 18 03.94 | 14:15 | 31 08.70 | 36 09.65 | 575 | 8000 |
| 30 03.94 | 14:15 | 31 08.55 | 36 09.56 | 475 | 6500 |
| 05 05 94 | 14:15 | 31 08.95 | 36 09.65 | 275 | 6700 |
| 16 05.94 | 14:15 | 31 08.95 | 36 09.75 | 315 | 6000 |
| 02 04.95 | 12:22 | 29 55.05 | 36 10.95 | 850 | 15600 |
| 04 04.95 | 1:30 | 29 55.10 | 36 10.95 | 750 | 14000 |
| 24 04.95 | 11:45 | 29 54.60 | 36 10.45 | 900 | 15000 |
| 25 04.95 | 12:40 | 29 54.65 | 36 10.45 | 800 | 14000 |
| 30 04.95 | 11:50 | 29 54.73 | 36 10.45 | 950 | 16000 |

THOMAS AHRENS
SEISMOLOGICAL LABORATORY 252-21
CALIFORNIA INSTITUTE OF TECHNOLOGY
PASADENA, CA 91125

RALPH ALEWINE
NTPO
1901 N. MOORE STREET, SUITE 609
ARLINGTON, VA 22209

SHELTON ALEXANDER
PENNSYLVANIA STATE UNIVERSITY
DEPARTMENT OF GEOSCIENCES
537 DEIKE BUILDING
UNIVERSITY PARK, PA 16801

LOS ALAMOS NATIONAL LABORATORY
ATTN: TECHNICAL STAFF (PLS ROUTE)
PO BOX 1663, MS F659
LOS ALAMOS, NM 87545

LAWRENCE LIVERMORE NATIONAL LABORATORY
ATTN: TECHNICAL STAFF (PLS ROUTE)
PO BOX 808, MS L-200
LIVERMORE, CA 94551

MUAWIA BARAZANGI
INSTITUTE FOR THE STUDY OF THE CONTINENTS
3126 SNEE HALL
CORNELL UNIVERSITY
ITHACA, NY 14853

RICHARD BARDZELL
ACIS
DCI/ACIS
WASHINGTON, DC 20505

T.G. BARKER
MAXWELL TECHNOLOGIES
P.O. BOX 23558
SAN DIEGO, CA 92123

DOUGLAS BAUMGARDT
ENSCO INC.
5400 PORT ROYAL ROAD
SPRINGFIELD, VA 22151

SANDIA NATIONAL LABORATORY
ATTN: TECHNICAL STAFF (PLS ROUTE)
DEPT. 5791
MS 0567, PO BOX 5800
ALBUQUERQUE, NM 87185-0567

THERON J. BENNETT
MAXWELL TECHNOLOGIES
11800 SUNRISE VALLEY DRIVE SUITE 1212
RESTON, VA 22091

WILLIAM BENSON
NAS/COS
ROOM HA372
2001 WISCONSIN AVE. NW
WASHINGTON, DC 20007

JONATHAN BERGER
UNIVERSITY OF CA, SAN DIEGO
SCRIPPS INSTITUTION OF OCEANOGRAPHY IGPP, 0225
9500 GILMAN DRIVE
LA JOLLA, CA 92093-0225

ROBERT BLANDFORD
AFTAC
1300 N. 17TH STREET
SUITE 1450
ARLINGTON, VA 22209-2308

LOS ALAMOS NATIONAL LABORATORY
ATTN: TECHNICAL STAFF (PLS ROUTE)
PO BOX 1663, MS F665
LOS ALAMOS, NM 87545

LAWRENCE LIVERMORE NATIONAL LABORATORY
ATTN: TECHNICAL STAFF (PLS ROUTE)
PO BOX 808, MS L-207
LIVERMORE, CA 94551

STEVEN BRATT
NTPO
1901 N. MOORE STREET, SUITE 609
ARLINGTON, VA 22209

SANDIA NATIONAL LABORATORY
ATTN: TECHNICAL STAFF (PLS ROUTE)
DEPT. 5704
MS 0655, PO BOX 5800
ALBUQUERQUE, NM 87185-0655

LAWRENCE LIVERMORE NATIONAL LABORATORY
ATTN: TECHNICAL STAFF (PLS ROUTE)
PO BOX 808, MS L-221
LIVERMORE, CA 94551

RHETT BUTLER
IRIS
1616 N. FORT MEYER DRIVE
SUITE 1050
ARLINGTON, VA 22209

1

SANDIA NATIONAL LABORATORY
ATTN: TECHNICAL STAFF (PLS ROUTE)
DEPT. 5736
MS 0655, PO BOX 5800
ALBUQUERQUE, NM 87185-0655

LESLIE A. CASEY
DOE
1000 INDEPENDENCE AVE. SW
NN-40
WASHINGTON, DC 20585-0420

SANDIA NATIONAL LABORATORY
ATTN: TECHNICAL STAFF (PLS ROUTE)
DEPT. 9311
MS 1159, PO BOX 5800
ALBUQUERQUE, NM 87185-1159

DR. STANLEY DICKINSON
AFOSR
110 DUNCAN AVENUE
SUITE B115
BOLLING AFB, WASHINGTON D.C. 20332-001

SEAN DORAN
ACIS
DCI/ACIS
WASHINGTON, DC 20505

DIANE I. DOSER
DEPARTMENT OF GEOLOGICAL SCIENCES
THE UNIVERSITY OF TEXAS AT EL PASO
EL PASO, TX 79968

LAWRENCE LIVERMORE NATIONAL LABORATORY
ATTN: TECHNICAL STAFF (PLS ROUTE)
LLNL
PO BOX 808, MS L-175
LIVERMORE, CA 94551

SANDIA NATIONAL LABORATORY
ATTN: TECHNICAL STAFF (PLS ROUTE)
SNL, DEPT. 4115
MS 0329, PO BOX 5800
ALBUQUERQUE, NM 87185-0329

RICHARD J. FANTEL
BUREAU OF MINES
DEPT OF INTERIOR, BLDG 20
DENVER FEDERAL CENTER
DENVER, CO 80225

JOHN FILSON
ACIS/TMG/NTT
ROOM 6T11 NHB
WASHINGTON, DC 20505

MARK D. FISK
MISSION RESEARCH CORPORATION
735 STATE STREET
P.O. DRAWER 719
SANTA BARBARA, CA 93102-0719

LAWRENCE LIVERMORE NATIONAL LABORATORY
ATTN: TECHNICAL STAFF (PLS ROUTE)
PO BOX 808, MS L-208
LIVERMORE, CA 94551

PACIFIC NORTHWEST NATIONAL LABORATORY
ATTN: TECHNICAL STAFF (PLS ROUTE)
PO BOX 999, MS K6-48
RICHLAND, WA 99352

ROBERT GEIL
DOE
PALAIS DES NATIONS, RM D615
GENEVA 10, SWITZERLAND

LORI GRANT
MULTIMAX, INC.
311C FOREST AVE. SUITE 3
PACIFIC GROVE, CA 93950

HENRY GRAY
SMU STATISTICS DEPARTMENT
P.O. BOX 750302
DALLAS, TX 75275-0302

CATHERINE DE GROOT-HEDLIN
SCRIPPS INSTITUTION OF OCEANOGRAPHY
UNIVERSITY OF CALIFORNIA, SAN DIEGO
INSTITUTE OF GEOPHYSICS AND PLANETARY PHYSICS
LA JOLLA, CA 92093

I. N. GUPTA
MULTIMAX, INC.
1441 MCCORMICK DRIVE
LARGO, MD 20774

PACIFIC NORTHWEST NATIONAL LABORATORY
ATTN: TECHNICAL STAFF (PLS ROUTE)
PO BOX 999, MS K7-34
RICHLAND, WA 99352

PACIFIC NORTHWEST NATIONAL LABORATORY
ATTN: TECHNICAL STAFF (PLS ROUTE)
PO BOX 999, MS K6-40
RICHLAND, WA 99352

DAVID HARKRIDER
PHILLIPS LABORATORY
EARTH SCIENCES DIVISION
29 RANDOLPH ROAD
HANSCOM AFB, MA 01731-3010

JAMES HAYES
NSF
4201 WILSON BLVD., ROOM 785
ARLINGTON, VA 22230

THOMAS HEARN
NEW MEXICO STATE UNIVERSITY
DEPARTMENT OF PHYSICS
LAS CRUCES, NM 88003

MICHAEL HEDLIN
UNIVERSITY OF CALIFORNIA, SAN DIEGO
SCRIPPS INSTITUTION OF OCEANOGRAPHY IGPP, 0225
9500 GILMAN DRIVE
LA JOLLA, CA 92093-0225

DONALD HELMBERGER
CALIFORNIA INSTITUTE OF TECHNOLOGY
DIVISION OF GEOLOGICAL & PLANETARY SCIENCES
SEISMOLOGICAL LABORATORY
PASADENA, CA 91125

EUGENE HERRIN
SOUTHERN METHODIST UNIVERSITY
DEPARTMENT OF GEOLOGICAL SCIENCES
DALLAS, TX 75275-0395

ROBERT HERRMANN
ST. LOUIS UNIVERSITY
DEPARTMENT OF EARTH & ATMOSPHERIC SCIENCES
3507 LACLEDE AVENUE
ST. LOUIS, MO 63103

VINDELL HSU
HQ/AFTAC/TTR
1030 S. HIGHWAY A1A
PATRICK AFB, FL 32925-3002

ANTHONY IANNACCHIONE
BUREAU OF MINES
COCHRANE MILL ROAD
PO BOX 18070
PITTSBURGH, PA 15236-9986

RONG-SONG JIH
PHILLIPS LABORATORY
EARTH SCIENCES DIVISION
29 RANDOLPH ROAD
HANSCOM AFB, MA 01731-3010

THOMAS JORDAN
MASSACHUSETTS INSTITUTE OF TECHNOLOGY
EARTH, ATMOSPHERIC & PLANETARY SCIENCES
77 MASSACHUSETTS AVENUE, 54-918
CAMBRIDGE, MA 02139

THORNE LAY
UNIVERSITY OF CALIFORNIA, SANTA CRUZ
EARTH SCIENCES DEPARTMENT
EARTH & MARINE SCIENCE BUILDING
SANTA CRUZ, CA 95064

ANATOLI L. LEVSHIN
DEPARTMENT OF PHYSICS
UNIVERSITY OF COLORADO
CAMPUS BOX 390
BOULDER, CO 80309-0309

DONALD A. LINGER
DNA
6801 TELEGRAPH ROAD
ALEXANDRIA, VA 22310

GARY MCCARTOR
SOUTHERN METHODIST UNIVERSITY
DEPARTMENT OF PHYSICS
DALLAS, TX 75275-0395

KEITH MCLAUGHLIN
MAXWELL TECHNOLOGIES
P.O. BOX 23558
SAN DIEGO, CA 92123

PACIFIC NORTHWEST NATIONAL LABORATORY
ATTN: TECHNICAL STAFF (PLS ROUTE)
PO BOX 999, MS K7-22
RICHLAND, WA 99352

BRIAN MITCHELL
DEPARTMENT OF EARTH & ATMOSPHERIC SCIENCES
ST. LOUIS UNIVERSITY
3507 LACLEDE AVENUE
ST. LOUIS, MO 63103

RICHARD MORROW
USACDA/IVI
320 21ST STREET, N.W.
WASHINGTON, DC 20451

JOHN MURPHY
MAXWELL TECHNOLOGIES
11800 SUNRISE VALLEY DRIVE SUITE 1212
RESTON, VA 22091

3

JAMES NI
NEW MEXICO STATE UNIVERSITY
DEPARTMENT OF PHYSICS
LAS CRUCES, NM 88003

CHARLES ODDENINO
BUREAU OF MINES
810 7TH ST. NW
WASHINGTON, DC 20241

JOHN ORCUTT
INSTITUTE OF GEOPHYSICS AND PLANETARY PHYSICS
UNIVERSITY OF CALIFORNIA, SAN DIEGO
LA JOLLA, CA 92093

FRANK PILOTTE
HQ/AFTAC/TT
1030 S. HIGHWAY A1A
PATRICK AFB, FL 32925-3002

KEITH PRIESTLEY
DEPARTMENT OF EARTH SCIENCES
UNIVERSITY OF CAMBRIDGE
MADINGLEY RISE, MADINGLEY ROAD
CAMBRIDGE, CB3 OEZ UK

JAY PULLI
RADIX SYSTEMS, INC.
6 TAFT COURT
ROCKVILLE, MD 20850

PACIFIC NORTHWEST NATIONAL LABORATORY
ATTN: TECHNICAL STAFF (PLS ROUTE)
PO BOX 999, MS K5-72
RICHLAND, WA 99352

PAUL RICHARDS
COLUMBIA UNIVERSITY
LAMONT-DOHERTY EARTH OBSERVATORY
PALISADES, NY 10964

DAVID RUSSELL
HQ AFTAC/TTR
1030 SOUTH HIGHWAY A1A
PATRICK AFB, FL 32925-3002

PACIFIC NORTHWEST NATIONAL LABORATORY
ATTN: TECHNICAL STAFF (PLS ROUTE)
PO BOX 999, MS K6-84
RICHLAND, WA 99352

LAWRENCE LIVERMORE NATIONAL LABORATORY
ATTN: TECHNICAL STAFF (PLS ROUTE)
PO BOX 808, MS L-202
LIVERMORE, CA 94551

CHANDAN SAIKIA
WOOODWARD-CLYDE FEDERAL SERVICES
566 EL DORADO ST., SUITE 100
PASADENA, CA 91101-2560

THOMAS SERENO JR.
SCIENCE APPLICATIONS INTERNATIONAL
CORPORATION
10260 CAMPUS POINT DRIVE
SAN DIEGO, CA 92121

AVI SHAPIRA
SEISMOLOGY DIVISION
THE INSTITUTE FOR PETROLEUM RESEARCH AND
GEOPHYSICS
P.O.B. 2286, NOLON 58122 ISRAEL

ROBERT SHUMWAY
410 MRAK HALL
DIVISION OF STATISTICS
UNIVERSITY OF CALIFORNIA
DAVIS, CA 95616-8671

MATTHEW SIBOL
ENSCO, INC.
445 PINEDA COURT
MELBOURNE, FL 32940

SANDIA NATIONAL LABORATORY
ATTN: TECHNICAL STAFF (PLS ROUTE)
DEPT. 5704
MS 0979, PO BOX 5800
ALBUQUERQUE, NM 87185-0979

LOS ALAMOS NATIONAL LABORATORY
ATTN: TECHNICAL STAFF (PLS ROUTE)
PO BOX 1663, MS D460
LOS ALAMOS, NM 87545

DAVID SIMPSON
IRIS
1616 N. FORT MEYER DRIVE
SUITE 1050
ARLINGTON, VA 22209

LAWRENCE LIVERMORE NATIONAL LABORATORY
ATTN: TECHNICAL STAFF (PLS ROUTE)
PO BOX 808, MS L-195
LIVERMORE, CA 94551

JEFFRY STEVENS
MAXWELL TECHNOLOGIES
P.O. BOX 23558
SAN DIEGO, CA 92123

LOS ALAMOS NATIONAL LABORATORY
ATTN: TECHNICAL STAFF (PLS ROUTE)
PO BOX 1663, MS C335
LOS ALAMOS, NM 87545

BRIAN SULLIVAN
BOSTON COLLEGE
INSITUTE FOR SPACE RESEARCH
140 COMMONWEALTH AVENUE
CHESTNUT HILL, MA 02167

DAVID THOMAS
ISEE
29100 AURORA ROAD
CLEVELAND, OH 44139

NAFI TOKSOZ
EARTH RESOURCES LABORATORY, M.I.T.
42 CARLTON STREET, E34-440
CAMBRIDGE, MA 02142

LAWRENCE TURNBULL
ACIS
DCI/ACIS
WASHINGTON, DC 20505

FRANK VERNON
UNIVERSITY OF CALIFORNIA, SAN DIEGO
SCRIPPS INSTITUTION OF OCEANOGRAPHY IGPP, 0225
9500 GILMAN DRIVE
LA JOLLA, CA 92093-0225

GREG VAN DER VINK
IRIS
1616 N. FORT MEYER DRIVE
SUITE 1050
ARLINGTON, VA 22209

TERRY WALLACE
UNIVERSITY OF ARIZONA
DEPARTMENT OF GEOSCIENCES
BUILDING #77
TUCSON, AZ 85721

LAWRENCE LIVERMORE NATIONAL LABORATORY
ATTN: TECHNICAL STAFF (PLS ROUTE)
PO BOX 808, MS L-205
LIVERMORE, CA 94551

DANIEL WEILL
NSF
EAR-785
4201 WILSON BLVD., ROOM 785
ARLINGTON, VA 22230

JAMES WHITCOMB
NSF
NSF/ISC OPERATIONS/EAR-785
4201 WILSON BLVD., ROOM785
ARLINGTON, VA 22230

RU SHAN WU
UNIVERSITY OF CALIFORNIA SANTA CRUZ
EARTH SCIENCES DEPT.
1156 HIGH STREET
SANTA CRUZ, CA 95064

JIAKANG XIE
COLUMBIA UNIVERSITY
LAMONT DOHERTY EARTH OBSERVATORY
ROUTE 9W
PALISADES, NY 10964

PACIFIC NORTHWEST NATIONAL LABORATORY
ATTN: TECHNICAL STAFF (PLS ROUTE)
PO BOX 999, MS K5-12
RICHLAND, WA 99352

SANDIA NATIONAL LABORATORY
ATTN: TECHNICAL STAFF (PLS ROUTE)
DEPT. 6116
MS 0750, PO BOX 5800
ALBUQUERQUE, NM 87185-0750

JAMES E. ZOLLWEG
BOISE STATE UNIVERSITY
GEOSCIENCES DEPT.
1910 UNIVERSITY DRIVE
BOISE, ID 83725

OFFICE OF THE SECRETARY OF DEFENSE
DDR&E
WASHINGTON, DC 20330

DEFENSE TECHNICAL INFORMATION CENTER
8725 JOHN J. KINGMAN ROAD
FT BELVOIR, VA 22060-6218 (2 COPIES)

TACTEC
BATTELLE MEMORIAL INSTITUTE
505 KING AVENUE
COLUMBUS, OH 43201 (FINAL REPORT)

PHILLIPS LABORATORY
ATTN: XPG
29 RANDOLPH ROAD
HANSCOM AFB, MA 01731-3010

PHILLIPS LABORATORY
ATTN: GPE
29 RANDOLPH ROAD
HANSCOM AFB, MA 01731-3010

PHILLIPS LABORATORY
ATTN: TSML
5 WRIGHT STREET
HANSCOM AFB, MA 01731-3004

PHILLIPS LABORATORY
ATTN: PL/SUL
3550 ABERDEEN AVE SE
KIRTLAND, NM 87117-5776 (2 COPIES)